UNIVERSITAT DE BARCELONA

Analytic Derivation of Non-Linear Dark Matter Clustering from the Filtering of the Primordial Density Field

Enric Juan Rovira

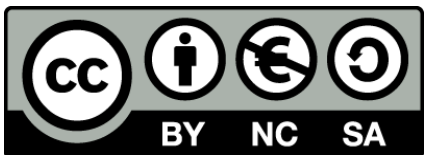

UNIVERSITAT DE BARCELONA

UNIVERSITAT DE BARCELONA

Departament d'Astronomia i Meteorologia

Analytic Derivation of Non-Linear Dark Matter Clustering from the Filtering of the Primordial Density Field

Enric Juan Rovira

Barcelona (Catalonia), February 2016

Programa de Doctorat en Física

Línia de recerca en Astronomia i Astrofísica

2010-2016

Memòria presentada per **Enric Juan Rovira**

per optar al grau de Doctor per la Universitat de Barcelona

Director i Tutor

Dr. Eduard Salvador-Solé i Dr. Alberto Manrique

Acknowledgements

First of all, I would like to spend some words in order to thank some of the people who have been by my side during all these years, some of them since the day I signed up for a college degree in Physics.

Of course, first of all I want to thank Dr. Eduard Salvador-Solé, my thesis supervisor and a great advisor. It has been a great honor working with him, and this thesis would have not been possible without his support and insights. I would also like to thank Dr. Alberto Manrique for his help and the great advice he has given me during all these years. I am also really grateful to all the people at the Astronomy Department (DAM).

I would also like to thank Dr. Ravi K. Sheth and all the people at Trieste's International Centre for Theoretical Physics. It was a really enlightening experience working there with such diverse and competent people.

Voldria, a continuació, agrair a la meva família i en especial als meus pares, per tot el suport rebut durant tots aquests anys i que han fet possible que hagi arribat fins aquí.

A la Lucía, per la paciència i el suport rebut durant tot aquest temps i per tots els moments que hem passat junts... i els que ens queden.

Al Xavier Caner, per haver estat allà durant tants anys i per totes les nits esbojarrades a la Taberna del Minotauro.

A tota la colla de "frikis" del Club de Rol de la UB, especialment al Jordi, l'Efrem, l'Alex, l'Adrià i el Daniel, per crear un espai per a desconectar ja sigui jugant a rol, fent timbes, barbacoes o discutint sobre geopolítica fent una cervesa.

Al Rubén i l'Isra, especialment per a concedir-me l'honor de ser un dels testimonis el dia de la seva boda.

A tots aquells amb qui he compartit la meva altra gran passió, la música:

- Als membres d'*Anaxenon*: Nil, Mireia, Lucía, Marcel, Jordi, Jofre, Edgar i Roque. Per moments com el famós *"Onion incident"*.
- Als membres de *Lemmings Cover Band*: Ferri, Viku, Edgar, Ona, Gabri, David i Alex. Vam arribar a fer de Garci una segona casa, ens anirem veient als escenaris amb els nostres respectius projectes!
- Als membres de *Versya*: Noelia, Jaime i Jerry. Tornar a tenir un grup amb temes que m'omplin tant ha estat una de les millors maneres de recuperar forces per a acabar aquesta tesi.

A Nerea, "Nana" para los amigos, por todas esas largas tardes de marujeos y, especialmente, por convertir las sartenes en un arma con la que repartir karma.

Al Xavier Ramírez, per tot el suport i carinyo i fondues i cotilleos i salmiakki rebut i donat durant tots aquests anys.

A Iraide, por tantos años de amistad, de componer juntos, de aguantarnos en los mejores y en los peores momentos y, por supuesto, por esas noches jugando al DDO... pero sobretodo por siempre seguir a mi lado.

I, finalment, a la Irene, per aguantar i donar-me forces en aquesta recta final... que no deixa de ser el principi d'un nou viatge.

Resum de la tesi

El major misteri que ens brinda l'Univers no és la vida, és el tamany.
Stephen King

Tractament Analític de l'Agregació No Lineal de Matèria Fosca a través del Filtrat del Camp de Densitat Primordial

Des de l'inici dels temps, la humanitat s'ha preguntat sobre l'origen i la naturalesa del nostre Univers. Totes les religions conegudes, des de l'antiga Mesopotàmia a les presents avui en dia, han intentat respondre a preguntes com *Quin és l'origen de l'Univers?* i *De que es compòn el món que ens envolta?*. La gran majoria de filòsofs tambe han indagat en la naturalesa de l'Univers durant segles i, finalment, la cosmologia ha estat un dels camps de recerca més important dels últims temps.

La formació d'estructures a l'Univers ha estat un tema que ha desafiat als científics durants segles i, encara avui en dia, és un dels principals camps de recerca en cosmologia. La resposta més acceptada a la pregunta de com es formen les estructures a gran escala de l'Univers és que petites inhomogeneitats al camp primordial de densitat varen colapsar, després de la recombinació, degut a la seva inestabilitat gravitacional, donant lloc a les llavors de les estructures que observem avui en dia.

El descobriment de les galàxies i de l'expansió del Univers per part d'Edwin Hubble (Hubble 1929) als inicis del segle XX i, més endavant, el descobriment dels fons còsmic de microones (CMB, degut a les seves sigles en anglès)(Penzias & Wilson 1965) van fixar el marc on construir una teoria per a explicar les inestabilitats gravitacionals. Aquesta teoria es va basar en el treball de James Jeans (Jeans 1902), que ja en el segle XIX va demostsrar que si les forces de pressió en un fluid són negligibles en comparació amb l'atracció gravitatòria genereada per les seves pròpies partícules, les regions amb més densitat acabaran col·lapsant. Aquest resultat va

dur a diversos autors (Doroshkevich et al. 1967; Silk 1967, 1968; Peebles & Yu 1970; Field 1971; Weimberg 1971; Chibisov 1972) a intentar desenvolupar una teoria de la formació d'estructura a través de la inestabilitat gravitacional.

Per altra banda, tot i que la matèria fosca va ser proposada per primera vegada als anys 30 del segle passat(Zwicky 1933; Babcock 1939), no va ser fins als anys 70 que la idea de que les galàxies i els *clusters* es trobaven dins d'halos massius de matèria fosca va ser àmpliament acceptada. Aquesta acceptació va dur als primers models de formació de galàxies dincs d'halos de matèria fosca (White & Rees 1978). Des d'aleshores, el camp de la formació de galàxies ha estat extensament estudiat, tant de manera analítica com, sobretot, usant simulacions numèriques de N-cosos.

En aquesta tesi, demostrem com les propietats dels halos de matèria fosca poden ser derivades directament del camp primordial de densitat si s'usa un filtre adequat i, en aquest marc, desenvolupem el *ConflUent System of Peak trajectories* (CUSP). Aquest treball és el resultat d'un llarg procés, encetat per Manrique & Salvador-Solé (1995) i Manrique & Salvador-Solé (1996), essent més endavant reprès per Salvador-Solé et al. (2012a) i Salvador-Solé et al. (2012b). Tot i això, aquests treballs es basaven, per una banda, en el *Ansatz* de que existeix una correspondència unívoca entre pics de densistat del camp primordial i els halos i; per l'altra, també requeria que els halos creixessin de dins cap enfora (és a dir, sense alterar la seva estructura interna), punt que es basava en arguments teòrics consistents però que no havia pogut ser comprovat. Aquests inconvenients feien que el formalisme CUSP quedés incomplet i perdés bona part del seu poder predictiu.

Aquest treball completa aquest tractament analític acurat de la formació no linear d'estructura a través del filtrat del camp primordial de densitat. En primer lloc, fem un repàs al formalisme, les seves bases teòriques i expliquem com pot ser usat per a derivar les propietats típiques dels halos. A la vegada:

1. Hem demostrat l'existència d'una correspondència unívoca entre halos i pics, tot i que aquests col·lapsin de forma el·lipsoidal.

2. Hem demostrat que els halos que es formen a través de fusions i els que es formen per acreció pura tenen les mateixes propietats, que depenen de les propietats dels pics progenitors a la major escala.

3. En conseqüència, hem explicat perquè les propietats típiques dels halos depenen només de la seva massa i dels temps d'observació, independentment de si han patit una fusió, en cas d'haver-la tingut, de quan ha tingut lloc.

Un cop establert el formalisme CUSP i demostrats els punts en els quals es basa, hem procedit a usar-lo per tal d'estudiar el creixement dels halos. En particular:

1. Hem demostrat que els halos creixent de dins cap a fora, ingredient crucial en el desenvolupament dels formalisme CUSP.

2. Hem establert unes relacions analítiques per a les relacions massa-concentració-forma dels ajustos NFW i Einasto, vàlides per a tots els *redshifts* i masses rellevants.

3. Hem comprovat els dominis de validesa, tant en massa com en *redshift*, de les relacions mencionades en el punt anterior.

Finalment, també hem aplicat al CUSP per a estudiar les funcions de massa i multiplicitat, i la seva dependència en la definició de massa feta servir. En particular:

1. Hem demostrat que l' algoritme de busqueda d'halos FoF(0.2) (molt usat en simulacions numèriques) és equivalent a la definició SO(Δ_{vir}), habitualment usada en tractaments analítics de la formació i evolució dels halos de matèria fosca. Conseqüentment, hem pogut explicar el perquè la distància 0.2 de l'algoritme FoF sembla ser una definició privilegiada.

2. Hem demostrat el motiu pel qual els radis virials dels halos són propers als halos *top-hat* descrits pel model de col·lapse esfèric i perquè la funció de mases dels halos té una forma tant similar a la de Press-Schechter.

3. Hem explicat perquè la funció de multiplicitat dels halos és pràcticament universal ens els dos casos equivalents descrits més amunt.

Tot i no haver-se inclòs en aquesta tesi, el formalisme CUSP també es ppot aplicar en l'estudi acurat de la subestructura dels halos, treball que ara mateix s'està efectuant. Altres camps on el formalisme CUSP podria ser aplicat per tal d'estudiar-los són

- La dispersió de les propietats dels halos.
- L'*assembly bias* dels halos.
- La correlació espacial entre halos de diferents masses.
- La formació d'estructures en forma de filament a grans escales.

- Les propietats dels fluxos i esferoides estel·lars que es troben al centre dels halos de matèria fosca.

Així doncs, amb aquesta tesi completem l'estudi purament analític dels halos de matèria fosca, trobant de forma rigurosa i autoconsistent les seves propietats. Donem una resposta analítica a un problema normalment estudiat a través de simulacions numèriques i, a la vegada, expliquem el perqué dels resultats trobats en les citades simulacions.

Contents

If I were not a physicist, I would probably be a musician.
I often think in music. I live my daydreams in music.
I see my life in terms of music.
Albert Einstein

1
Introduction

The greatest mystery the Universe offers is not life, but size.
Stephen King

Since the dawn of time, humanity has wondered about the origin and nature of our Universe. All known religions, from ancient Mesopotamia to the present day, include their own explanations to questions such as *what is the origin of the Universe?* and *what is it made of?* Most philosophers also worked on the nature of the Universe through the centuries and, finally, Cosmology has been one of the major scientific topics for the last centuries.

Structure formation in the Universe is a subject that challenged scientists for centuries and is still one of the main research fields of modern Cosmology. The most widely accepted answer to this issue is that small inhomogeneities in the primordial density field grew and collapsed, after the time of matter-radiation equality, via gravitational instability to give rise to the structures we observe today.

Afer the discovery of galaxies and the expansion of the Universe by Edwin Hubble (Hubble 1929) at the beginning of the 20th century and the discovery of the Cosmic Microwave Background (CMB) (Penzias & Wilson 1965), the framework for a gravitational instability theory was set. This theory was based on the work by James Jeans (Jeans 1902) who, in the 19th century, showed that if the pressure forces of a homogeneous fluid are negligible compared to the self-gravitational attraction generated by its particles, overdense regions will collapse into gravitationally

bound objects. This brought several authors (Doroshkevich et al. 1967; Silk 1967, 1968; Peebles & Yu 1970; Field 1971; Weimberg 1971; Chibisov 1972) to attempt the derivation of a theory of structure formation through grativational instability in the cosmological framework.

Although dark matter was first proposed in the 1930's (Zwicky 1933; Babcock 1939), it was not until the 1970's that the idea that galaxies and clusters are embedded in massive dark matter halos was widely accepted. This led to the first models of galaxy formation in dark matter halos (White & Rees 1978). Since then, the issue of galaxy formation has been extensively studied, approached both by analytical models and, specially, by N-body numerical simulations.

In this Thesis, we show how the properties of dark matter halos can be directly derived from the proper filtering of the primordial density field. This work is the result of a long process, started by Manrique & Salvador-Solé (1995) and Manrique & Salvador-Solé (1996), retaken by Salvador-Solé et al. (2012a) and Salvador-Solé et al. (2012b). However, those works relied, on the one hand, on the *Ansatz* that there is a one-to-one correspondence between peaks and halos and, in the other hand, on the condition that halos grow in an inside-out fashion, based on simple theoretical arguments but not checked against simulations.

In the present Thesis we complete the formalism, proving the existence of a one-to-one correspondence between halos and primordial denstiy peaks and confirming the inside-out growth of halos. The formalism has also been applied to better characterise halo growth, as well as the halo mass and multiplicity functions.

The structure of the Thesis is as follows. In Chapter 2 we review the basics of dark matter structure formation theory. In Chapter 3 we give an overview of the CUSP formalism and its application to the derivation of halo properties. In Chapter 4 we study how halo density profiles evolve with time and present some useful analytical fits to their typical density properties. In Chapter 5 we study the link between halo mass definitions and halo mass and multiplicity functions. Finally, in Chapter 6 we present the conclusions of this work and mention some possible developments of the CUSP formalism to the study and better understanding of structure formation in our Universe.

2

Structure Formation - Theory

I want to see gamma rays, I want to hear X-rays...
and I want to smell dark matter.
Brother Cavil

In this Chapter we give an overview of several approaches followed in the analytic study of the evolution of primordial dark matter density perturbations. In §2.1 we explain the linear theory for small fluctuations. In §2.2 we study the nonlinear regime. In §2.3 we review the spherical collapse model and its application to the study of collapsed objects through the excursion set formalism. Finally, in §2.5 we introduce the peak theory on which the CUSP formalism is based.

2.1 Linear Regime

As mentioned, dark matter structure forms from small inhomogeneites of the primordial density field. Therefore, it is convinient to define the mass density contrast δ, as the departure from the mean density around a point $\mathbf{x}$

$$\delta(\mathbf{x}, t) \equiv \frac{\rho(\mathbf{x}, t) - \bar{\rho}(t)}{\bar{\rho}(t)}\,, \tag{2.1}$$

being $\bar{\rho}(t)$ the mean background density at a given time t. Using comoving spatial coordinates, the matter density field at a point $\mathbf{x}$ given time t is:

$$\rho(\mathbf{x},t) = \bar{\rho}(t)[1+\delta(\mathbf{x},t)]\,. \tag{2.2}$$

In order to use the linear approximation, we must assume that perturbations are small, meaning that $\delta << 1$, and that their size is smaller than the horizon scale[1] $r \ll r_H \sim c/H$ (Lifshitz 1946). Under these circumstances, the gravitational potential is weak enough to allow us to treat the gravitational unstability in a non-relativistic way, using Newtonian mechanics.

If the mean free path between collisions of a particle is also small, matter can be treated as an ideal fluid which satisfies both the mass conservation equation

$$\left(\frac{\partial\rho}{\partial t}\right)_{\mathbf{r}} + \nabla_{\mathbf{r}}\cdot(\rho\mathbf{u}) = 0\,, \tag{2.3}$$

and the Euler equation of motion

$$\left(\frac{\partial\mathbf{u}}{\partial t}\right)_{\mathbf{r}} + (\mathbf{u}\cdot\nabla_{\mathbf{r}}\mathbf{u})\mathbf{u} = -\nabla_{\mathbf{r}}\Phi - \frac{1}{\rho}\nabla_{\mathbf{r}}P\,, \tag{2.4}$$

where Φ is the gravitational potential that verifies Poisson's equation

$$\nabla^2_{\mathbf{r}}\Phi = 4\pi G\rho\,. \tag{2.5}$$

where $\mathbf{r}$ and $\mathbf{u}$ are, respectively, the position and velocity of a fluid element measured in an inertial frame.

Given that the Universe is expanding, it is better suited to use the comoving coordinates $\mathbf{x} = \mathbf{r}/a(t)$, where is the cosmic scale factor, instead of an inertial coordinate system. In this new reference frame the velocity field can be written as

$$\mathbf{u} = \dot{a}\mathbf{x} + \mathbf{v}(\mathbf{x},t)\,, \tag{2.6}$$

where the first term on the right hand side is the Hubble flow due to the expansion of the Universe, $H\mathbf{r} = \dot{a}\mathbf{x}$, and the last one is the peculiar velocity relative to the velocity imprinted by the general expansion, $\mathbf{v}(\mathbf{x},t) = a\dot{\mathbf{x}}$.

We will use ϕ to denote the perturbations of the gravitational potential Φ due to the inhomogeinities in the matter distribution.

[1]The largest structure known in the Universe, the "*el Gordo*" cluster, is over 400kpc (Menanteau et al. 2012), about one order of magnitude smaller than the Horizon scale.

After changing the position variables to comoving coordinates, the time derivative at a fixed $\mathbf{r}$ and the gradient along the same direction at a fixed t have respectively the form

$$\left(\frac{\partial}{\partial t}\right)_{\mathbf{r}} = \left(\frac{\partial}{\partial t}\right)_{\mathbf{x}} - \frac{\dot{a}}{a}\,\mathbf{x}\cdot\nabla_{\mathbf{x}} \tag{2.7}$$

$$\nabla_{\mathbf{r}} = \frac{1}{a}\,\nabla_{\mathbf{x}}\,. \tag{2.8}$$

We can apply these transformations to equations (2.3)–(2.5) and after some algebra, we are led to the analog equations, but in the comoving frame and expressed in terms of the density contrast δ, the peculiar velocity v and the perturbed part of the gravitational potential ϕ

$$\frac{\partial\rho}{\partial t} + 3\,\frac{\dot{a}}{a}\,\rho + \frac{1}{a}\,\nabla_{\mathbf{x}}(\rho\mathbf{v}) = 0\,, \tag{2.9}$$

$$\frac{\partial(a\mathbf{v})}{\partial t} + (\mathbf{v}\cdot\nabla_{\mathbf{x}})\,\mathbf{v} = -\frac{1}{\rho}\,\nabla_{\mathbf{x}}P - \nabla_{\mathbf{x}}\phi\,, \tag{2.10}$$

$$\nabla^2_{\mathbf{x}}\phi = 4\pi G a^2(\rho-\bar{\rho}) = 4\pi G a^2\bar{\rho}\,\delta\,. \tag{2.11}$$

In linear perturbation theory, we can compute δ and $\mathbf{v}$ by considering only small amplitude perturbations in the mass density, which leads to small streaming motions and small values of the perturbed gravitational potential ϕ. This is equivalent to expanding perturbatively the density field, the velocity field and the gravitational potential in equations (2.3)–(2.5), then cut at first order this expansion, and work out the equations containing only those first order terms. These operations will lead to the following linearised expressions for the continuity, Euler and Poisson equations, respectively

$$\frac{\partial\delta}{\partial t} + \frac{1}{a}\,\nabla_{\mathbf{x}}\cdot\mathbf{v} = 0\,, \tag{2.12}$$

$$\frac{\partial\mathbf{v}}{\partial t} + \frac{\dot{a}}{a}\,\mathbf{v} + \frac{1}{a}\,\nabla_{\mathbf{x}}\phi = -\frac{1}{\rho a}\nabla_{\mathbf{x}}P\,, \tag{2.13}$$

$$\nabla^2_{\mathbf{x}}\phi = 4\pi G a^2\bar{\rho}\,\delta\,, \tag{2.14}$$

Given that in the early epochs of the Universe density fluctuations are still small, (2.12)-(2.14) provide an excellent description of their evolution. Furthermore, the linear regime is also a good approximation on large scales for an approximately

homogeneous mass distribution in a hierarchical scenario. In this case, large-scale fluctuations evolve linearly ($\delta < 1$) even if at smaller scales they already were in a highly nonlinear regime ($\delta \gg 1$).

2.1.1 Pressureless Fluids

Let us consider an expanding ideal fluid with negligible pressure, for instance, the Universe in the matter dominated era. In this case, the linearised equations describe the evolution of small density perturbations under the exclusive action of gravity. Therefore, we will obtain a secon-order differential equation for the time evolution of a given density contrast by removing the peculiar velocity from equation (2.12) and (2.13).

$$\ddot{\delta} + 2\,\frac{\dot{a}}{a}\,\dot{\delta} - 4\pi G\bar{\rho}\,\delta = 0\,. \tag{2.15}$$

Perturbation Growth in an Einstein-de Sitter universe

In the classic and well-known Einstein-de Sitter model, which assumes a critical Universe without dark energy or cosmological constant (i.e. $\Lambda = 0$, $\Omega = 1$), the scale factor increases as $a(t) \propto t^{2/3}$, and, therefore, the background density decreases as $\bar{\rho}(t) \equiv \rho_{cr} \propto t^{-2}$. In this framework, equation (2.15) takes the form:

$$\ddot{\delta} + \frac{4}{3t}\,\dot{\delta} - \frac{2}{3t^2}\,\delta = 0\,. \tag{2.16}$$

This second-order differential equation admits two solutions: the first one proportional to $t^{2/3}$ ($\propto a$), known as "growing mode", and the second one, proportional to t^{-1}, known as "decaying mode". For those perturbations with amplitude $\delta = \delta_i$ at an initial time t_i that begin to grow from rest [i.e. $\dot{\delta}(t_i) = 0$], the solution is a linear combination of both modes

$$\delta(t) = \delta_i \left[\frac{3}{5}\left(\frac{t}{t_i}\right)^{2/3} + \frac{2}{5}\left(\frac{t}{t_i}\right)^{-1}\right], \tag{2.17}$$

From this equation it is clear that the growing mode contributes 60% to the density contrast at the initial time, whereas the decaying mode contributes only with a 40%. Due to the monotonical amplitude decrement as time proceeds, the decaying mode will go to zero asymptotically. As it does not actually play any relevant role in structure formation, from now one we will deal only with the growing mode.

Perturbation Growth in Open and Closed Models

Let us now derive the growing solution in a general cosmological model following the development by Sahni & Coles (1995). Defining D_+ as the growin mode and D_- as the decaying mode, we can write the the Wronskian equation (2.15) as

$$W(t) = \dot{D}_+ D_- - \dot{D}_- D_+ \tag{2.18}$$

is proportional to a^{-2}. Once the decaying mode is known, and given the previous relation between those two modes, a differential equation for the growing mode can be found. Taking into account the Wronskian definition, we can write

$$\frac{W(t)}{D_-^2(t)} = \frac{\mathrm{d}}{\mathrm{d}t}\left(\frac{D_+(t)}{D_-(t)}\right) . \tag{2.19}$$

Isolating $D_+(t)$ and integrating over t we have

$$\begin{aligned} D_+(t) &= D_-(t)\int^t W(t')D_-^{-2}(t')\mathrm{d}t' = H(t)\int^t \frac{\mathrm{d}t'}{a^2(t')H^2(t')}, \\ D_+(a) &= H(a)\int^a \frac{\mathrm{d}a}{(Ha)^3} . \end{aligned} \tag{2.20}$$

In order to compute this integrals, it is preferable to use the redshift z instead of the scale factor as the integration variable. We can write the relation between both variables and the expression for $H(z)$ as

$$\begin{aligned} a(z) &= a_0\,(1+z)^{-1} , \\ H(z) &= H_0\,(1+z)\,(1+\Omega_0 z)^{1/2} , \end{aligned} \tag{2.21}$$

where a_0, H_0 and Ω_0 are the present time scale factor (usually taken as 1), Hubble parameter and total density parameter, respectively. Taking all these relations into account, equation (2.20) can be writen as

$$D_+(z) = (a_0 H_0)^{-2}(1+z)(1+\Omega_0 z)^{1/2}\int_z^\infty \frac{\mathrm{d}z'}{(1+z')^2(1+\Omega_0 z')^{3/2}} . \tag{2.22}$$

This integral has an analytical solution that leads to

$$D_+(z) = \frac{1 + 2\,\Omega_0 + 3\,\Omega_0 z}{|1 - \Omega_0|^2} + 3\,\Omega_0 \frac{(1+z)(1+\Omega_0 z)^{1/2}}{|1-\Omega_0|^{5/2}}\, f(\Omega_0, z)\,, \tag{2.23}$$

where $f(\Omega_0, z)$ can be written as

$$\begin{aligned} f(\Omega_0, z) &= -\frac{1}{2}\log\left[\frac{(1+\Omega_0 z)^{1/2} + (1-\Omega_0)^{1/2}}{(1+\Omega_0 z)^{1/2} - (1-\Omega_0)^{1/2}}\right]\,, \\ f(\Omega_0, z) &= \arctan\left[\frac{1+\Omega_0 z}{\Omega_0 - 1}\right]^{1/2}\,, \end{aligned} \tag{2.24}$$

for the cases $\Omega_0 < 1$ and $\Omega_0 > 1$, respectively. In the simpler case where $\Omega_0 = 1$, we have

$$D_+(z) \propto\ (1+z)^{-1}\,. \tag{2.25}$$

Perturbation Growth in Models with Cosmological Constant

To study models with a cosmological constant, we will follow the same strategy as in the previous case, but taking into account that the dynamics of the Universe are affected by the presence of a cosmological constant Λ. Like we have seen before, the decaying mode is proportional to $H(a)$, and the growing mode is given by equation (2.20). Let us consider a spatially flat universe ($\Omega_0 + \Omega_\Lambda = 1$). In this kind of universe, the Hubble parameter can be written as

$$H(a) \propto a^{-3/2}\left(1 + \frac{\Omega_0}{\Omega_\Lambda}\, a^3\right)^{1/2}\,, \tag{2.26}$$

and the integration of equation (2.20) leads to

$$D_+(a) = C\,\frac{5}{6}\,\mathcal{B}_x\left(\frac{5}{6}, \frac{2}{3}\right)\,\left(\frac{\Omega_0}{\Omega_\Lambda}\right)^{1/3}\left[1 + \frac{\Omega_0}{\Omega_\Lambda a^3}\right]^{1/2}\,, \tag{2.27}$$

where

$$x = \frac{\Omega_\Lambda a^3}{\Omega_0 + \Omega_\Lambda a^3}\,, \tag{2.28}$$

C is an arbitrary constant, and $\mathcal{B}_x(\alpha, \beta)$ is the incomplete Beta function.

In models including a cosmological constant, the expansion rate passes through two distinct stages. As the density of matter decreases ($\rho_m \propto a^{-3}$) the expansion rate growth experiences a deceleration, which leads to an almost constant scale factor with time when the repulsive force, driven by the cosmological constant, and the gravitational attraction, driven by matter, cancel out. During this epoch density perturbations grow increasingly faster approaching the exponential Jeans rate, characteristic of a non-expanding universe. At later times, when the dynamics are completely dominated by the cosmological constant, the scale factor begins to grow again and tends to the value $a(t) = \exp(\sqrt{\Lambda/3}\, t)$. This acceleration in the expansion rate of the Universe keeps the perturbation amplitude from growing. From equation (2.27), we can see that the growing mode becomes constant for $z \ll z_\Lambda = (\Omega_\Lambda/\Omega_0)^{1/3} - 1$.

Perturbation Growth in Models with Two Components

Let us now consider the universe filled with pressureless matter, contributing with ρ_m to the total density ρ_{tot}, and radiation, contributing with ρ_r. We also consider a flat universe, and assume that the radiation component is not perturbed[2], the resulting equations are

$$\begin{aligned} &\ddot{\delta} + 2\left(\frac{\dot{a}}{a}\right)\dot{\delta} - 4\pi G\bar{\rho}\,\delta = 0\,, \\ &\left(\frac{\dot{a}}{a}\right)^2 = \frac{8\pi G}{3}(\rho_m + \rho_r) = \frac{8\pi G}{3}\rho_{tot}\,. \end{aligned} \tag{2.29}$$

If we now change the time variable to $\tau = \rho_m/\rho_r \propto a(t)$, the second-order differential equation can be rewritten as

$$\frac{\mathrm{d}^2\delta}{\mathrm{d}\tau^2} + \frac{(2+3\tau)}{2\tau(1+\tau)}\frac{\mathrm{d}\delta}{\mathrm{d}\tau} - \frac{3}{2\tau(1+\tau)}\,\delta = 0\,. \tag{2.30}$$

The growing solution of this equation is $D_+(\tau) \propto 1 + 3\tau/2$. We can see that for $\tau \ll 1$ the growing mode is a constant, so fluctuations do not grow. This behaviouris a consequence of radiation dominating the dynamics of the universe at early times, causing the scale factor to evolve as $t^{1/2}$. As time goes on, the contribution of radiation to the total energy density diminishes rapidly, with matter taking its place as the dominant component, allowing for density inhomogeneities

[2]Primordial adiabatic perturbations do affect radiation as well as matter. However, this simplification leads to a correct qualitative result

to grow. Since,during the matter dominated era, the scale factor increases as $t^{2/3}$, it is clear that the expansion rate will experience an acceleration throughout the transition. Therefore, the growth of density perturbations is suppressed as long as $\rho_r \gg \rho_m$.

The Peculiar Velocity

To see how perturbations in the Hubble flow evolve with time, we have to consider the linearised continuity equation with $P = 0$, Poisson's equation and the solution of the second-order differential equation describing the density contrast growth. Since the growing mode dominates the general solution of equation (2.15), we can write $\delta(\mathbf{x}, t) \equiv \delta(\mathbf{x})D_+(t)$. Substituting this result in the linearised mass conservation equation [eq. (2.12)] we see that the relation between density and velocity is

$$\nabla_{\mathbf{x}} \cdot \mathbf{v} = -a \frac{\partial \delta}{\partial t} = -a\,\delta \frac{\dot{D_+}}{D_+} = -a\,\delta H f\,, \tag{2.31}$$

where the dimensionless velocity factor is

$$f = \frac{a}{\dot{a}}\frac{\dot{D_+}}{D_+} = \frac{1}{H}\frac{\dot{D_+}}{D_+} = \frac{\mathrm{d}\log\delta}{\mathrm{d}\log a} \simeq \Omega_0^{0.6} + \frac{\Omega_\Lambda}{70}\left(\Lambda + \frac{\Omega_0}{2}\right)\,. \tag{2.32}$$

In order to isolate the density contrast, we use Poisson's equation, and equation (2.31) yields

$$\nabla_{\mathbf{x}} \cdot \mathbf{v} = -\nabla_{\mathbf{x}} \cdot \left(\frac{Hf}{4\pi G a}\nabla_{\mathbf{x}}\phi\right)\,, \tag{2.33}$$

which, after integration, leads to

$$\mathbf{v} = -\frac{2f}{3\Omega H a}\nabla_{\mathbf{x}}\phi + \frac{\mathrm{const}}{a(t)}\,. \tag{2.34}$$

These linearised equations show that the peculiar velocity field associated with the growing mode can be expressed in terms of a velocity potential exclusively (i.e., the peculiar velocity field is irrotational) $\mathbf{v} = -\nabla_{\mathbf{x}}\phi_v/a$. In this case we can write

$$\phi_v = \frac{2\,f}{3\Omega H}\phi\,. \tag{2.35}$$

This interesting property of the velocity field has been applied to several cosmological topics, such as some analytical approximations to the non-linear regime (Zel'dovich 1970) or reconstruction techniques used to obtain the density field by measuring the peculiar motions of galaxies relative to the cosmological frame defined

by the microwave background (Bertschinger & Dekel 1989; Dekel et al. 1990, 1993), assuming that galaxies trace the velocity field.

The presence of gravitational forces causes an acceleration field of magnitude $\mathbf{g} = -\nabla_{\mathbf{x}}\phi/a$. Taking equation (2.34) and setting the integration constant equal to zero, we get

$$\mathbf{v} = \frac{2\,f}{3\Omega H}\,\mathbf{g}\,. \tag{2.36}$$

It is clear from this equation that the peculiar velocity is parallel to the acceleration. In an Einstein-de Sitter model, with negligible cosmological constant and density parameter equal to unity, we would have $f = 1$ and $H = 3/2\,t^{-1}$. In this case the peculiar velocity field would adopt the simple form $\mathbf{v} = \mathbf{g}\,t$. In the absence of a gravitational field ($\phi = 0$), the linearised Euler equation for pressureless fluids can be written as

$$\frac{\partial \mathbf{v}}{\partial t} + \frac{\dot{a}}{a}\,\mathbf{v} = \frac{1}{a}\frac{\partial (a\mathbf{v})}{\partial t} = 0\,, \tag{2.37}$$

and any initial peculiar velocity decays as $a^{-1}(t)$.

2.1.2 Pressure Effects

So far we have only considered simple models assuming a pressureless fluid. However, at some scales and at given epochs, pressure cannot be simply neglected. Therefore, we will study what happens on those scales when pressure is introduced in the linearised equations. Assuming pressure is only a function of density, making use of equation (2.2) and remembering that the "sound speed" is defined as $c_s = (dP/d\rho)^{1/2}$, the pressure force in an expanding fluid can be written as

$$\mathbf{F} = -\frac{1}{a}\,\nabla_{\mathbf{x}} P = -\frac{\mathrm{d}P}{\mathrm{d}\rho}\frac{\nabla_{\mathbf{x}}\rho}{a} = -c_s^2\,\bar{\rho}\,\frac{\nabla_{\mathbf{x}}\delta}{a}\,. \tag{2.38}$$

Going back to the linearised equations, substituting the former result in the Euler equation (2.13) leads to

$$\frac{\partial \mathbf{v}}{\partial t} + \frac{\dot{a}}{a}\,\mathbf{v} + \frac{1}{a}\,\nabla_{\mathbf{x}}\phi = -\frac{c_s^2}{a}\,\nabla_{\mathbf{x}}\,\delta\,. \tag{2.39}$$

Following the same steps as in the pressureless case, we get to the perturbation equation

$$\frac{\partial^2\delta}{\partial t^2} + 2\,\frac{\dot{a}}{a}\frac{\partial\delta}{\partial t} - \left(\frac{c_s}{a}\right)^2 \nabla_{\mathbf{x}}{}^2\delta - 4\pi G\bar{\rho}\delta = 0\,. \tag{2.40}$$

It is convenient to expand the density contrast in Fourier series

$$\delta = \sum_k \delta_k \exp(-i\mathbf{k}\cdot\mathbf{x})\,, \tag{2.41}$$

where $k \equiv |\mathbf{k}| = 2\pi a/\lambda$ is the comoving wavenumber. All the coefficients in equation (2.41) are independent from $\mathbf{x}$, therefore the amplitude $\delta_k(t)$ associated with the wavenumber k satisfies the second-order differential equation

$$\ddot{\delta}_k + 2H\dot{\delta}_k + \omega_k^2\delta_k = 0\,. \tag{2.42}$$

This is the well known damped oscillator equation with a damping factor equal to $2H$ and a proper frequency

$$\omega_k^2 = \left(\frac{kc_s}{a}\right)^2 - 4\pi G\rho\,. \tag{2.43}$$

According to equation (2.42), density perturbations are damped due to the expansion of the universe as long as the frequency ω_k^2 is positive. When it becomes negative, we have to abandon the damped oscillator interpretation and reconsider the solutions for a pressureless fluid. The limiting case is given by the condition $\omega_k^2 = 0$, which defines the so-called *Jeans length*

$$\lambda_J = c_s\left(\frac{\pi}{G\rho}\right)^{1/2}\,. \tag{2.44}$$

At scales larger than the Jeans length, $\lambda > \lambda_J$, perturbations do not feel the influence of pressure and grow just like they do in a pressureless fluid, whereas on smaller scales, $\lambda < \lambda_J$, pressure gradients force perturbations to oscillate as acoustic waves with steadily decreasing amplitude. This behaviour can also be discussed in terms of characteristic times. From equation (2.44) we see that, for perturbations of a scale equal to the Jeans length, the characteristic time of gravitational growth ($\sim \sqrt{G\bar{\rho}}$) is comparable to the crossing time of pressure waves ($\sim \lambda_J/c_s$). On scales larger than that, the crossing time is longer than the gravitational growth time for the density contrast. Therefore, pressure effects can be neglected. On scales smaller than the Jeans scale, the opposite is true, and the density contrast behaves as a damped oscillator.

From equation (2.44), it can be seen that the Jeans length is extremely sensitive to the sound speed within the fluid. On the radiation dominated era, electrons are tightly coupled to radiation via Thomson scattering, in such a way that we are

allowed to consider the mixture as a single fluid with an adiabatic speed of sound

$$c_s = \frac{1}{\sqrt{3}} \left(\frac{3\rho_m}{4\rho_r} + 1 \right)^{-1/2} . \tag{2.45}$$

Taking into account that $\rho_r \gg \rho_m$ and $\rho_r \propto t^{-2}$, it can be seen that the Jeans length is proportional to t. Said otherwise, during the radiation dominated era the Jeans length scales with the cosmological horizon. During recombination, the coupling between electrons and radiation breaks down, and pressure becomes supported by neutral hydrogen atoms instead of radiation. This change in the physical properties of the fluid causes an abrupt decrease in the value of the sound speed. If the mass associated with the Jeans length at recombination is $M_J \simeq 9 \times 10^{16} (\Omega h^2)^{-2} M_\odot$ (of the same order than that of superclusters of galaxies), the corresponding value after recombination drops to $M_J \simeq 1.3 \times 10^5 (\Omega h^2)^{-\frac{1}{2}} M_\odot$, which is comparable to the mass of a globular cluster

Another phenomenon, known as Silk damping, begins to play a relevant role on the evolution of baryonic density perturbations just before recombination. As recombination approaches, the mean free path of photons increases due to the progressive weakening of the coupling between matter and radiation. As a result, photons are able to escape from the potential wells created by overdensities, and carry with them still tightly coupled electrons. This free-streaming causes an effective damping of perturbations in the photon-baryon mixture on scales smaller than a characteristic length known as the Silk length. The associated Silk mass at recombination is $M_s \simeq 1.3 \times 10^{12} (\Omega h^2)^{-3/2} M_\odot$ similar to that of a galaxy.

Although pure baryonic models are simpler than multicomponent models, they suffer a number of problems, such as the difficulty of reconciling the predictions based on primordial nucleosynthesys and not being able to predict the CMB temperature fluctuations in the detected range. On the other hand, non-baryonic dark matter is not coupled to radiation after the epoch of matter-radiation equality, so it is not subject to this kind of collisional damping. However, given that dark matter is free-streaming, particles may travel through regions of high density into regions of low density, and vice versa. If the dark matter particles are relativistic, the phase mixing caused by this free-streaming movement may be efficient enough to wash out all the fluctuations on scales smaller than the free-streaming distance (i.e., the mean distance a particle travels until its momentum becomes non-relativistic). While important in Hot Dark Matter (HDM) models, in Cold Dark Matter (CDM) models the free-streaming cut-off scale is too small to be relevant, either because non-

baryonic particles are very massive (e.g., gravitinos) or because they were created out of thermal equilibrium (e.g. axions). This is enough to rule out pure HDM models in favour of CDM ones, as the cut-off power spectrum of the first ones fails to predict the formation of objects at galactic scales.

2.2 Nonlinear Regime

As the amplitude of a fluctuation approaches unity at a given scale, the spatial Fourier modes [eq. (2.41)] begin to couple and the and the linear approximation is no longer valid. The perturbation starts to evolve in the nonlinear regime, with no known exact treatment. Therefore, some kind of approximation is needed in order to be able to follow the collapse of density perturbations and the formation of nonlinear structures. One possible approach is to derive some quantity using linear theory and extrapolate the result to the nonlinear regime, as in the case of the Zel'dovich approximation. Another possibility is to make some assumptions on the collapse process (e.g., self-similarity). In either case the direct comparison with numerical simulations has proven to be a necessary test of the validity of these assumptions that, most of the times, are not fully physically justified.

2.2.1 Mildly Nonlinear Regime: the Zel'dovich Approximation

Given that the density contrast is still close enough to the linear regime ($\delta \lesssim 1$), Zel'dovich (1970) proposed an elegant solution to follow the evolution of density fluctuations in a mildly nonlinear regime (for an extensive review of the Zel'dovich approximation see also Shandarin & Zel'dovich 1989).

In this approach, perturbations are considered to grow in an expanding Friedmann universe filled with dust (pressure-free matter) in the Newtonian approximation. Only growing perturbation are considered, thus, from equation (2.17), $\delta(\mathbf{x}, t) = \delta(\mathbf{x})D_+(t)$. If the initial (unperturbed) Lagrangian coordinates of a dust particle are described by $\mathbf{q}$, then its trajectory in linear theory (i.e., its Eulerian coordinates $\mathbf{x}$ at time t) is given by

$$\mathbf{r}(\mathbf{q}, t) = a(t)\mathbf{x}(\mathbf{q}, t) = a(t)[\mathbf{q} + D_+(t)\,\mathbf{u}(\mathbf{q})]\,. \tag{2.46}$$

The term $\mathbf{u}(\mathbf{q})$ is the initial velocity field of the particle and its related to the linear velocity potential, which is proportional to the Newtonian gravitational potential

[eq. (2.35)], according to

$$\mathbf{u}(\mathbf{q}) = -\nabla_{\mathbf{x}}\phi_v(\mathbf{q})/a\,. \tag{2.47}$$

This implies that the initial velocity flow is irrotational (see §2.1.1), which is generally true since expansion would damp any rotations potentially present at the initial time.

The approximation proposed by Zel'dovich consists in extrapolating equation (2.46), valid in the linear regime ($\delta \ll 1$), into the region where the density contrast is not so small ($\delta \lesssim 1$).

Equation (2.46) is formally analogous to the equation of motion of a particle moving with constant velocity $\mathbf{u}$,

$$\mathbf{x} = \mathbf{q} + \tau\mathbf{u}(\mathbf{q})\,, \tag{2.48}$$

except for the presence of the $a(t)$ term accounting for the cosmic expansion and of the $D_+(t)$ term accounting for the presence of gravity. Taking this into account, note that a typical feature of inertial motion given random initial condition is that particles intersect trajectories, which leads to the formation of singularities in the density field. A similar effect is also encountered by the Zel'dovich approximation by requiring the conservation of the mass

$$\rho(\mathbf{r},t)\mathrm{d}\mathbf{r} = \rho_0\mathrm{d}\mathbf{q}\,, \tag{2.49}$$

where ρ_0 is the density at the initial time. Defining the deformation tensor as

$$\mathcal{D}_{ij} = \frac{\partial r_i}{\partial q_j} = a(t)\,\delta_{ij} + D_+(t)\,\frac{\partial u_i}{\partial q_j}\,, \tag{2.50}$$

we can choose the eigensystem formed by its eigenvectors as a basis and diagonalise it, so that the density field is given by

$$\rho(\mathbf{r},t) = \frac{\bar{\rho}}{[1 - D_+(t)\,\alpha(\mathbf{q})][1 - D_+(t)\,\beta(\mathbf{q})][1 - D_+(t)\,\gamma(\mathbf{q})]}\,, \tag{2.51}$$

where $\bar{\rho} = \rho_0/a^3$ is the mean density at time t, and $-\alpha$, $-\beta$ and $-\gamma$ are the eigenvalues of the tensor of deformation.

In the linear regime, $|D_+\,\alpha| \ll 1$, $|D_+\,\beta| \ll 1$ and $|D_+\,\gamma| \ll 1$, therefore equation (2.51) is simplified to

$$\rho(\mathbf{r}, t) \approx \bar{\rho}\,[1 + D_+(t)(\alpha + \beta + \gamma)]\,, \tag{2.52}$$

or equivalently

$$\delta \approx D_+(t)(\alpha + \beta + \gamma)\,. \tag{2.53}$$

Therefore, at the linear stage, the spatial structure of the density distribution is given by the trace of the deformation tensor.

As $D_+(t)$ grows with time, we will reach a moment when a singularity appears in equation (2.51) causing the density to become formally infinite in a region where at least one of the eigenvalues is positive. Specifically, if the eigenvalues are ordered in such a way that $\alpha \geq \beta \geq \gamma$, then the first singularity will occur when α attains its maximum positive value, α_{max} , at the time $t_{max} = 1/\alpha_{max}$, such that $D_+(t) = \alpha_{max}^{-1}$. When this happens, particle trajectories have crossed and two points with different Lagrangian coordinates may coincide at the same Eulerian coordinate, meaning that the mapping (2.46) is no longer unique. This corresponds to the collapse along the corresponding axis and the formation of a *pancake* (a flattened, sheet-like structure of quasi-two-dimensional nature). Generally, α is not equal to β or γ. However, in the improbable case that two or three eigenvalues take the same positive values, the collapse will result in a filament or a knot (point) respectively. Doroshkevich (1970) computed the probability distribution of the three eigenvalues in the case of a Gaussian random field and showed that the simultaneous vanishing of more than one of them is very unlikely. Pancakes are therefore expected to be the generic result of nonlinear gravitational clustering.

The Zel'dovich approximation describes well the evolution of density perturbations after they have left the linear regime, up to the point were some crossings in the particle trajectories occur in numerical simulations (e.g., Coles et al. 1993). After this point the collapse enters the highly nonlinear regime ($\delta > 1$) and the approximation is no longer valid.

2.2.2 Highly Nonlinear Regime

At the time of last scattering the density distribution of the Universe was almost homogeneous ($\delta\rho/\rho < 1$). As we have already seen, linear theory can only explain the evolution of density fluctuations at early epochs (or at very large scales) and the Zel'dovich approximation, while holding also at later times, ceases to be valid when the firsts crossing between particle orbits (i.e., shell-crossing) occurs. However, the

structures observed today are highly nonlinear ($\delta > 1$)[3]. Therefore, a nonlinear gravitational instability theory is needed to account for structure formation. Nevertheless, it is not possible to follow in detail the evolution of a given perturbation in such a regime; some other assumption about the characteristics of the collapse is needed.

One possible solution is to apply the Zel'dovich approximation, not to the actual density field, but to a smoother field obtained by filtering out small scale fluctuations from the initial conditions which are responsible for shell crossing, leaving only perturbations of protogalactic scale (White 1984). However, this approximations ignores the effects of shell crossing and assumes that small scale (nonlinear) fluctuations have no influence on the large scale (quasilinear) ones, which is a not physically justified assumption.

Therefore, the Zel'dovich approximation is valid on scales relevant only to clusters and superclusters, whereas for smaller scales, which rapidly become nonlinear, another approximation is needed. The only exact solution in such a nonlinear regime is provided by the spherical collapse model, which is the subject of the next Section.

2.3 The Spherical Collapse Model

The spherical collapse model assumes a universe which i sspherically symmetric about one point, filled with pressureless matter behaving as an ideal fluid. This approach was originally proposed by Peebles (1967) and extended by Gunn & Gott (1972) in the Secondary Infall context. In this approach, any tidal effect of the neighbouring structure upon the perturbation itself and any deviation from sphericity of the potential well due to the distribution of matter inside or outside the volume element whose evolution is being followed are neglected. Under these conditions, the Gauss theorem (or the Birkhoff theorem in the context of General Relativity) guarantees that the motion of a spherical mass shell depends only on the mass inside the shell's radius. This model also assumes that the perturbation initially expands according to the Hubble flow, i.e. with null initial peculiar velocity. Due to having density higher than the cosmic mean density, the overdensity will decelerate faster than the background medium because of its own gravitational pull. Eventually it will begin to collapse after reaching its maximum expansion radius, known

[3]The density contrast corresponding to a galaxy cluster is of the order of several hundreds, at least.

as "turnaround radius".

The model also assumes that the density profile of the perturbation is monotonically decreasing with increasing radius in order to avoid shell crossing and, hence, to ensure mass conservation inside evolving spherical shells. It has to be noted that this is not the case for the subsequent collapse phase which involves crosses between the infalling shells and the more internal ones that have already collapsed and are expanding again. In this phase, the system oscillates around an equilibrium state and shells mix, thereby exchanging energy. This leads to the so called "phase mixing" and "violent relaxation" mechanisms (Lynden-Bell 1967; Shu 1978; Stiavelli & Bertin 1987; Spergel & Hernquist 1992; Kull et al. 1997; Nakamura 2000; Trenti & Bertin 2005) which are responsible for the virialisation of the system.

Under these simplifying assumptions an exact analytical treatment of the nonlinear stage of gravitational instability is possible.

2.3.1 Energy Balance and Maximum Expansion Radius

Let us consider a spherical density inhomogeneity of radius R_i centered around a point $\mathbf{x}$ at an initial time t_i and containing a mass $M = \rho_b(1+\delta_i)(4/3)\pi R_i^3$, where δ_i is the initial overdensity, and ρ_b is the density of the background. For simplicity, we will assume that the shell has a flat ("top hat") density profile

$$\begin{aligned} \rho(r) &= \rho_b\,(1+\delta_i) \quad \text{for } r \le R_i, \\ \rho(r) &= \rho_b \qquad\qquad\quad \text{for } r > R_i. \end{aligned}$$

At early times the expansion of the shell is virtually indistinguishable from that of the rest of the universe, so that the velocity of the shell relative to the centre is governed by the Hubble flow $\dot{R}_i = H_i R_i$, being H_i the Hubble parameter at the initial time. Thus, the kinetic energy per unit mass at a distance R_i from the centre is $K_i = H_i^2 R_i^2/2$, and the potential energy per unit mass can be expressed as

$$U_i = -GM/R_i = -\frac{4\pi G}{3H_i^2}\rho_b(1+\delta_i)H_i^2R_i^2 = -\Omega_i K_i(1+\delta_i)\,. \tag{2.54}$$

Conservation of energy guarantees that the sum of the kinetic and potential energies is a constant. In particular, at the initial time we have

$$E = K_i + U_i = K_i\Omega_i[\Omega_i^{-1} - (1+\delta_i)]\,. \tag{2.55}$$

The requirement for a shell to be gravitationally bound is that its total energy E must be negative. In this case, the shell keeps on expanding until it reaches a maximum radius, turns around and begins to collapse. According to equation (2.55), the condition ensuring $E < 0$ is $1 + \delta_i > \Omega_i^{-1}$. Taking into account that the initial time t_i corresponds to a given redshift z, the former condition can be rewritten as

$$\delta(z) > \Omega^{-1}(z) - 1 = \frac{1 - \Omega_0}{\Omega_0(1+z)}\,. \tag{2.56}$$

For those shells that are gravitationally bound, it is straightforward to relate the maximum expansion radius to its initial values R_i, and δ_i (or, equivalently, $R(z)$ and $\delta(z)$). Owing to the monotonically decreasing density profile of the spherical perturbation, a shell with a given radius does not cross with other shells until after turnaround, so the mass contained inside the shell remains constant with time while the expansion is taking place. On the other hand, the shell velocity at turnaround is zero, $\dot{R}|_{ta} = 0$. Therefore, only potential energy contributes to the total energy at turnaround

$$E = U_{ta} = -\frac{GM}{R_{ta}} = -\frac{R_i}{R_{ta}} K_i \Omega_i (1 + \delta_i)\,. \tag{2.57}$$

Equating this equation and (2.55) due to energy conservation, we obtain the relation

$$\frac{R_{ta}}{R_i} = \frac{1+\delta_i}{\delta_i - (\Omega_i^{-1} - 1)} \equiv [1 + \delta(z)] \left[\delta(z) - \frac{1-\Omega_0}{\Omega_0(1+z)}\right]^{-1}\,. \tag{2.58}$$

Dynamics of a Mass Shell

The radius $R(t)$ of a spherical shell comprising a mass M satisfies the following equation of motion

$$\frac{\mathrm{d}R^2}{\mathrm{d}^2 t} = -\frac{GM(<R)}{R^2}\,. \tag{2.59}$$

Its first integral leads to the energy equation

$$\frac{1}{2}\left(\frac{\mathrm{d}R}{\mathrm{d}t}\right)^2 = \frac{GM}{R} + C\,, \tag{2.60}$$

where the constant of integration C is just the total energy E. Taking $E < 0$ ($E > 0$) we recover the case of a gravitationally bound (unbound) spherical shell. The solution of equations (2.59) and (2.60) can be expressed in a parametric form

$$R = A(1 - \cos\theta) \qquad t = B(\theta - \sin\theta)\,, \tag{2.61}$$

for the case of a bound shell ($E < 0$), and

$$R = A(\cosh\theta - 1) \qquad t = B(\sinh\theta - \theta)\,, \tag{2.62}$$

for the case of an unbound shell ($E > 0$). The constants A and B are not independent, but related through $A^3 = GMB^2$. As we have noted above, the dynamical evolution of a spherical mass shell is similar to that of the whole universe. In fact, the corresponding parametric solution for a closed universe is (see Peebles 1980)

$$R_b = A_b(1 - \cos\mu) \qquad t = B_b(\mu - \sin\mu)\,, \tag{2.63}$$

and for an open universe

$$R_b = A_b(\cosh\mu - 1) \qquad t = B_b(\sinh\mu - \mu)\,. \tag{2.64}$$

If we assume that $a(t) = R_b(t)$, then the spherical portion of the universe contains the same mass as the shell, and the constraint between A_b and B_b just writes $A_b^3 = GMB_b^2$.

At this point we are able to compute the density contrast in each mass shell. Since mass is conserved we get, using $M = 4\pi R^3\rho/3$ and equation (2.61),

$$\rho(t) = \frac{3M}{4\pi A^3(1 - \cos\theta)^3}\,. \tag{2.65}$$

Working on a spatially flat, matter dominated universe the background density scales as

$$\rho_b(t) = \frac{1}{6\pi G t^2} = \frac{1}{6\pi G B^2(\theta - \sin\theta)^2}\,. \tag{2.66}$$

So, from the definition of the density contrast in terms of the ratio $\rho(t)/\rho_b(t)$ [eq. (2.2)], and using equations (2.65) and (2.66), we have

$$\delta(\theta) \equiv \frac{\rho(t)}{\rho_b(t)} - 1 = \frac{9}{2}\frac{(\theta - \sin\theta)^2}{(1 - \cos\theta)^3} - 1\,, \tag{2.67}$$

for gravitationally bound density perturbations, and

$$\delta(\theta) = \frac{9}{2}\frac{(\theta - \sinh\theta)^2}{(\cosh\theta - 1)^3} - 1\,, \tag{2.68}$$

for unbound density fluctuations.

We can expresse constants A and B in terms of the maximum expansion radius and the time at which it is reached. According to equation (2.61), maximum expansion occurs for $\theta = \pi$. Then, for this specific value of the developing angle, constants A and B are

$$A = R_{ta}/2 \qquad\qquad B = t_{ta}/\pi \,. \tag{2.69}$$

However, these relations are only valid for gravitationally bound shells. If we use initial quantities instead of the "turnaround" ones, we can obtain the expressions for a more general case. This is achieved by applying equation (2.58), the constrain $A^3 = GMB^2$ and expressing the constant mass M in terms of R_i and ρ_i. The final result is

$$\begin{aligned} A &= \left(\frac{R_i}{2}\right) \frac{1+\delta_i}{\delta_i - (\Omega_i^{-1} - 1)} \,, \\ B &= \frac{1+\delta_i}{2H_i \Omega_i^{1/2} [\delta_i - (\Omega_i^{-1} - 1)]^{3/2}} \,. \end{aligned} \tag{2.70}$$

Bearing in mind that initial conditions are set in an early epoch, it is reasonable to assume $\delta_i \ll 1$. Then, in a flat cosmological model equation (2.70) becomes,

$$A \simeq \frac{R_i}{2\delta_i} \qquad\qquad B \simeq \frac{3}{4}\, t_i\, \delta_i^{-3/2} \,. \tag{2.71}$$

From equations (2.67) and (2.71) we can recover the density contrast limit for small θ (or small t):

$$\lim_{\theta \to 0} \delta(\theta) \simeq \frac{3\theta^2}{20} \simeq \frac{3}{20} \left(\frac{6\,t}{B}\right)^{2/3} = \frac{3}{5}\, \delta_i \left(\frac{t}{t_i}\right)^{2/3} \,, \tag{2.72}$$

that correspond to the linear theory growth law for a purely growing mode if the initial peculiar velocity is set to zero [see eq. (2.17)]. In view of equation (2.72) the critical condition (2.56) turns into $\delta_i > 3(\Omega_i^{-1} - 1)/5$.

Turnaround and Collapse

The spherical model provides us with a variety of relations between quantities computed at turnaround ($\theta = \pi$) and at collapse ($\theta = 2\pi$) for bound shells. Let us

consider a flat background cosmology with negligible cosmological constant. From equation (2.61), we have that *the collapse time t_{coll} is twice the turnaround time* t_{ta}. From equation (2.67), we find that $\delta(\theta = \pi) \simeq 4.6$ at the maximum expansion radius, whereas at collapse the overdensity tends to infinity due to the fact that the radius becomes zero. Exact spherical collapse breaks down as the density perturbation starts to collapse due to physical processes, such as shell crossing and rebounding, and the subsequent violent relaxation ensures that the system reaches virial equilibrium at a finite density, and, therefore $\delta_{coll} \to \infty$ is never achieved. The typical radius of the virialised perturbation can be estimated by means of energetic arguments. At the time of turnaround, only the potential energy contributes to the total energy of the spherical shell. After relaxation, the system satisfies the virial theorem, i.e., $2K = |W|$. Energy conservation leads to

$$U(R = R_{ta}) = E = U(R = R_{vir})/2\,, \tag{2.73}$$

being $U(R) = -GM/R$. Since the shell mass is conserved along the process, then *the final virial radius R_{vir} is half the turnaround radius R_{ta}*. This result assumes that the uniform density profile is preserved during the relaxation process. But virialised objects exhibit an outward-decreasing density profile instead of a flat one. In this case, the final potential energy does not take the same form that it had at the turnaround epoch, and consequently the relation $2R_{vir} = R_{ta}$ does not hold. Therefore, the following calculations should be taken only as raw estimations. Bearing in mind this warning, let us compute the typical overdensity of a virialised object $\delta_{vir} = \rho_{vir}/\bar{\rho}_{vir} - 1$ where $\bar{\rho}_{vir}$ is the background density at the epoch of virialisation. From the previous results, we know that

$$\rho_{vir} = 8\rho_{ta} = 8\bar{\rho}_{ta}(4.6 + 1)\,. \tag{2.74}$$

Taking into account that the background density scales as t^{-2}, and assuming that $t_{vir} \simeq t_{coll} \simeq 2t_{ta}$ then $\delta_{vir} = 8 \times 5.6 \times 4 - 1 = 178.2$[4]. From here, it is easy to calculate the density of the relaxed system in terms of the present mean density and the collapse redshift z_{vir}

$$\rho_{vir} \simeq 179.2(1 + z_{vir})^3\rho_0\,. \tag{2.75}$$

Sometimes it is interesting to know extrapolated values of the density contrast assuming that the perturbation always evolves in the linear regime. This is equivalent to consider the limit of equation (2.67) for small values of the developing angle

[4]This result has been used by Navarro et al. (1997) to define the virialised regions of dark matter halos. For a more accurate treatment see Bryan & Norman (1998) and Henry (2000).

θ (small t). Given that we have set initial conditions at an early epoch, the linear behaviour of the perturbation is ensured. So, the extension to any epoch of the limit (2.72), only valid for times close to the initial one, gives the wanted extrapolation. Equations (2.61) and (2.71) bring this limit to

$$\delta_L(\theta) \simeq \frac{3}{5}\left(\frac{3}{4}\right)^{2/3}(\theta - \sin\theta)^{2/3}\,. \tag{2.76}$$

In particular, $\delta_L(\pi) \simeq 1.063$ for the linear density contrast at turnaround, and $\delta_L(2\pi) \simeq 1.686$ at recollapse (Gunn & Gott 1972). In an Einstein-de Sitter universe, perturbations in the linear regime grow as the scale factor $a(z) \propto (1+z)^{-1}$. Then, known the linear density contrast of a given spherical perturbation, the corresponding true redshifts at which the perturbation reached the maximum expansion and collapsed are, respectively,

$$\begin{aligned} 1 + z_{ta} &\simeq \frac{\delta_L}{1.063} \\ 1 + z_{coll} &\simeq \frac{\delta_L}{1.686}\,. \end{aligned} \tag{2.77}$$

However, the spherical collapse model is founded on strong assumptions. As already discussed, there is no physical motivation for the assumption that the virial radius equals half the turnaround radius, and that virialisation happens at twice the turnaround time. Moreover, a spherical model is far from giving an adequate description of the collapse of protogalaxies or protoclusters, since, as proved by Lin, Mestel & Shu (1965), departures from spherical symmetry are amplified once the almost spherical density perturbation starts collapsing. During this stage the perturbation develops non-radial motions which invalidate the applicability of the spherical model. However, this phenomenon can be incorporated to the analysis by modelling the collapsing perturbation as a homogeneous ellipsoid of ideal fluid with negligible pressure. Classical studies on the motion of homogeneous spheroids, neglecting the tidal field of surrounding matter, show that collapse occurs along the minor axis at a faster rate than that of an equivalent spherical overdensity, while the other axes tend to contract or expand in finite factors, so the perturbation finally reaches a pancake configuration.

Nonetheless, this model can be successfully applied to some astrophysical problems, such as the statistical description of dark matter clustering or the growth

of individual virialised objects from the monolithic infall of matter onto an initial overdensity according to the so-called Secondary Infall (SI) model. In the following section we give an overview on the work done based on the SI model over the last decades.

2.4 The Excursion Set Formalism

The spherical collapse model, although being simple, allows us to relate linear density perturbations to relaxed objects in a straightforward (although not completely accurate) way. In the present section, we show how this simple model can be used to obtain some information on highly non-linear structures from the statistics of the linear density field. We deal with the mass function of halos, that is, the number density of relaxed objects per unit volume with mass in an infinitesimal range at a given epoch, which gives a valuable but incomplete information about the clustering history of objects.

2.4.1 Statistics of Primordial Density Fluctuations

The primordial density field $\delta(\mathbf{x}, t_i)$ can be mathematically described as a homogeneous and isotropic three-dimensional scalar Gaussian random field, as long as perturbation amplitudes remain small. There are physical and statistical arguments which support the Gaussianity assumption. The physical argument relies on inflation. According to this theory, small amplitude curvature perturbations generated by quantum fluctuations in the inflationary phase are very likely to be Gaussian. The statistical argument is based on the *central limit theorem*, which states that the superposition of a large number of independent random variables (all having the same form of distribution) gives rise to a new random variable whose probability distribution is Gaussian. We have already showed that the density field $\delta(\mathbf{x})$ can be written as an infinite sum (2.41) with coefficients δ_k, which are statistically independent in a homogeneous universe (see below) and come from the same shaped distribution. Furthermore, the phases between the different modes are supposed to be random and uniformly distributed from 0 to 2π, unless density fluctuations arise from gravitational fall into topological defects such as cosmic strings.

For statical purposes, it is convenient to express the density field in the Fourier space by using the Fourier transform (the continuous limit of the series [2.41])

$$\delta(\mathbf{x}) = \frac{1}{(2\pi)^3}\int \mathrm{d}^3\mathbf{k}\,\delta(\mathbf{k})\,e^{-i\mathbf{k}\cdot\mathbf{x}} \tag{2.78}$$

$[\delta(\mathbf{k}) \equiv \delta(\mathbf{k},t)]$, which has the inverse relation

$$\delta(\mathbf{k}) = \int \mathrm{d}^3\mathbf{x}\,\delta(\mathbf{x})\,e^{i\mathbf{k}\cdot\mathbf{x}}. \tag{2.79}$$

Notice that, in k-space, the Dirac delta function can be written in the form

$$\delta^D(\mathbf{k}) = \frac{1}{(2\pi)^3}\int \mathrm{d}^3\mathbf{x}\,e^{\pm i\mathbf{k}\cdot\mathbf{x}}\,. \tag{2.80}$$

The most relevant quantity in the statistical description of the density field is the *two-point correlation function or autocovariance function* defined as the volume average of the product of the function $\delta(\mathbf{x})$ evaluated at points $\mathbf{x}_1$ and $\mathbf{x}_2 = \mathbf{x}_1 + \mathbf{r}$ [5]

$$\langle\delta(\mathbf{x}_1)\delta(\mathbf{x}_2)\rangle = \xi(|\mathbf{x}_1 - \mathbf{x}_2|) = \xi(r)\,, \tag{2.81}$$

where we have used the fact that the field is homogeneous and isotropic (i.e., invariant under translations and rotations), which means that the covariance function only depends on the relative distance between points. Developing equation (2.81) in the k-space and taking into account that $\delta(\mathbf{x})$ is real, we have

$$\begin{aligned}\xi(r) = \langle\delta(\mathbf{x}_1)\delta(\mathbf{x}_2)\rangle &= \left\langle \int \frac{\mathrm{d}^3\mathbf{k}_1}{(2\pi)^3}\delta(\mathbf{k}_1)\,e^{-i\mathbf{k}_1\cdot\mathbf{x}_1} \int \frac{\mathrm{d}^3\mathbf{k}_2}{(2\pi)^3}\delta(\mathbf{k}_2)\,e^{-i\mathbf{k}_2\cdot\mathbf{x}_2}\right\rangle = \\ &= \int\int \frac{\mathrm{d}^3\mathbf{k}_1}{(2\pi)^3}\frac{\mathrm{d}^3\mathbf{k}_2}{(2\pi)^3}\langle\delta(\mathbf{k}_1)\,\delta^*(\mathbf{k}_2)\rangle e^{-i\mathbf{k}_1\cdot\mathbf{x}_1}\,e^{i\mathbf{k}_2\cdot\mathbf{x}_2} = \\ &= \int \frac{\mathrm{d}^3\mathbf{k}}{(2\pi)^3}P(k)\,e^{-i\mathbf{k}\cdot(\mathbf{x}_1-\mathbf{x}_2)}\,,\end{aligned} \tag{2.82}$$

where the Fourier transform of the autocovariance function, $P(k)$, is the *primordial power spectrum*, defined as [6]

[5] Since random Gaussian processes are ergodic, volume averages are equivalent to ensemble averages.

[6] Given that $\delta(\mathbf{x})$ is real, $\delta(-\mathbf{k}) = \delta^*(\mathbf{k})$, and expression (2.83) is equivalent to

$$P(k)\,\delta^D(\mathbf{k}_1 + \mathbf{k}_2) = \langle(\delta(\mathbf{k}_1)\,\delta(\mathbf{k}_2)\rangle\,.$$

$$P(k)\,\delta^D(\mathbf{k}_1 - \mathbf{k}_2) = \langle(\delta(\mathbf{k}_1)\,\delta^*(\mathbf{k}_2)\rangle\,, \tag{2.83}$$

where * denotes complex conjugation.

The power spectrum describes the amplitude of fluctuations on different length scales or, equivalently, on different mass scales. The Dirac delta function δ^D in (2.83) indicates that, because of homogeneity, $\xi \equiv \xi(\mathbf{x}_1 - \mathbf{x}_2)$, modes of different spatial frequency are statistically independent (and,therefore, have vanishing covariance). On the other hand, isotropy implies that the power spectrum should depend on the modulus of $\mathbf{k}$ and not on its direction. When the condition $\mathbf{k}_1 = \mathbf{k}_2$ is enforced, we obtain the expression $P(k) = \langle|\delta(k)|^2\rangle$ which is sometimes used as a definition of the power spectrum. In the case of a density field in which the fluctuations are drawn from a Gaussian distribution, the two-point correlation function or its Fourier transform, $P(k)$, gives a complete statistical description of the fluctuations and can be used to fully characterize the random field.

Many physical properties of the primordial density field can be related to the power spectrum. For example, the mean square density fluctuation is defined as the average $\langle\delta(\mathbf{x})\,\delta(\mathbf{x})\rangle$, so from equations (2.81) and (2.83) we get

$$\left\langle\left(\frac{\delta\rho}{\rho}\right)^2\right\rangle = \langle\delta(\mathbf{x})\,\delta(\mathbf{x})\rangle = \frac{1}{2\pi^2}\int_0^\infty \mathrm{d}k\,k^2 P(k)\,. \tag{2.84}$$

In hierarchical scenarios of structure formation the linear density field contains perturbations on all scales. In order to single out a given scale, one has to to smooth the density field using a spherically symmetric window with the appropriate size. The filtering operation brings equation (2.84) to

$$\left\langle\left(\frac{\delta\rho}{\rho}\right)^2\right\rangle_R \equiv \sigma_0^2(R) = \frac{1}{2\pi^2}\int_0^\infty \mathrm{d}k\,k^2 W^2(kR) P(k), \tag{2.85}$$

where $W(kR)$ is the Fourier transform of the filter function used to smooth the density field in real space. It tends to unity for small values of the argument, and falls off rapidly beyond the value $k_c \sim 1/R$ suppressing the contribution to the filtered density field from modes of wavelength smaller than the size of the smoothing function. The most used filters are the top hat (or spherical) and the Gaussian ones, which have the following form in the real and Fourier space:

top hat:

$$W(r;R_T) = \left(\frac{4\pi}{3}\,R_{TH}^3\right)^{-1}\theta\left(1-\frac{r}{R_{TH}}\right)$$
$$W(k;R_T) = 3\,\frac{\sin(kR_T)-kR_T\,\cos(kR_T)}{(kR_T)^3}\,; \tag{2.86}$$

Gaussian:

$$W(r;R_G) = \frac{1}{(2\pi)^{3/2}R_G^3}\exp\left(-\frac{r^2}{2R_G^2}\right)$$
$$W(k;R_G) = \exp\left(-\frac{k^2R_G^2}{2}\right)\,; \tag{2.87}$$

where $\theta(x)$ is the Heaviside step function. The rms fluctuation can be interpreted as the zero-order spectral moment. It is straightforward to extend the definition (2.85) to include moments of higher order

$$\sigma_j^2(R) = \frac{1}{2\pi^2}\int_0^\infty \mathrm{d}k\,k^{2(j+1)}\,W^2(kR)P(k)\,. \tag{2.88}$$

where j indicates the order of the spectral moment $\sigma_j(R)$.

Quantities such as the mean square velocity smoothed on a scale R and the mean square gravitational potential fluctuation can be calculated by using the linearised continuity equation and Poisson's equation expressed in the Fourier space. The contribution of these quantities, along with the mass fluctuation, per logarithmic interval of wavenumber is

$$\begin{aligned}
\frac{\mathrm{d}\sigma^2}{\mathrm{d}\log k} &= 4\pi k^3 P(k)\,;\\
\frac{\mathrm{d}\sigma_v^2}{\mathrm{d}\log k} &= 4\pi(aHf)^2 kP(k)\,;\\
\frac{\mathrm{d}\sigma_\phi^2}{\mathrm{d}\log k} &= 4\pi\left(\frac{3}{2}\Omega_0 H^2a^2\right)^2\frac{P(k)}{k}\,.
\end{aligned} \tag{2.89}$$

In order to complete this statistical description, we should specify the fluctuation

spectrum. Inflationary theories predict a scale-invariant power spectrum with a power-law form

$$P(k) = A\,k^n\,, \tag{2.90}$$

usually with index $n = 1$. This special case, known as the *Harrison-Zel'dovich power spectrum* (Harrison 1970; Zel'dovich 1972), results also from assuming that density fluctuations on all scales enter the horizon with the same amplitude. However, due to the evolution of density perturbations, the slope of the shape of the primordial spectrum is not conserved. Perturbations that exceed the horizon size grow through self-gravity and leave the power spectrum unchanged, but, on smaller scales, even in the linear regime, the growth of density perturbations after the horizon entry is affected by collisional processes (see §2.1.2) and depends on the nature of the matter which dominates the expansion. To account for this change in shape, the primordial power spectrum is expressed in terms of the *transfer function* $T(k, t_f)$ from t_i to t_f

$$P(k, t_f) = T^2(k, t_f)\,P(k, t_i)\,. \tag{2.91}$$

When perturbation evolution is only driven by gravity, the transfer function adopts the simple form $T(k, t_f) \propto D_+(k, t_f)$. Transfer functions depend on the values of the cosmological parameters and convey the information about the matter content of the universe. If the dynamics of the universe is driven by weakly interacting massive particles which left the relativistic regime at a very late epoch, then a Hot Dark Matter transfer function, which eliminates power on small and intermediate scales, has to be applied. On the other hand, if the matter content of the universe is dominated by weakly interacting massive particles non-relativistic in all epochs of interest, the Cold Dark Matter transfer function, which gently bends the primordial power-law power spectrum from $n = 1$ on large scales to $n \approx -3$ on small scales, is more suited (Bond & Efstathiou 1984; Eisenstein & Hu 1999). Expressions of these transfer functions are given in Appendix G of Bardeen et al. (1986, hereafter BBKS).

The primordial amplitude A is usually determined observationally. The first attempts were based on galaxy counts on scales large enough to ensure linear regime. One approach uses the statistics J_3, which is the integral of the two-point correlation function $\xi(r)$ times r^2. In terms of the power spectrum, J_3 becomes

$$J_3(R) \equiv \int_0^R \xi(r) r^2 dr = \frac{R^3}{3}\,\frac{1}{(2\pi)^3}\int_0^\infty \mathrm{d}\mathbf{k}\,W^2(kR)\,P(k)\,. \tag{2.92}$$

The variance of the galaxy counts-in-cells is easily related to the power spectrum

by means of equation (2.85). Galaxy surveys seem to indicate that perturbations on scales of $8h^{-1}$ Mpc are currently entering the non-linear regime ($\delta \approx 1$) (Bond & Szalay 1983; Loveday et al. 1996). However, this result assumes that galaxies trace the mass, and there is no evidence that this has to be true. It is believed that fluctuations in galaxy counts can be proportional to mass perturbations

$$\left(\frac{\delta N}{N}\right) = b\left(\frac{\delta\rho}{\rho}\right), \tag{2.93}$$

with the bias factor b likely dependent on the scale. Therefore, by definition, the galaxy biasing provides a measure of the difference between the distribution of luminous and dark matter. Taking into account the proportionality (2.93), the normalisation condition writes

$$\sigma_8 = \sigma_0(8\,h^{-1}\mathrm{Mpc})_{t_0} = b^{-1}\,, \tag{2.94}$$

by means of which the primordial amplitude A is fixed.

After COBE (and more accurate CMB probes such as WMAP and Planck), another method to normalise the primordial amplitude of the fluctuation spectrum appeared, based on the level of the CMB anisotropies at large scales. It can be shown (see e.g., Sahni & Coles 1995) that the quadrupole moment, which appears after the expansion of temperature fluctuations in spherical harmonics, can be expressed in terms of the primordial power spectrum.

2.4.2 The Press-Schechter Formalism

With all these tools, it is possible to develop a method capable of retrieveing the analytical mass function of relaxed objects in terms of statistical properties of the initial density field. The following formalism was originally derived by Press & Schechter (1974) (PS) and, therefore, it is commonly referred as the PS formalism. It is based on the linear extrapolation, for the growing mode, of the growth of density fluctuations according to the spherical collapse. Despite ignoring some of the difficulties of gravitational collapse, it is a very simple approximation that is able to reproduce the results of numerical simulations and, therefore, has many practical uses. Scales and densities are henceforth assumed to be expressed in comoving coordinates. To turn comoving lengths into physical ones, they must be multiplied by the factor $a(t)/a_0$.

According to the spherical model (see §2.3.1), the collapse time for a shell of radius R around the centre, located at $\mathbf{x}$, of a spherically symmetric, outwards

decreasing (to avoid shell crossing), linear density fluctuation at t_i only depends on the mean value of δ inside it. More exactly, the value of the average density contrast for collapse at t in an Einstein-de Sitter universe is $\delta_c(t) = \delta_{c0}\, a(t_i)/a(t)$ with $\delta_{c0} = 1.686$. Of course, the collapse of the shell of radius R represents the appearance, at t, of a virialised object of mass equal to $4\pi/3\,\bar{\rho}R^3$ to 0th order in δ_c[7]. This therefore suggests that any point in the real density field at t_i smoothed with a top hat filter of scale R with density contrast *above* a positive linear threshold δ_c should tend to collect matter so to reach, at a time t related to δ_c through the previous expression, a mass M *larger than* $4\pi/3\,\bar{\rho}R^3$. Since we are dealing with a Gaussian density field (as a consequence of assuming uncorrelated phases for the various Fourier components of the density field via the central limit theorem), the probability that a given point has a density contrast above some critical value δ_c when the field is smoothed on the scale R adopts the simple form

$$P(\delta > \delta_c, R) = \frac{1}{\sqrt{2\pi}\sigma_0(R)} \int_{\delta_c}^{\infty} \mathrm{d}\delta \exp\left[-\frac{\delta^2}{2\sigma_0^2(R)}\right] \equiv$$
$$\equiv \frac{1}{2}\,\mathrm{erf}\left[\frac{\delta_c}{\sqrt{2}\sigma_0(R)}\right], \tag{2.95}$$

where $\sigma_0(R)$ is the linear rms fluctuation on scale R given by equation (2.85) and $\mathrm{erf}(x)$ is the error function. According to the PS formalism, this probability can also be interpreted as the probability that a given point has ever been embedded in a collapsed object on scales greater than R. This assumes that if a point has a density contrast exceeding δ_c on a given scale, then it will reach the value δ_c when filtered on some larger scale and will be computed as a distinct object of the larger scale. In other words, it assumes that the only objects which exist at epoch t are those that have just collapsed. But, what happens to underdense regions which seem to contain half of the matter of the universe? PS proposed that the matter of underdense regions was efficiently accreted by overdense regions, and therefore, the correct probability was obtained by adding a factor 2.

The probability $P(\delta > \delta_c, R)$ gives the volume fraction occupied by points with overdensity above the threshold δ_c when the density field is smoothed on scale R with a top hat window. Consequently, by differentiating this probability over M one should obtain the volume fraction contributing at t with objects of mass between

[7]Since the mean density within the spherical perturbation is $\rho = \bar{\rho}(1+\delta_c)$, then the actual mass contained inside a radius R is $M(R) = 4\pi/3\,\bar{\rho}(1+\delta_c)\,R^3$.

M and $M + \mathrm{d}M$, and by dividing the result by $M/\bar{\rho}$ to the number density of such objects

$$N(M,t)\,\mathrm{d}M = 2\,\frac{\bar{\rho}}{M}\left|\frac{\partial P(\delta > \delta_c, R)}{\partial R}\right|\frac{\mathrm{d}R}{\mathrm{d}M}\,\mathrm{d}M = \\ = \sqrt{\frac{2}{9\pi}}\,\frac{\bar{\rho}}{M^2}\,\frac{\delta_c}{\sigma_0}\left|\frac{\mathrm{d}\ln\sigma_0}{\mathrm{d}\ln R}\right|\,\exp\left[-\frac{\delta_c^2}{2\sigma_0^2}\right]\,\mathrm{d}M\,. \tag{2.96}$$

Assuming that every particle in the Universe is at any time t within some virialised object with the appropriate mass, then the mass function must verify the normalisation condition

$$\int_0^\infty \mathrm{d}M\,M\,N(M) = \bar{\rho}\,. \tag{2.97}$$

The factor 2 in the right-hand member of equation (2.96) is the one interpreted as accounting for the underdense regions and must be inserted in order to properly normalize the mass function (i.e, the total mass of the Universe remains constant). This is a weak point of the PS theory that has been frequently criticised (e.g., Bond et al. 1991; Peacock & Heavens 1990; Bower 1991) and is related with the so-called "cloud-in-cloud" problem (above-threshold regions lying inside of other above threshold regions), which is not treated by the PS formalism, especially in the case of underdense regions embedded in overdense regions(Jedamzik 1995).

Another quantity closely related to the mass function is the mass fraction (or multiplicity function) contained in objects of mass M, defined as

$$f(M)dM = \frac{M}{\bar{\rho}}N(M)\mathrm{d}M = \\ = \frac{1}{M}\sqrt{\frac{2}{9\pi}}\,\frac{\delta_c}{\sigma_0}\left|\frac{\mathrm{d}\ln\sigma_0}{\mathrm{d}\ln R}\right|\,\exp\left[-\frac{\delta_c^2}{2\sigma_0^2}\right]\,\mathrm{d}M\,. \tag{2.98}$$

For a power-law power spectrum $P(k) \propto k^n$, the rms fluctuation on scale R is $\sigma_0(R) \propto R^{-(n+3)/2}$, or in terms of the mass $\sigma_0(M) \propto M^{-(n+3)/6}$. Let us define the characteristic mass M_* as the mass for which the rms fluctuation is equal to the threshold value $\sigma_0(M_*) = \delta_c$. In this case the mass function and the mass fraction of objects in an infinitesimal interval of the variable M/M_* have the respective forms

$$N\left(\frac{M}{M_*}\right) = \sqrt{\frac{2}{\pi}}\,\frac{n+3}{6}\,\frac{\bar{\rho}}{M_*}\left(\frac{M}{M_*}\right)^{\frac{n}{6}-\frac{3}{2}} \exp\left[-\frac{1}{2}\left(\frac{M}{M_*}\right)^{\frac{n+3}{3}}\right]$$
$$f\left(\frac{M}{M_*}\right) = \sqrt{\frac{2}{\pi}}\,\frac{n+3}{6}\left(\frac{M}{M_*}\right)^{\frac{n}{6}-\frac{1}{2}} \exp\left[-\frac{1}{2}\left(\frac{M}{M_*}\right)^{\frac{n+3}{3}}\right]. \tag{2.99}$$

Notice that for a scale invariant power spectrum the mass fraction when expressed in terms of the variable M/M_* is time invariant, as it is expected in self-similar models of structure evolution.

The PS theory provides a simple analytical description for the evolution of gravitational structure in a hierarchical universe. Nonetheless, the PS mass function is not fully satisfactory. The origin of the factor two added "by hand" in (2.96) is unclear and the disappearance of objects of any given mass swallowed by previously collapsed ones owing to "cloud-in-cloud" configurations is not accounted for. In addition, the real density field is not spherically symmetric and outwards decreasing around any point. As a consequence, the growth of density fluctuations leaving the linear regime deviates from spherical collapse and involves complicated non-local, nonlinear, dynamics. Therefore, it is by no means obvious that the PS prescription can provide a good description of the formation of bound virialised objects. In fact, small changes in some aspects strongly connected with the spherical collapse model might be suitable. Moreover, this method does not allow to follow the evolution of halos that accrete into larger systems.

Yet, the PS mass function gives reasonably good fits to the mass function inferred from N-body simulations. For this reason numerous authors have tried to properly justify it by greatly refining and extending it. A rigorous solution to the cloud-in-cloud problem, which also naturally recovers the factor 2 in the mass functions (but see also Peacock & Heavens 1990), has been proposed by Bond et al. (1991) by means of the powerful "excursion set formalism"[8]. Bond et al. also showed how the mass function depends on the filter used to define the spatial smoothing, particularly, that the only case in which exact analytical results can be obtained is the case of the k-sharp window, for which the standard PS formula is recovered. An identical expression for the conditional mass function was derived independently by

[8]In the theory of stochastic processes, an excursion set is defined as a region in wich the linear density contrast is larger than some threshold.

Bower (1991).

Jedamzik (1995) got rid of the cloud-in-cloud problem by considering only isolated regions, defined as those regions lying above the threshold on a given scale, and lying below the threshold for any larger scale. He obtained a correctly normalised mass function that seems to agree much better with mass distributions derived from N-body simulations than the PS one. The effects of the departure from spherical collapse have also been studied (Monaco 1995, 1998; Lee & Shandarin 1998; Sheth et al. 2001). Monaco (1995, 1998) showed that when the assumption of spherical collapse is relaxed, δ_c becomes a function of the local shape of the perturbation spectrum.

The PS formalism has also been extended to calculate other properties, notably the merger histories of dark matter halos. In particular, Lacey & Cole (1993), were able to calculate analytically the fraction of the total number of halos with mass M at t, which give rise per unit time to halos with mass in the range M', $M' + \mathrm{d}M'$ through instantaneous mergers of any amplitude This is usually referred as the EPS (Extended Press-Schechter) theory. However, in the EPS model, the formation and destruction of halos is modelled trough an unrealistic prescription (Kitayama & Suto 1996; Percival et al. 2000, see e.g.,) where the age and survival time of an object are defined arbitrarily in terms of some relative mass variation. On the other hand, the so called Modified Press-Schechter formalism (MPS) (Salvador-Solé et al. 1998; Raig et al. 1998, 2001; Hiotelis 2003; Manrique et al. 2003) solves this problem through the distinction between major and minor merger events, defined according to whether they cause the complete rearrangement of the system (based on the comparison of the resulting fractional mass increase with respect to the reference halo with a given threshold $\Delta_{\mathrm{m}} \approx 0.6$) or not. Thus, the halo formation and destruction times are unambiguously defined as the times corresponding to their last and next major merger[9].

All these improvements only apply to the PS original prescription dealing with undefined regions above the threshold overdensity. However there is no reason for every point above the threshold overdensity to tend to accrete matter. This is expected to happen rather onto density maxima or "peaks" (Doroshkevich 1970; Kaiser 1984; Doroshkevich & Shandarin 1978; Peacock & Heavens 1985; Bardeen

[9]Whithout distinguishing between merger and accretion this would not have been possible. Since the number density of objects diverges at small masses, objects continuously experience captures. If a unique process of mass increase is considered(generically called merger, as in the Lacey & Cole 1993 model), it cannot be defined any specific event to mark the beginning or the end of any stable entity.

et al. 1986; Bernardeau 1994; Manrique & Salvador-Solé 1995, 1996; Bond & Myers 1996; Manrique et al. 1998). In the PS framework there is no satisfactory derivation of the theoretical mass function for peaks as seeds of virialised objects. Furthermore, none of the former studies has supplied a well justified relation between the window used to filter the density field and the mass of the collapsed object, or the one between the critical overdensity and the time of collapse (Manrique & Salvador-Solé 1995, 1996; Manrique et al. 1998).

Despite the good agreements with numerical simulation, the PS formalism has to be taken as a useful simplification to a far more complex problem. Nevertheless, the above arguments are enough to demand a more rigorous approach than that given by the PS theory. An alternative is to assume that objects form from peaks in the initial density field. This possibility has been extensively investigated in the study of clustering of galaxies and clusters (Peacock & Heavens 1985, BBKS), but has been less used in calculating mass functions because of the mathematical difficulties that arise when trying to solve the cloud-in-cloud problem, with the risk of miscounting the number of objects, and of identifying what mass object forms from a given size peak.

This formalism was adopted in subsequent refinements carried out with the aim to account for the more realistic ellipsoidal collapse (Monaco 1995; Lee & Shandarin 1998; Sheth & Tormen 2002).

But the assumptions made in this derivation are not fully satisfactory: i) Every overdense region does not collapse into a distinct halo; only those around peaks do. Unfortunately, the extension of the excursion set formalism to peaks is not trivial (Paranjape et al. 2012; Paranjape & Sheth 2012); ii) Real haloes (and peaks) are not spherically symmetric but triaxial, so halo seeds do not undergo spherical but ellipsoidal collapse. Unfortunately, the implementation in this approach of ellipsoidal collapse is hard to achieve due to the dependence on M of the corresponding critical density contrast (Sheth & Tormen 2002; Paranjape et al. 2012; Paranjape & Sheth 2012). iii) The formation of haloes involves not only the collapse of the seed, but also the virialisation (through shell-crossing) of the system, which is hard to account for. And iv) there is a slight inconsistency between the top-hat filter used to monitor the dynamics of collapse and the sharp k-space window used to correct for nesting. The use of the top-hat filter with this latter purpose is again hard to implement due to the correlation between fluctuations at different scales in top-hat smoothing (Musso & Paranjape 2012).

The excursion set formalism has also recently been modified (Paranjape et al.

2012; Paranjape & Sheth 2012) to account for the fact that density maxima (peaks) in the initial density field are the most probable halo seeds (Hahn & Paranjape 2014).

2.5 The Peak Formalism

As we have seen, the PS formalism considers any positive perturbation as the seed of some object at a given epoch. These overdense regions evolve linearly until their density contrast reaches a value about unity, and then experience a collapse analog to that of a perfect spherical, isolated inhomogeneity. This picture implies a rapid transition from linear to non-linear regime and a good correspondence between overdense regions and final objects. In other words, in the PS formalism, any point with density contrast above a critical value when the density field is smoothed on a specific scale gives rise to a collapsed object with the appropriate mass at t. This means that, somehow, points have to efficiently accrete the surrounding matter in order to achieve the mass corresponding to the filtering radius at the appropriate collapse time.

However, this simple model is not accurate enough. Numerical simulations have shown that not all the overdense regions in the linear density field end up in collapsed objects at a given epoch (Bond et al. 1991). Density maxima (also known as peaks) have been shown to be seeds of virialized halos (Hahn & Paranjape 2014). Only $15 - 20\%$ of haloes arise from two nodes (Porciani et al. 2002; Ludlow & Porciani 2011), which is compatible with them being currently undergoing a major merger. Indeed, for steep power-law spectra ($n < -1$) and moderately high amplitudes ($\nu \equiv \delta/\sigma_0 \geq 2$), the non-linear evolution of peaks is well-described by the spherical collapse (Bernardeau 1994).

This is the basis of the so-called peak formalism. The study of peak statistics in Gaussian random fields was first introduced by Doroshkevich (1970) and has been extensevely extended and refined by man other authors (Doroshkevich & Shandarin 1978; Kaiser 1984; Peacock & Heavens 1985; Bardeen et al. 1986; Cline et al. 1987; Couchman 1987; Heavens & Peacock 1988; Coles 1989; Bernardeau 1994; Bond & Myers 1996; Avila-Reese et al. 2005; Del Popolo et al. 2000; Ascasibar et al. 2004).The Ansatz of the peak formalism (which will later be proved to be correct, see section 3.2) states that virialized objects of a mass M at a time t emerge from maxima of the density field with a density contrast that is a *monotonously decreasing* function of t when the density field is filtered at a scale R_f that is *monotonously*

increasing with M. Said otherwise, there is a one-to-one correspondence between virialized halos with mass M at a time t and *non-nested* peaks with density contrast $\delta(t)$ at the filtering radius $R(M)$. Under this assumption, the evolution of peaks in the filtering of the density field at t_i automatically traces the dynamical growth of halo mases in the CDM clustering process.

The confluent system formalism of peak trajectories (CUSP), introduced by Manrique & Salvador-Solé (1995, 1996); Manrique et al. (1998) and further developed by Salvador-Solé et al. (2012a) (hereafter SVMS); Salvador-Solé et al. (2012b) (hereafter SSMG) and Viñas et al. (2012), is an extension of the peak theory that makes it possible to derive the theoretical mass function of relaxed objects and their inner properties, relying on the peak model Ansatz. In what follows, we will review the general peak theory, while in the following sections we further develop the CUSP formalism and show the results obtained by it.

2.5.1 Basic Theory

Let us consider a homogeneous and isotropic Gaussian random field $\delta(\mathbf{r})$ characterised by a power spectrum $P(k)$. If the random field describes the primordial density field, then the power spectrum gives information about the distribution of density perturbations as a function of the scale. In order to give rise to a cosmology with hierarchical gravitational clustering, the power spectrum must have power at all scales. Moreover, in order to have a well defined set of local maxima, the field has to be smooth and differentiable, therefore having its harmonic content limited at high wavenumbers. Finally, the density field has to be filtered with a smoothing function at a given scale in order to single out one of the maxima. This additional dependence on scale should be always born in mind, although it will not always be explicitly specifiedfor the sake of notation.

The Joint Probability Function

In §2.3.1, we used the properties of a random Gaussian field to calculate the probability of finding a point above a threshold when the density field is smoothed on a given scale (equation [2.95]). In that case, the probability density can be writen as

$$P(\delta)\, d\delta = \frac{1}{\sqrt{2\pi}\,\sigma_0} \exp\left(\frac{\delta^2}{2\sigma_0^2}\right) d\delta\,. \tag{2.100}$$

The extension of the distribution probability function to two points separated by a distance r requires the use of the covariance function $\xi(r)$, because the values

of the density field at different points are not statistically independent. Then the probability that one of the points has density contrast in the interval δ_1 to $\delta_1 + \mathrm{d}\delta_1$, and the other point has density contrast in the interval δ_2 to $\delta_2 d + \mathrm{d}\delta_2$ is

$$P(\delta_1, \delta_2)\,\mathrm{d}\delta_1\mathrm{d}\delta_2 = \frac{1}{2\pi\sigma_0^2}\frac{1}{\sqrt{1-w^2(r)}}\,\exp\left[-\frac{\delta_1^2+\delta_2^2-2w(r)\delta_1\delta_2}{2\sigma_0^2[1-w^2(r)]}\right]\,\mathrm{d}\delta_1\mathrm{d}\delta_2\,, \quad (2.101)$$

where $w(r) = \xi(r)/\sigma_0^2$ is the scaled correlation function. Notice that if the points were not correlated [$\xi(r) = 0$] the above probability would be simply equal to the product $P(\delta_1)\,P(\delta_2)$. It is easy to generalise the former Gaussian joint probability distribution for m points

$$P(\delta_1, ..., \delta_m)\prod_i^m \mathrm{d}\delta_i = \frac{\exp(-Q)}{[(2\pi)^m\det(\mathbf{M})]^{1/2}}\prod_i^m \mathrm{d}\delta_i\,, \quad (2.102)$$

$$Q \equiv \frac{1}{2}\sum_{ij}^m \delta_i(\mathbf{M}^{-1})_{ij}\delta_j\,,$$

where we have taken the means of random variables $\langle\delta_i\rangle = 0$. In this case, only the covariance matrix $M_{ij} \equiv \langle\delta_i\delta_j\rangle = \xi(r_{ij})$ is required to specify the distribution. The successive derivatives of a random Gaussian field are random Gaussian fields, which implies that expression (2.102) for the joint probability function does not hold exclusively for the values of the density field at different points, but for the values of its derivatives as well.

The Maximum Constraint

The characterisation of maxima for one-dimensional functions is reduced to finding those points with null first derivative and negative second derivative. In the case of random Gaussian fields, we need the joint probability function for the value of the field δ, and its first $\delta' \equiv \eta$, and second $\delta'' \equiv \zeta$ derivatives at a given point. By enforcing $\eta = 0$, and $\zeta < 0$, the integration over these variables in the appropriate domains leads to the probability of finding a maximum at the point with density contrast in the interval δ to $\delta + \mathrm{d}\delta$. However, this procedure cannot be applied because the set comprising those points with $\eta = 0$ has null measure, so the corresponding probability seems to be zero. Luckily enough, it is possible to substitute

$\mathrm{d}\eta$ for $|\zeta|\mathrm{d}x$ [10], because, owing to ergodicity, the integral over x is equivalent to the integral over the probability distribution, being x the spatial coordinate. In this way, the measure problem is avoided and a peak number density, instead of a probability, is achieved by dividing by $\mathrm{d}x$.

In three-dimensional Gaussian random fields (as the one describing the density field), the process to characterise peaks is the same than in the one dimensional case, but taking into account that the first Cartesian derivatives of the field involve three components, $\eta_i = \nabla_i \delta$, (one for each possible direction), and second derivatives $\zeta_{ij} = \nabla_i \nabla_j \delta$ make a symmetric 3×3 matrix with six independent components. Therefore, the probability of having a maximum at a given point with density contrast in the range from δ to $\delta + \mathrm{d}\delta$ is

$$p_{pk}(\delta)\,\mathrm{d}\delta = \mathrm{d}\delta \int \mathrm{d}^3\eta\ \mathrm{d}^6\zeta\ P(\delta, \boldsymbol{\eta} = \mathbf{0}, \zeta)\,, \tag{2.103}$$

integrated over the domain for which the second derivatives are negative. To overcome the problem of null measure sets, we turn the ensemble average into a volume average. The Jacobian of the transformation is $J = \det \zeta$, then the probability (2.103) becomes

$$p_{pk}(\delta)\,\mathrm{d}\delta = \mathrm{d}\delta\,\mathrm{d}^3 r \int \mathrm{d}^6\zeta\,|\det\zeta|\,P(\delta, \boldsymbol{\eta} = \mathbf{0}, \zeta)\,. \tag{2.104}$$

By dividing both sides by the volume element $\mathrm{d}^3 r$ we obtain the number density of peaks per infinitesimal range of height[11]. Given that the Gaussian field is homogeneus and isotropic, the probability (i.e., number density) of peaks does not depend on the position. For simplicity, we will hereafter evaluate the joint probability functions at $\mathbf{r} = \mathbf{0}$.

The expression (2.104) can also be derived considering a point process. In this case the number density of points p selected to be maxima of the field $\delta(\mathbf{r})$ is

$$n_{pk} = \sum_p \delta^{(3)}(\mathbf{r} - \mathbf{r}_p)\,, \tag{2.105}$$

[10] The Taylor expansion of the first derivative of the field in the neighbourhood of a maximum located at x_p is

$$\eta(x) \approx \zeta(x_p)(x - x_p).$$

[11] In peak statistics, the density contrast is usually referred as the peak "height".

where $\delta^{(3)}$ is the three-dimensional Dirac delta function. The following step is to express this point process in terms of the random field and its derivatives. To do so, let us expand the field and its gradient in Taylor series around the maximum located at $\mathbf{r}_p$

$$\begin{aligned} \delta(\mathbf{r}) &\approx \delta(\mathbf{r}_p) + \frac{1}{2}\sum_{ij}\zeta_{ij}\,(r-r_p)_i\,(r-r_p)_j, \\ \eta_i(\mathbf{r}) &\approx \sum_j \zeta_{ij}\,(r-r_p)_j\,. \end{aligned} \tag{2.106}$$

If the matrix ζ_{ij} is non-singular (i.e., it can be inverted) we can write

$$\begin{aligned} \mathbf{r}-\mathbf{r}_p &\approx \zeta^{-1}(\mathbf{r}_p)\,\boldsymbol{\eta}(\mathbf{r}), \\ \delta^{(3)}(\mathbf{r}-\mathbf{r}_p) &= |\det\zeta(\mathbf{r}_p)|\,\delta^{(3)}[\boldsymbol{\eta}(\mathbf{r})]\,. \end{aligned} \tag{2.107}$$

Notice that the δ-function picks out all the points satisfying $\boldsymbol{\eta}(\mathbf{r})=\mathbf{0}$. For now, we can only obtain the number density of extrema

$$n_{ext} = |\det\zeta(r_p)|\,\delta^{(3)}[\boldsymbol{\eta}(\mathbf{r})]\,. \tag{2.108}$$

In practice, only the ensemble average of expression (2.108) can be calculated. This average involves the joint probability function $P(\delta,\boldsymbol{\eta},\zeta)$ evaluated at $\mathbf{r}=\mathbf{0}$. Integrating over the domain where ζ is negative one gets the number density of peaks with height in the interval δ to $\delta+\mathrm{d}\delta$

$$\langle n_{pk}(\delta)\rangle\,\mathrm{d}\delta = \mathrm{d}\delta\int \mathrm{d}^6\zeta\,|\det\zeta|\,P(\delta,\boldsymbol{\eta}=\mathbf{0},\zeta)\,. \tag{2.109}$$

In Appendix A we show how to calculate the number density of peaks per infinitesimal $\nu\equiv\delta/\sigma_0$ range at a given scale R_f, following the derivation of BBKS. However, the quantity needed in order to compute the halo mass function (both unconditional and conditional) is the number density of peaks with a given δ per infinitesimal R_f range. The CUSP formalism allows us to compute these quantities and mass functions, as well as other important halo properties, such as their inner structure.

3

The Confluent System of Peak Trajectories

Simplicities are enormously complex. Consider the sentence "I love you".
Richard O. Moore

In the present Chapter, we give a general overview of the Confluent System of Peak Trajectories (CUSP) and its application to the analytic derivation of halo properties from the filtering of the primordial density field. The CUSP formalism was introduced by Manrique & Salvador-Solé (1995, 1996); Manrique et al. (1998) to deal with the properties of relaxed halos within the general peak formalism. Some years later, SVMS and SSMG managed to establish the whole link between the characteristics of triaxial peaks (abundance, height, ellipticity, prolateness, curvature and nesting) and the properties of virialised halos (abundance, structure, kinematics, shape and substructure), taking into account ellipsoidal collapse and virialisation. These results opened the possibility to build a complete accurate analytic treatment of non-linear clustering in any hierarchical (cold as well as warm; Viñas et al. 2012) dark matter cosmology from the filtering of the linear density perturbation field. Unfortunately, the peak Ansatz was not proved and the functions describing the a one-to-one correspondence between virialised haloes with mass M at t and non-nested peaks with density contrast $\delta(t)$ at the filtering radius $R(M)$ were determined by fitting the halo MF to the PS one, which caused the formalism to loose its predicting power. In addition, it was argued although not checked that halos grow inside-out, a condition that plays a crucial role in the formalism. Last but no the least, the theory focused on halos formed in smooth accretion, assumin that major mergers lead to halos with identical properties due to the fact that virialisation is a

real relaxation process.

In this overview we include the proof by Juan et al. (2014a) that these relations hold as well as the formal justification that the formalism developed for accretion is valid, indeed, for major mergers.. In Chapter 4 we check the inside-out growth of accreting halos and, in Chapter 5, apply the formalism to derive the halo mass and multiplicity functions that correspond to realistic halo mass definitions.

3.1 Filtering vs. Gravitational Clustering

In this Section, we show that the Gaussian filter allows one to establish a one-to-one correspondence between virialised halos with mass M (according to any given mass definition) at time t and non-nested peaks with density contrast $\delta(t)$ at scale $R(M,t)$ in the density field at t_i. In other words, the Gaussian filter is the best adapted to monitor the gravitational collapse and virialisation of density perturbations through the filtering evolution of the initial density field.

3.1.1 Gaussian Filter

The density contrast $\delta(\mathbf{r})$ at any arbitrary point $\mathbf{r}$ of the density field filtered with a Gaussian window satisfies the relation

$$\frac{\partial\delta(\mathbf{r})}{\partial R} = R\nabla^2\delta(\mathbf{r},R) \tag{3.1}$$

that warrants the negative sign of the R-derivative of δ *at density maxima* of scale R. The fixed sign of $\delta(\mathbf{r})$ in peaks is only ensured for that particular window, so the existence of a monotonous dependency of δ on R (or of R on δ) as needed in order to trace the monotonous mass growth of halos with time is only possible for that filter (Manrique & Salvador-Solé 1995).

3.1.2 Ellipsoidal Collapse

Provided spherical symmetry, the sphere of radius R around a peak with δ in the density field at t_i filtered with a *top-hat* window of that radius collapses at a time t satisfying $\delta(t) = \delta_\mathrm{c}^\mathrm{th}(t)D(t_\mathrm{i})/D(t)$, where $\delta_\mathrm{c}^\mathrm{th}(t)$ is a time- and cosmology-dependent critical value, equal to 1.686 in the Einstein-de Sitter universe. In these circumstances, a one-to-one correspondence can thus be established between peaks at t_i

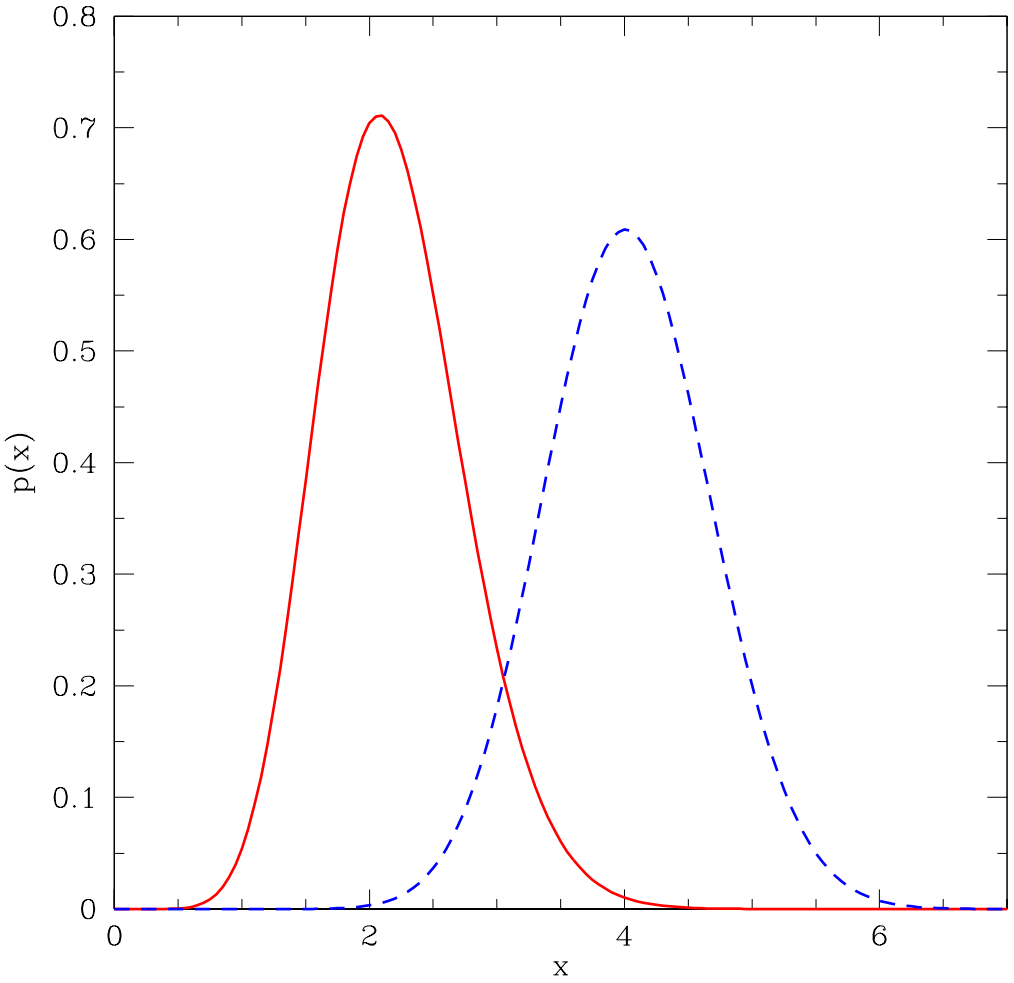

Figure 3.1: Distribution of curvatures for peaks corresponding to current haloes with extreme masses of 10^8 $M_\odot$(red solid line) and 10^{16} $M_\odot$(blue dashed line), for which $\langle (x - \langle x \rangle)^2 \rangle^{1/2} / \langle x \rangle$ are respectively equal to 0.25 and 0.16.

with δ at R and halos at t with mass $M = 4\pi/3\,\bar{\rho}(t_\mathrm{i})\,R^3$, where $\bar{\rho}(t_\mathrm{i})$ is the mean cosmic density at t_i.

Unfortunately, in the Universe, peaks are triaxial and undergo ellipsoidal collapse. In this case, the time of collapse of spheres of any radius R around a peak depends not only on δ but also on the ellipticity and prolateness of the peak as well as on the spherically averaged density profile around it (Peebles 1980).

However, for the Gaussian filter, the ellipticity and prolateness of peaks with δ at R depends only on their curvature and so does also the spherically averaged density profile around them (BBKS). The curvature x of a peak of scale R is defined as minus the Laplacian over the rms value of such a quantity on that scale, equal to the second order spectral moment

$$x \equiv -\nabla^2\delta/\sigma_2. \tag{3.2}$$

Therefore, we can rewrite Equation 3.1 as

$$\frac{\partial\delta(\mathbf{r})}{\partial R} = R\nabla^2\delta(\mathbf{r},R) \equiv -x\sigma_2(R)R. \tag{3.3}$$

In addition, the distribution of peak curvatures is sharply peaked at its maximum (BBKS, 3.1) due to Laplace transform being linear

$$\frac{\left\langle \left(\frac{\mathrm{d}\rho_\mathrm{p}}{\mathrm{d}r} - \left\langle\frac{\mathrm{d}\rho_\mathrm{p}}{\mathrm{d}r}\right\rangle\right)^2\right\rangle^{1/2}}{\left\langle\frac{\mathrm{d}\rho_\mathrm{p}}{\mathrm{d}r}\right\rangle} \approx \frac{\langle(x-\langle x\rangle)^2\rangle^{1/2}}{\langle x\rangle} \ll 1\,, \tag{3.4}$$

so all peaks with δ at R have similar ellipticity and prolateness as well as similar spherically averaged density profiles. Consequently, all spheres with mass equal to a function of R and δ, $M(R,\delta)$, around peaks with δ at R collapse and virialise[1] at approximately the same time (Juan et al. 2014a).

Of course, the scatter around the mean curvature will cause some scatter in the properties of virialised halos derived under the approximation of identical time of collapse and virialisation. The distribution of any halo property around the typical value should be possible to be calculated for halos with M at t from the well-known distribution of curvatures of the corresponding peaks. But we will concentrate here in the typical (mean) halo properties, without caring about their scatter.

3.1.3 Peak Nesting

Strictly, not all spheres with $M(R,\delta)$ around peaks with δ at R will collapse and virialise at t. This would be the case provided peaks were isolated. But, in the Universe, *peaks are often located within the collapsing cloud of other peaks with identical*

[1]The time of virialisation of a collapsed system depends on its mass (and its radius determined by the the former and the cosmic time; see below), so the full time of collapse and virialisation depends indeed on R and δ.

density contrast at larger-scales. When such a peak nesting happens, the halos the former peaks would eventually evolve into are swallowed by those of their larger scale hosts, which aborts their growth.

Therefore, besides the use of a Gaussian filter, another necessary condition for the existence of a halo-peak one-to-one correspondence is that *peaks are corrected for nesting*. The higher a peak,[2] the rarer it is and the lower the probability of being nested in other peaks with identical δ at even larger scales. The correction for nesting will thus depend on the peak height. We will comeback to this correction in Section 3.4.1.

3.1.4 The Halo-Peak Correspondence

According to that correspondence, for suited functions $\delta(t)$ and $R(M,t)$, every virialised halo with M at t arises from the collapse and virialisation of a non-nested peak with δ at the Gaussian filtering scale R.

But, what mass M are we talking about? As mentioned, the mass of a virialised halo is a rather fuzzy concept. One can adopt, for instance, the mass of the region with the time-dependent virial overdensity, $\Delta_{\rm vir}(t)$, relative to the cosmic mean density $\bar{\rho}(t)$ predicted by the top-hat spherical collapse model, which defines the so-called virial mass, $M_{\rm vir}$, or with a fixed overdensity, say $\Delta = 200$, relative to the critical density $\rho_{\rm c}(t)$, which defines the mass usually denoted by M_{200}. The question then rises: is the one-to-one correspondence only possible for one specific mass definition and, if this is the case, which is it? We will come back to this question later (see section 5.3).

3.2 Setting the one-to-one correspondence between peaks and halos

In any given cosmology, we can take any desired monotonous decreasing $\delta(t)$ function[3] and find non-nested peaks with fixed δ at any scale R in the density field at $t_{\rm i}$ filtered with a Gaussian window. Then, taking at t the mass definition matching

[2]The height ν of a peak of scale R is defined as its density contrast over the rms value of such a quantity on that scale, equal to the zero order spectral moment, i.e. $\nu \equiv \delta/\sigma_0(R)$.

[3]The only constraint is that it must be proportional $D(t_{\rm i})/D(t)$ for consistency with the arbitrariness of $t_{\rm i}$ (see Juan et al. (2014a)).

the masses $M(R,\delta) \equiv M(R,t)$ of the collapsed clouds arising from different R's, we will end up with a one-to-one correspondence between virialised halos with M at t and non-nested peaks at t_i with δ at R. The mass definition corresponding to any given monotonous $\delta(t)$ function can be found following the prescription described further in this section.

But the converse is also feasible and even more interesting: for any chosen halo mass definition, we can determine, at the arbitrary small time t_i, one only couple of $\delta(t)$ and $R(M,t)$ functions defining non-nested peaks giving rise to halos with M at t. This is achieved by enforcing the two following consistency conditions: the total mass density locked into halos must be equal to the mean cosmic density[4] and the mass of a halo must coincide with the integral of its density profile times $4\pi r^2$. The result takes the form (Juan et al. 2014a)

$$\delta(t) = \delta_c(t)\frac{D(t_\mathrm{i})}{D(t)} \tag{3.5}$$

$$\sigma_0(M,t) = \frac{1}{2\pi^2}\int_0^\infty \mathrm{d}k\, k^2 P(k)\, \exp\left(-\frac{k^2R^2}{2}\right) = \sigma_0^{th} + \delta(t)\cdot S(t) \tag{3.6}$$

where $S(t)$ is a function of time that will be specified later on (eq. [3.10]).

It should be noted that, due to using the Guassian filter instead of the top-hat one, the deffinition of the filtering radius is slightly different

$$R(M,t) = \frac{1}{q(M,t)}\left[\frac{3M}{4\pi\bar{\rho}(t_\mathrm{i})}\right]^{1/3} \tag{3.7}$$

The dependence on t_i on the right of equations (3.5)–(3.7) ensures the arbitrariness of that initial time. Equation (3.5) defines the density contrast $\delta_c(t)$ of peaks with $\delta(t)$ at t_i linearly extrapolated to the time t, and equation (3.7) defines the radius $q(M,t)$ of halo seeds in units of the radius $R(M,t)$ of the Gaussian filter. As shown by several authors (e.g. Hahn & Paranjape (2014)), the density contrast of density perturbations undergoing ellipsoidal collapse depends on M, while in the CUSP formalism it does not. We note however that in all those works the filter used is top-hat, while in the CUSP formalism it is Gaussian. This introduces a freedom in $R(M,t)$ associated to a given halo mass M through the function $q(M,t)$. We can

[4]This is for ideal hierarchical cosmologies with divergent rms density fluctuation at vanishing scales. If the power spectrum is truncated (e.g. below the free streaming mass of the DM particle), the normalisation should be taken equal to that of the non-truncated power-spectrum at the same large enough masses.

then chose $\delta(t)$ independent of M and let the radius of the seed in units of $R(M,t)$ to depend on M.

Note that the relation between the filtering radius R and the mass M of the final halo (equal to that of the collapsing cloud around the peak) is given by equations (3.5)–(3.6), so it is different in general from the mass of the sphere of radius R. Furthermore, a peak with δ on the top-hat filtering scale R is not the seed of a halo with the corresponding mass M at the time t. It is therefore not surprising that the mass of *top-hat* peaks may substantially deviate from those of their corresponding halos in spherical collapse; no tidal compression is actually needed to explain that difference.

As we have already seen, for halos with a well known trajectory, equation (3.21) is a Fredholm integral equation of first kind for $\delta_{\rm p}(r)$ which allows us to obtain the typical spherically averaged density profile of the protohalo. Then, bringing the profile $\rho_{\rm p}(r) = \bar{\rho}_{\rm i}[1+\delta_{\rm p}(r)]$ into equations (3.41) and (3.42), we can calculate $E_{\rm p}(M)$ and, through equation (3.40), obtain the mean spherically averaged density profile $\rho_{\rm h}(r)$ for haloes with M at t.

Each boundary condition $\delta(t_0)$ at $R = R(M_0, t_0)$ for the integration of equation (3.13) gives rise to one peak trajectory $\delta(R)$ leading to one specific density profile whose integration out to $r = R_0$ yields a value of the mass different from M_0 in general. Only one particular value of $R(M_0, t_0)$ or, equivalently, of $q(M_0, t_0)$, ensures the equality $M(R_0) = M_0$. Consequently, imposing this constraint, we can find the desired value of $q(M_0, t_0)$ for any couple of values M_0 and t_0. Note that, by changing the value of $\delta(t_0)$ the resulting value of $q(M_0, t_0)$ will change, but neither the solution $\delta(R)$ of equation (3.13) nor the associated final density profile will, so the particular value of $\delta(t_0)$ used is irrelevant at this stage. And, repeating the same procedure for different masses M_0, we can determine the whole function $q(M, t_0)$ corresponding to any arbitrary value of $\delta(t_0)$ for any given time t_0 (see Fig. 3.2).

The mean spherically averaged density profiles so predicted for current haloes with three spherical overdensity, SO($\Delta_{\rm vir}$), masses encompassing the whole mass range covered in simulations are compared, in Figure 3.3, to the best NFW fits (Navarro et al. 1997) for simulated haloes with identical masses obtained by Zhao et al. (2009). The deviations observed are typically less than 10 %. Only at the outermost radii in the less massive halo, where the density profile of simulated haloes is the most uncertain, do they reach 30 %. Given the absence of any free parameter in the theory, the agreement found over 4 decades in mass and two decades in radii

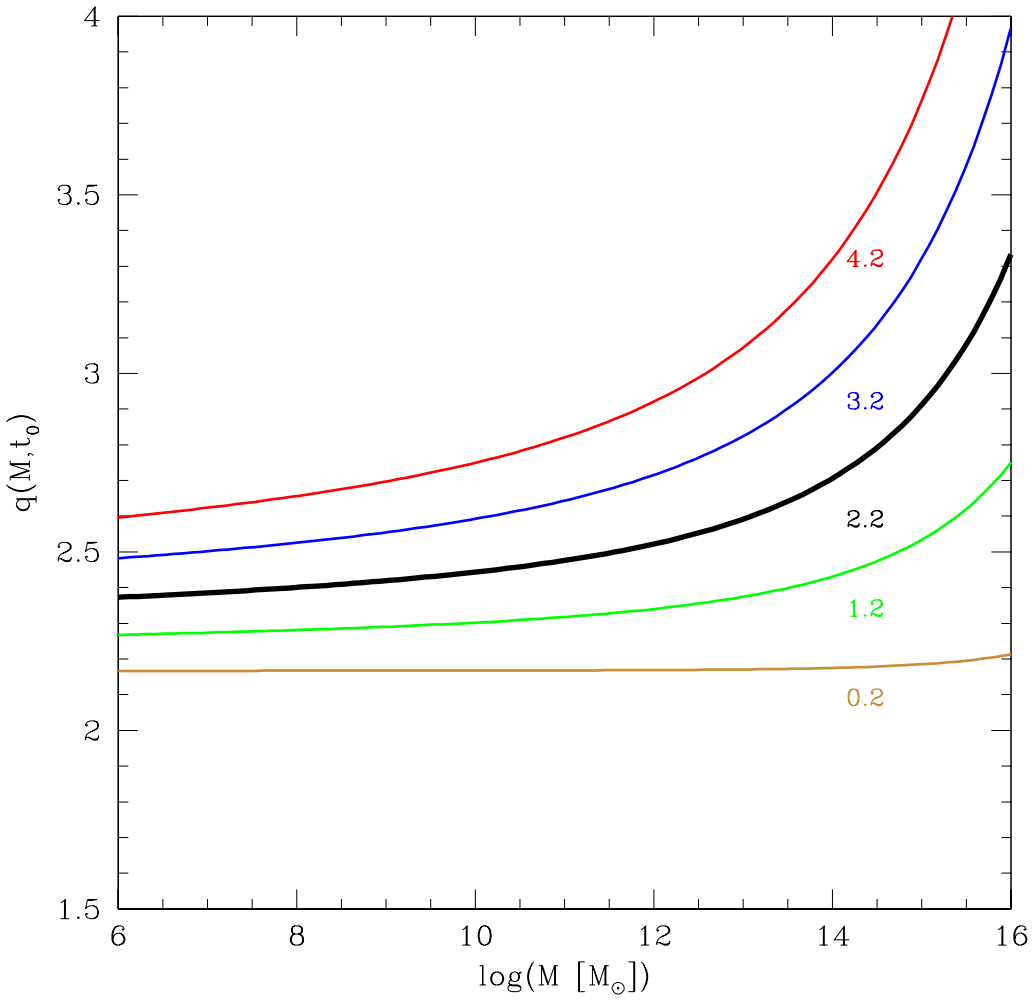

Figure 3.2: Radius of seeds, in units of Gaussian filtering radius, of present haloes with SO($\Delta_{\rm vir}$) masses (solid lines) and Friends of Friends, FoF(0.19), masses (dashed lines) for the quoted values of $\delta(t_0)$. The two kinds of curves fully overlap, but this is not the case for any arbitrary mass definition. The thick black line is for the value of $\delta(t_0)$ yielding the right normalisation of the associated MF.

is remarkable.

The previous result refers to the mean halo density profile. A scatter is expected arising from that in individual peak trajectories (due to the scatter in x at each R), added to the scatter in the peak ellipticity and density slope. In fact, an "assembly

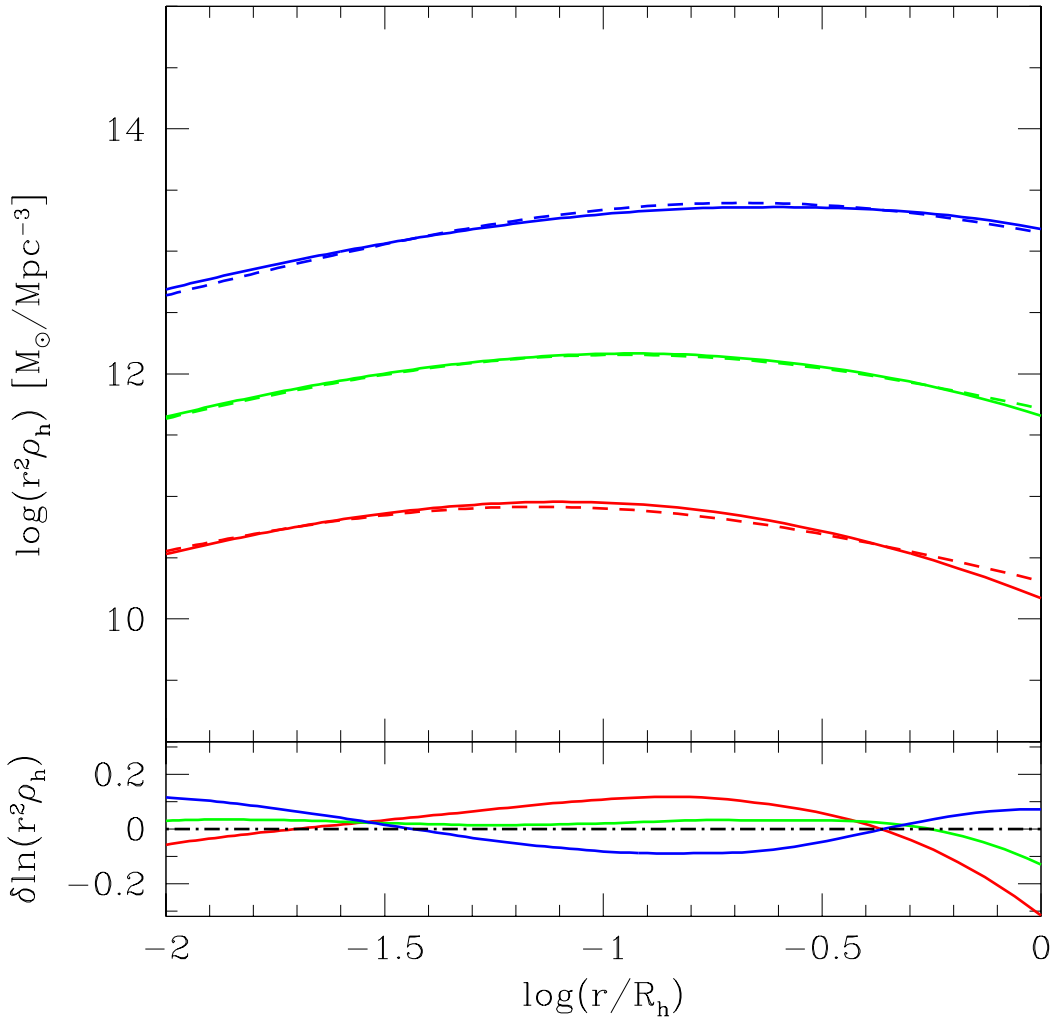

Figure 3.3: Typical spherically averaged density profiles (solid lines) predicted for current haloes with SO(Δ_{vir}) masses equal to 5×10^{10} $M_\odot$(red), 5×10^{12} $M_\odot$(green) and 5×10^{14} $M_\odot$(blue), compared to the typical NFW profiles of simulated haloes (dashed lines) with identical masses and the same cosmology according to Zhao et al. (2009).

bias" is foreseen as the peak trajectory $\delta(R)$ of individual haloes will slightly deviate from the average peak trajectory and, consequently, the final density profile of individual haloes and the time at which they reach a given mass fraction will slightly depend on their mass aggregation history.

In order to find the correct value for $\delta(t_0)$, we need to impose another condition. As we have already said, in Manrique & Salvador-Solé (1995), the CUSP mass function was fitted to the PS one in orther to find the proper values of the parameters. However, if one uses the normalization of the mass function, one can rigorously find the proper value and time dependence of $\delta(t_0)$, giving the CUSP formalism full predictive power. See Section 3.4 for the detailed explanation on how the CUSP formalism can be used in order to compute the halo mass function and how to correct the nesting effect.

Using this prescription, every function $q(M, t_0)$ obtained above for each value of $\delta_c(t_0)$ will give rise to one possible MF, although not necessarily satisfying the right normalisation condition

$$\bar{\rho} = \int_0^\infty M(R)\, N^{\rm nest}(R, \delta)\, {\rm d}R\,. \tag{3.8}$$

Thus, imposing this constraint, we can determine the right value of $\delta_{\rm c}(t_0)$ and the corresponding function $q(M, t_0)$. And repeating the same procedure at any time t, we can determine the whole functions $\delta_{\rm c}(t)$ and $q(M, t)$.

The MF for FoF(0.19) or SO($\Delta_{\rm vir}$) masses is compared in Figure 3.4 to the MFs of simulated FoF(0.2) haloes at three redshifts encompassing the interval studied by Lukić et al. (2007). Once again, there is overall agreement, particularly if we directly compare the theoretical predictions with the empirical data. Peaks with very low ν's will often be disrupted by the velocity shear caused by massive neighbours. But peaks suffering such strong tides will be nested, so they will not counted in the MF. This explains why the theoretical MF is well-behaved even at small masses.

For FoF(0.2) or more exactly FoF(0.19) masses, the functions $\delta_{\rm c}(t)$ and $q(M, t)$ are found to be identical to those for SO($\Delta_{\rm vir}$) masses. Generally, for any given cosmology and mass definition, one can write

$$\delta_c(t) = \delta_c^{\rm th}(t)\frac{a^d(t)}{D(t)} \tag{3.9}$$

$$\sigma_0(M, t) = \sigma_0^{\rm th}(M, t) + \left\{s_0 + s_1 a(t) + \log\left[\frac{a^{s_2}(t)}{1 + a(t)/a_1}\right]\right\}\delta(t). \tag{3.10}$$

where $a(t)$ is the cosmic scale factor, $\delta_c(t)$ is the density contrast for spherical collapse at t and $\sigma_0^{\rm th}(M, t)$ is the top-hat 0th order linear spectral moment at t. The

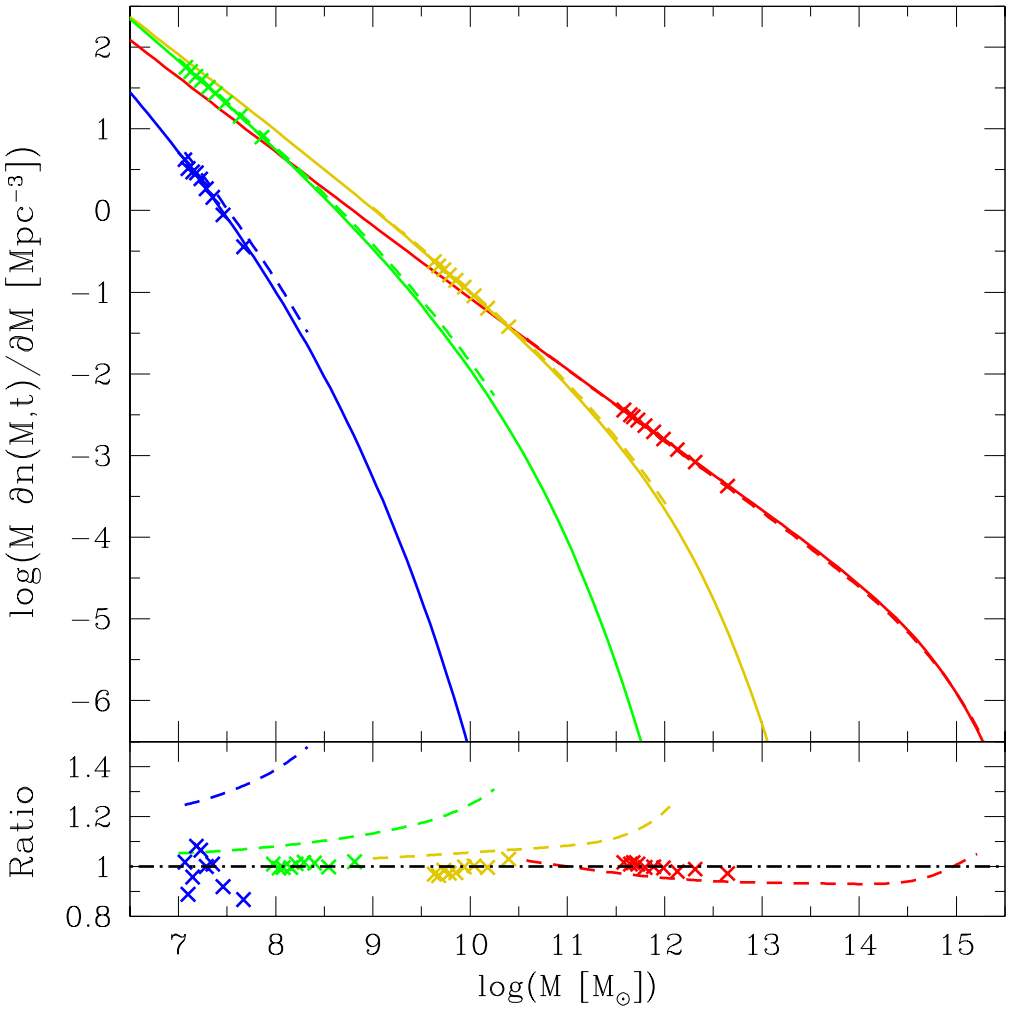

Figure 3.4: MFs predicted for haloes with FoF(0.2) masses (solid lines), compared to Warren et al. (2006) analytic fits to the MFs of simulated haloes (dashed lines) at $z = 20$ (blue lines), 10 (green lines), 5 (yellow lines) and 0 (red lines), from left to right. The dashed curves cover the ranges analysed in simulations. The ratios in the bottom panel are with respect to the theoretical predictions. Points are the raw data obtained by Lukić et al. (2007) in simulations with box sizes around $\sim 128(1+z)^{-1}$ Mpc/h giving the best common resolution at all z's.

values of the coefficients d, s_0, s_1, s_2 and a_1 can be found on Table 3.1.

From the relation (3.10) and assuming a linear power spectrum $P(k)$ equal to

Table 3.1: Coefficients in the halo-peak correspondence.

Cosmology	Mass	d	s_0	s_1	s_2	a_1
Planck14[a]	$M_{\rm vir}$	0.928	0.0226	0.0610	0.0156	11.7
	M_{200}	0.928	0.0341	0.0684	0.0239	6.87
WMAP7[b]	$M_{\rm vir}$	1.06	0.0422	0.0375	0.0318	25.7
	M_{200}	1.06	0.0148	0.0630	0.0132	12.4

[a] Planck Collaboration et al. (2014)
[b] Komatsu et al. (2011)

a power law with spectral index equal to the effective one, $n(M)$, one can infer a simple approximation for the value of $q(M,t)$

$$q(M,t) \approx \left[Q(M)\frac{\sigma_0^{\rm th}(M,t)}{\sigma_0(M,t)}\right]^{-2/[n(M)+3]}, \tag{3.11}$$

where $Q(M)$ is defined as

$$Q^2(M) = \frac{\int_0^\infty {\rm d}x\, x^{2+n(M)}\, W_{\rm G}^2(x)}{\int_0^\infty {\rm d}x\, x^{2+n(M)}\, W_{\rm TH}^2(x)}, \tag{3.12}$$

and $W_{\rm TH}(x)$ and $W_{\rm G}(x)$ are the Fourier transforms of the top-hat and Gaussian windows of radius x/k, respectively. This means that for the CDM spectrum both n and Q depend slightly on M. However, $q(M,t)$ is only needed to calculate $\sigma_0(M,t)$, which can be readily inferred from the well-known value of $\sigma_0^{\rm th}(M,t)$ from the exact relation (3.10).

Now that we have fixed the one-to-one correspondance between halos and peaks using simple consistency arguments and have checked that the predictions of the CUSP formalism are in full agreement with those of simulations for two ΛCDM cosmologies, we will use this formalism to study further properties of halos and make some predictions of halo properties.

3.3 Peak Trajectories

The existence of the halo-peak one-to-one correspondence ensures the possibility to monitor halo clustering (via accretion and major mergers)[5] by means of the Gaussian filtering evolution of peaks in the δ–R plane. The fact that there is *at most* one peak at the immediate vicinity (i.e. at a distance $r \lesssim \Delta R$) from a peak at scale R when the scale is increased form R to $R + \Delta R$ with $\Delta R \ll R$ (Manrique & Salvador-Solé 1995) ensures the possibility to identify the peak tracing a given halo on infinitesimally contiguous scales, even though the exact location of peak varies with scale.

3.3.1 Peak Trajectories

The series of peaks tracing accreting halos describe continuous $\delta(R)$ trajectories in the δ–R plane.

Given the relation (3.1) and the definition of peak curvature, the trajectory $\delta(R)$ tracing a halo with M_0 at t_0 accreting at the typical (mean) instantaneous rate is the solution of the differential equation (Manrique & Salvador-Solé 1995)

$$\frac{\mathrm{d}\delta}{\mathrm{d}R} = -x_{\mathrm{e}}(\delta, R)\, \sigma_2(R) R\,, \tag{3.13}$$

for the boundary condition $\delta(t_0)$ at $R(M_0, t_0)$, where $x_{\mathrm{e}}(\delta, R)$ is the inverse of their mean inverse curvature, $\langle\!\langle 1/x \rangle\!\rangle^{-1}$ of peaks with δ at R. Given the sharply peaked curvature distribution, $x_{\mathrm{e}}(\delta, R)$ is in practice essentally equal to the mean curvature $\langle\!\langle x \rangle\!\rangle(R, \delta)$ calculated in BBKS.

The relations $\delta(t)$ and $R(M, t)$ (eqs. [3.5] and [3.6]) allow one to calculate the instantaneous mass accretion rate, $\mathrm{d}M/\mathrm{d}t$, of halos with M at t from the R-derivative of δ of their corresponding peaks. In particular, according to the definition of x_{e}, the derivative $\mathrm{d}R/\mathrm{d}\delta$ given by equation (3.13) yields the typical (mean) mass accretion rate of halos with M at t.

Taking into account that, for low and moderately high peaks as corresponding to ordinary halos, $\langle\!\langle x \rangle\!\rangle(R, \delta)$ is well-approximated by $\gamma\nu$, where γ is $\sigma_1^2/(\sigma_0\sigma_2)$, being σ_{j} the jth spectral moment (BBKS, equation 2.88), equation (3.13) leads to the

[5] We distinguish between minor mergers contributing to the smooth growth of the most massive partner without destroying it, the so-called accretion, and major mergers producing its destruction.

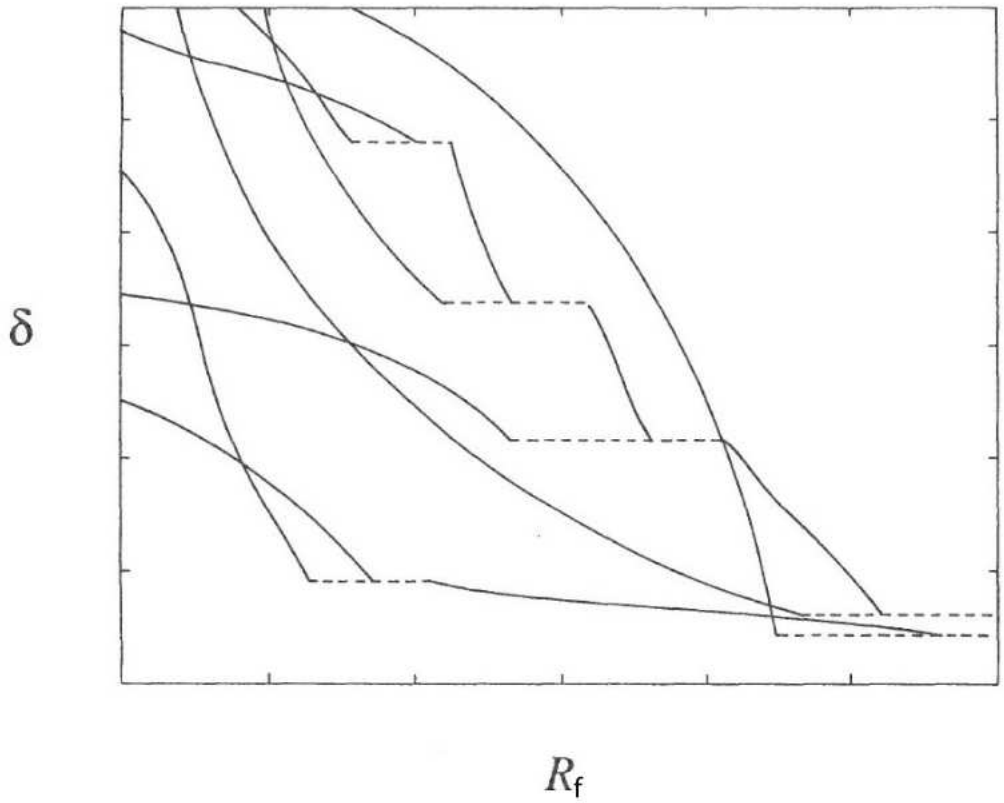

Figure 3.5: Idealized confluent system of peak trajectories for a limited sample volume. Solid lines represent the continuous filtering evolution of peaks undergoing accretion. Dashed lines represent the discontinuities caused by major mergers (figure from Manrique & Salvador-Solé 1995).

approximate relation

$$\frac{\mathrm{d}\ln\delta}{\mathrm{d}\ln R} \approx -\left(\frac{n+3}{2}\right)^{3/2}, \tag{3.14}$$

where n is the effective spectral index, $P(k) \propto k^n$. This demonstrates that the typical peak trajectory tracing purely accreting halos is roughly universal, i.e. very similar for all halo masses, redshifts and cold dark matter cosmologies.

In major mergers, the continuous peak trajectories $\delta(R)$ tracing the evolution by accretion of merging halos are *interrupted*[6] and a new peak *appears*[7] with the same δ as the disappeared peaks, but on a larger scale R corresponding to the sum of the masses of the progenitors (Manrique & Salvador-Solé 1995).

[6] At $R + \mathrm{d}R$, there is no peak at the immediate vicinity of the peak at R.
[7] At $R - \mathrm{d}R$, there is no peak at the immediate vicinity of the peak at R.

Major mergers are the only events where peak trajectories are interrupted and new trajectories arise, the peak trajectory interruption and appearance rates thus measure the halo destruction and formation rates through major mergers. The calculation of those rates involves the peak-peak correlation. A practical estimate of such a correlation, also useful for the calculation of peak nesting and halo substructure among other quantities, is given in (Manrique et al. 1998).

3.3.2 Subhalos and Nested Peaks

Since there is no destruction (or appearance of) peak trajectories when a halo is accreted by another more massive one, those peaks tracing halos accreted onto a more massive one necessarily become nested "in the collapsing cloud around the corresponding peak", or simply "in the corresponding peak". On the other hand, when two halos suffer a major merger, even though their peak trajectories are interrupted, those of their respective nested peaks are not, so they become nested in the new peak resulting from the merger.

This process of peak nesting truthfully traces the process of halo nesting taking place in real DM clustering. Indeed, in accretion, less massive halos (with higher concentrations) become first-level (second-level,...) subhalos of the accreting halo at the same time that their own first-level clumps become second-level ones, and so on. And, in major mergers of similarly massive halos (with similar concentrations), the merging objects meld but their respective first-level (second-level,...) subhalos survive as such in the new halo resulting from the merger.

3.4 Halo Mass Function and Subhalo Abundance

To infer the mass function of virialised halos at t and the abundance of first-level (second-level,...) subhalos in halos with M at t we can thus simply compute the comoving number density of non-nested peaks with δ per infinitesimal scale R in the density field at $t_{\rm i}$ and the number of first-level (second-level,...) peaks with δ nested in non-nested peaks with δ at R, respectively.

3.4.1 Non-Nested Peak Number Density

The number density of peaks with δ at scales between R and $R+{\rm d}R$ is the number density of peaks at scale R with density contrast $\tilde{\delta}$ greater than δ that cross such

a density contrast when the scale is increased to $R + \mathrm{d}R$ or, equivalently, with δ satisfying the condition

$$\delta < \tilde{\delta} \leq \delta + \sigma_2(R)\,\tilde{x}\,R\,\mathrm{d}R\,. \tag{3.15}$$

Therefore, it is simply the integral of the density of peaks with infinitesimal height $\tilde{\nu} = \tilde{\delta}/\sigma_0(R)$ and curvature $\tilde{x}$, $\mathcal{N}_{\rm pk}(\tilde{\nu}, \tilde{x}, R)\,\mathrm{d}\tilde{\nu}\,\mathrm{d}\tilde{x}$, calculated by BBKS, over the range (3.15) of $\tilde{\delta}$ and all possible $\tilde{x}$. The result is Manrique & Salvador-Solé (1995)

$$N_{\rm pk}(R,\delta)\,\mathrm{d}R = \frac{\langle\!\langle x \rangle\!\rangle(R,\delta)}{(2\pi)^2 R_\star^3}\,\exp\left(-\frac{\nu^2}{2}\right)\,\frac{\sigma_2(R)}{\sigma_0(R)}\,R\,\mathrm{d}R\,, \tag{3.16}$$

where $\nu' = \nu + [\sigma_2(R)/\sigma_0(R)]R\mathrm{d}R$ and $R_\star = \sqrt{3}\,\sigma_1/\sigma_2$.

But number density (3.16) refers to *all* peaks with δ between R and $R + \mathrm{d}R$, while virialised halos correspond to non-nested peaks only. We must thus correct that density for nesting. The number density of *non-nested* peaks with δ between R and $R + \mathrm{d}R$, $N(R,\delta)\mathrm{d}R$ is the solution of the Volterra integral equation

$$\begin{aligned} N(R,\delta) &= N_{\rm pk}(R,\delta) \\ &\quad -\frac{1}{\bar{\rho}(t_{\rm i})}\int_R^\infty dR' M(R')\,N(R',\delta)\,N_{\rm pk}^{\rm nest}(R,\delta|R',\delta). \end{aligned} \tag{3.17}$$

The comoving density (5.12) of peaks with δ is thus equal to the (differential) comoving mass function of halos at t. In Chapter 5 we will give a deeper insight on the halo mass function.

3.4.2 Abundance of Peaks Nested in another Peak

Following the same procedure from the conditional density of peaks with infinitesimal $\tilde{\nu}$ and $\tilde{x}$ at R subject to being located in peaks with ν' at R', $\mathcal{N}(\tilde{\nu}, \tilde{x}, R|\nu', R')\mathrm{d}\tilde{\nu}\mathrm{d}\tilde{x})$ calculated by BBKS, we can also compute the conditional number density of peaks with δ at scales between R and $R + \mathrm{d}R$ subject to being nested in non-nested peaks with δ' at R' Manrique et al. (1998). The result is

$$\begin{aligned} &N(R,\delta|R',\delta')\mathrm{d}R\,\mathrm{d}R' \\ &\quad = N_{\rm pk}^{\rm nest}(R,\delta|R',\delta')\,\mathrm{d}R\,N(R',\delta')\,\frac{M(R')}{\bar{\rho}(t_{\rm i})}\,\mathrm{d}R', \end{aligned} \tag{3.18}$$

where $M(R')/\bar{\rho}(t_{\rm i})$ is the volume of the collapsing cloud of peaks with δ' at R'.

Then, the total number of *first-level* peaks with δ at scales greater than $R_{\rm s}$ nested in a non-nested peak with δ at scale R is (see Chapter 5)

$$\mathcal{N}(>R_{\rm s},\delta|R,\delta)=\frac{M}{\bar{\rho}(t_{\rm i})}\int_{R_{\rm s}}^{R}{\rm d}R'\Big\{N_{\rm pk}^{\rm nest}(R',\delta|R,\delta) - \int_{R'}^{R}{\rm d}R''N_{\rm pk}^{\rm f\,nest}(R',\delta|R'',\delta)N_{\rm pk}^{\rm nest}(R'',\delta|R,\delta)\,\frac{M(R'')}{\bar{\rho}(t_{\rm i})}\Big\}, \tag{3.19}$$

where the integral over R' on the right corrects the number density of peaks nested in the peak with δ at R for nesting in peaks with δ at intermediate scales between $R_{\rm s}$ and R so to ensure that only first-level nested peaks are counted and the function $N_{\rm pk}^{\rm f\,nest}(R',\delta|R'',\delta)$, solution of the Volterra integral equation

$$N_{\rm pk}^{\rm f\,nest}(R',\delta|R'',\delta)\equiv N_{\rm pk}^{\rm nest}(R',\delta|R'',\delta) -\int_{R'}^{R''}{\rm d}R'''N_{\rm pk}^{\rm nest}(R',\delta|R''',\delta)N_{\rm pk}^{\rm f\,nest}(R''',\delta|R'',\delta)\frac{M(R''')}{\bar{\rho}(t_{\rm i})}, \tag{3.20}$$

is the conditional number density of peaks with δ at R' subject to be *directly* nested in peaks with δ at R''. This ensures that the correction for intermediate nesting is not over-counted.

Given that first-level subhalos with masses greater than $M_{\rm s}\equiv M(R_{\rm s},t)$ in a halo with M at t are traced by first-level peaks with $\delta=\delta(t)$ at scales greater than $R_{\rm s}=R(M_{\rm s},t)$ nested in the non-nested peak with $\delta=\delta(t)$ and $R=R(M,t)$, their abundance $\mathcal{N}(>M_{\rm s},t)$ is equal to the corresponding abundance of nested peaks, $\mathcal{N}(>R_{\rm s},\delta|R,\delta)$, given by equation (3.19). Needless to say that the abundance of subhalos of any other level can be derived in a similar way from the corresponding abundance of nested peaks. However, the higher the nesting level, the more complicate the calculation.

Actually, since accreted halos are truncated by the host potential well, their masses change when they become subhalos. For this rerason, the subhalo abundance given by equation (3.19) is right provided subhalo masses are estimated by means of the *maximum circular velocity*, $V_{\rm max}$, which is stable against truncation. To express it as a function of the real truncated mass we should take into account for truncation whose strength depends on the properties of the host halo.

3.5 Protohalo Properties

The properties of halos depend on those of their *unconvolved* seeds, i.e. the collapsing clouds around their corresponding peaks, hereafter simply protohalos. To distinguish from now on between the properties of protohalos and halos we denote them with subscripts p and h, respectively.

The velocity field in the protohalo is due to the perturbed Hubble-flow. Consequently, to fully characterise protohalos we only need their spherically averaged density, ellipticity and prolateness unconvolved profiles, which must be inferred from the height, curvature, ellipticity and prolateness of the peaks. Certainly, peaks refer to the filtered density field and the filtering (convolution) with a Gaussian window yields some loss of information, so the deconvolution of those peak properties may seem unfeasible. Actually, *for purely accreting halos*, we know the whole series of peaks on different scales along the corresponding $\delta(R)$ trajectory, which, as we will see, is enough to achieve the desired deconvolutions.

When the protohalo on a scale slightly larger than that of a given halo has only collapsed along the two first axes, the collapse along the third one will be seen as accretion along a filament, as often found in simulations (e.g. Dekel & Birnboim (2006)). Since no statement is made in the CUSP formalism on how isotropic accretion must be, such an extremely anisotropic accretion is accounted for.

3.5.1 Spherically Averaged Density Profile

As mentioned, the exact location of peaks along the trajectory traced by a purely accreting halo may vary with R. However, we have the right to re-locate the origin of the coordinate system at every R on the peak. Then, the density contrast δ at $\mathbf{r} = 0$ along the $\delta(R)$ trajectory is but the value at $\mathbf{r} = 0$ of the unconvolved density contrast field $\delta_{\rm p}(\mathbf{r})$ in the protohalo, convolved with the Gaussian window of radius R. Thus, after integration over the polar angles, we have

$$\delta(R) = \sqrt{\frac{2}{\pi}} \frac{1}{R^3} \int_0^\infty \mathrm{d}r\, r^2\, \delta_{\rm p}(r) \exp\left(-\frac{r^2}{2R^2}\right) , \tag{3.21}$$

where we have introduced the following compact notation: $F(r)$ stands for the spherical average of any function $F(\mathbf{r})$. Only in case of a product of two or more functions of $\mathbf{r}$ will the spherical average be hereafter written in angular brackets.

For halos with known $\delta(R)$ trajectory, equation (3.21) is a Fredholm integral equation of first kind for $\delta_{\rm p}(r)$, which can be solved in the way explained in Salvador-Solé et al. (2012a). In the case of halos accreting at the typical (mean) instantaneous rate, $\delta(R)$ is the typical (with mean inverse curvature at each point) trajectory solution of the differential equation (3.13). Consequently, we can readily deconvolve equation (3.21) and obtain the typical (mean) spherically averaged density profile $\delta_{\rm p}(r)$ for protohalos.

3.5.2 Ellipticity and Prolateness Profiles

The squared semiaxes of the peak with δ at R, $A_{\rm j}^2$, are defined as the second order spatial derivatives along the cartesian axes j, $\partial_{\rm i}^2$, at the peak of the filtered density contrast field $\delta_{\rm p}(\mathbf{r})$, scaled to the Laplacian so to have $A_1^2+A_2^2+A_3^2=1$. They thus satisfy the relation

$$A_{\rm i}^2 x\,\sigma_2^{-1} = \frac{-\partial_{\rm i}^2}{(2\pi R^2)^{3/2}}\left\{\int {\rm d}\mathbf{r}\,\delta_{\rm p}(\mathbf{r})\exp\left[-\frac{(\mathbf{r}-\mathbf{r}')^2}{2R^2}\right]\right\}_{\mathbf{r}'=0}. \tag{3.22}$$

Writing $\delta_{\rm p}(\mathbf{r})$ in terms of $\delta_{\rm p}(r)$ and the protohalo axis profiles $a_{\rm pj}(r)$ (see the Appendix B) and integrating over the polar angles, we arrive at (Salvador-Solé et al. 2012b)

$$\begin{aligned} &A_{\rm j}^2\left(\frac{{\rm d}\delta}{{\rm d}R},R\right)\,\frac{{\rm d}\delta}{{\rm d}R}+3\,\delta(R)\\ &=\sqrt{\frac{2}{\pi}}\frac{3}{5R^5}\int_0^\infty {\rm d}r\,r^4\delta_{\rm p}(r)\left[\frac{2a_{\rm p1}^2(r)}{a_{\rm pj}^2(r)G_{\rm p}(r)}+1\right]\exp\left(-\frac{r^2}{2R^2}\right), \end{aligned} \tag{3.23}$$

where we have taken into account that the axes $A_{\rm j}$ of peaks are well-known functions of their curvature (BBKS) and introduced the function $G_{\rm p}(r)$ defined in the Appendix B.

Hence, for peaks with known $\delta(R)$ trajectory, equation (3.23) is again a Fredholm integral equation, which can be solved in the same way as equation (3.21). In the case of halos accreting at the typical (mean) instantaneous rate, $\delta(R)$ is the solution of equation (3.21), so we can determine the typical profiles $a_{\rm p1}^2(r)/[a_{\rm pj}^2(r)G_{\rm p}(r)]$ for the three orientations j and, taking the ratios between them, we can infer the typical (mean) ellipticity and prolateness profiles (or, equivalently, eccentricity profiles; see the Appendix B for their definition) of protohalos.

3.6 The link between Halo and Protohalo

The properties of halos can be inferred from those of their protohalos thanks to the conservation of a few quantities over ellipsoidal collapse and virialisation. As we will see, these conserved quantities arise from the fact that, in ellipsoidal collapse and virialisation, there is no apocentre crossing of particles in the ellipsoidal shells (homeoids) of protohalos. This causes the *inside-out* growth of virialised halos. Such a growth will be confirmed later on (Chapter 4) against simulations.

3.6.1 "Spherical" Quantities

Given any arbitrary mass distribution, we can split the density and gravitational potential at a separation $\mathbf{r}$ from any arbitrary point, taken as origin of the coordinate system, in the sum of their spherical average and a residual

$$\rho(\mathbf{r}) = \rho(r) + \delta\rho(\mathbf{r}) \tag{3.24}$$

$$\Phi(\mathbf{r}) = \Phi(r) + \delta\Phi(\mathbf{r})\,. \tag{3.25}$$

The residual $|\delta\rho(\mathbf{r})|$ may be greater than $\rho(r)$ in some points over the sphere of radius r. But, in well-centred triaxial systems, the typical (rms) value is necessarily smaller because the minimum possible value is $-\rho(r)$ and, hence, the maximum value cannot be greater than $\rho(r)$. This implies that the quantities $\langle(\delta\rho/\rho)^2\rangle(r)$, $\langle(\delta\Phi/\Phi)^2\rangle(r)$ and $|\langle\delta\rho\delta\Phi/(\rho\Phi)\rangle(r)|$ are necessarily less than one (see Salvador-Solé et al. (2012b) for details).

Thanks to this splitting, any macroscopic quantity $X(r)$ takes the form $\mathcal{X}(r) + \delta\mathcal{X}(r)$, where $\mathcal{X}(r)$ coincides with the value of $X(r)$ were the system spherically symmetric, hence why quantities $\mathcal{X}(r)$ are dubbed "spherical", and a residual $\delta\mathcal{X}(r)$ measuring the deviation of the system "from spherical symmetry", or simply "from sphericity", necessarily smaller in absolute value than the spherical quantity (Salvador-Solé et al. 2012b).

In particular, the mass inside r,

$$M(r) = 4\pi \int_0^r \mathrm{d}\tilde{r}\, \tilde{r}^2\, \rho(\tilde{r})\,, \tag{3.26}$$

takes the form $M = \mathcal{M} + \delta\mathcal{M}$, with $\delta\mathcal{M}$ null. In turn, the total energy inside r,

$E(r)$, splits in the sum of

$$\mathcal{E}(r) = 4\pi \int_0^r \mathrm{d}\tilde{r}\, \tilde{r}^2\, \rho(\tilde{r}) \left[\frac{s^2(\tilde{r})}{2} - \frac{GM(\tilde{r})}{\tilde{r}} \right] \tag{3.27}$$

and

$$\delta\mathcal{E}(r) = 2\pi \int_0^r \mathrm{d}\tilde{r}\, \tilde{r}^2 \frac{\delta s^2(\tilde{r})}{2} + \langle \delta\rho\, \delta\Phi \rangle(\tilde{r})\,, \tag{3.28}$$

where G is the gravitational constant and $s^2(r)$ is a velocity variance, different in general from the real velocity variance, $\sigma^2(r)$, through the non-null residual $\delta s^2 \equiv \sigma^2(r) - s^2(r)$. Indeed, the spherical total energy, $\mathcal{E}(r)$, is taken equal to the total energy of the sphere with $M(r)$, accounting for the energy lost by shell-crossing (if any), but without including any possible gravitational energy exchange between the sphere and the rest of the system due to non-sphericity (it is instead included in the residual δs^2).

If the system is, in addition, in equilibrium, the steady collisionless Boltzmann equation leads to the virial relation Salvador-Solé et al. (2012b)

$$\frac{2\mathcal{E}(r)}{\mathcal{W}(r)} = 1 - \mathcal{S}(r)\,, \tag{3.29}$$

where

$$\mathcal{W}(r) = -4\pi \int_0^r \mathrm{d}\tilde{r}\, \tilde{r}^2\, \rho(\tilde{r})\, \frac{GM(\tilde{r})}{\tilde{r}} \tag{3.30}$$

and

$$\mathcal{S}(r) = 4\pi r^3 \rho(r)\, s_\mathrm{r}^2(r) \mathcal{W}^{-1}(r) \tag{3.31}$$

are respectively the spherical potential energy and spherical surface term, being $s_\mathrm{r}^2(r)$ the spherical radial velocity variance, equal to its ordinary counterpart $\sigma_\mathrm{r}^2(r)$ minus the residual

$$\delta s_\mathrm{r}^2(r) = \frac{1}{r^3\rho(r)} \int_0^r \mathrm{d}\tilde{r}\, \tilde{r}^2 \left[\delta s^2(\tilde{r}) - \tilde{r} \langle \delta\rho\, \partial_\mathrm{r} \delta\Phi \rangle(\tilde{r}) \right] . \tag{3.32}$$

Differentiating equations (3.26), (3.27) and (3.29), we arrive at the relations

$$\rho(r) = \frac{1}{4\pi r^2} \frac{\mathrm{d}M}{\mathrm{d}r}\,, \tag{3.33}$$

$$s^2(r) = 2 \left[\frac{\mathrm{d}\mathcal{E}/\mathrm{d}r}{\mathrm{d}M/\mathrm{d}r} + \frac{GM(r)}{r} \right], \tag{3.34}$$

and

$$s_{\rm r}^2(r) = \frac{2\mathcal{E}(r) - \mathcal{W}(r)}{r\,{\rm d}M/{\rm d}r}\,, \tag{3.35}$$

identical to the relations resulting for spherically symmetric systems with $E = \mathcal{E}$ and $W = \mathcal{W}$. Since these relations hold regardless of the exact deviation from sphericity, the profiles $\rho(r)$, $s^2(r)$ and $s_{\rm r}^2(r)$ cannot depend on the shape of the system, contrarily to the profiles $\sigma_{\rm h}^2(r)$ and $\sigma_{\rm rh}^2(r)$ (see eqs. [3.28] and [3.32]).

3.6.2 Conserved Quantities

In the linear regime, collapsing clouds expand radially through a factor $D(t)$ and, hence, homothetically, without any shell-crossing nor energy exchange between different regions. This ensures that homeoids reach turn-around orderly. After reaching turn-around, shells collapse non-radially (and non-homothetically) and, since DM is collisionless, they rebound and cross other infalling shells. The consecutive shell-crossing near pericentre and apocentre between any couple of shells with correlated oscillatory phases yields a net energy transfer from the shell having reached apocentre first to that having reached it later.

The energy lost in one orbit by particles in a homeoid is small, so the characteristic time of their apocentre decay is greater than the orbital period. Consequently, even though particles in that homeoid do not reach next apocentre simultaneously, they still define an apocentre locus which, for symmetry reasons, is also triaxial. Repeating the same reasoning as many times as required, we are led to the conclusion that particles in a homeoid at turnaround define a triaxial apocentre locus that progressively shrinks and varies its ellipticity and prolateness (or eccentricities; see the Appendix B). As a consequence, an energy flux is set from the old inner to the new outer homeoids of the system with its consequent contraction together with an increasing, circularisation of individual particle orbits. When the random shell-crossing causes the oscillatory phase of a shell to become uncorrelated from those of all the remaining shells, it stops contracting or, equivalently, it virialises.

Even though, neither the total energy E inside spheres of fixed mass M nor the eccentricities $e_{\rm p}$ and $e_{\rm s}$ of homeoids are conserved over collapse and virialisation, the following quantities are (Salvador-Solé et al. 2012b):

i) *The mass of ellipsoids.* Apocentre loci evolve (shrink) orderly without crossing each other. If two of them did intersect, particles at that point, with null radial

velocity, would always coincide at their respective apocentres, so the two apocentre loci would always intersect, which would contradict the fact that homeoids reaching turnaround are homothetic to the *non-intersecting* isodensity contours in the protohalo. Consequently, the mass inside those triaxial apocentre loci is conserved from t_i to t. Moreover, since particles stay much of the time at their apocentres, a good estimate of $\rho_\mathrm{h}(r)$ consists of considering all particles at their respective ellipsoidal apocentre loci. We thus have

$$M_\mathrm{h}(r) = M_\mathrm{p}(r_\mathrm{p})\,, \tag{3.36}$$

where $r_\mathrm{p}(r)$ is the radius of the ellipsoid in the protohalo (see Appendix B for its definition) evolving into to the ellipsoid of radius r in the halo.

ii) *The ellipsoid to sphere volume ratio.* To leading order in the deviation from sphericity, the volume of the ellipsoid with a given mass does not depend on its triaxial shape. Consequently, the ratio between the volumes of the ellipsoid and the sphere of the same mass is conserved, to leading order, from t_i to t,

$$\frac{a_\mathrm{h1}(r)\,a_\mathrm{h2}(r)\,a_\mathrm{h3}(r)}{a_\mathrm{p1}(r_\mathrm{p})\,a_\mathrm{p2}(r_\mathrm{p})\,a_\mathrm{p3}(r_\mathrm{p})} = \frac{r^3}{r_\mathrm{p}^3}\,. \tag{3.37}$$

iii) *The spherical to ordinary total energy ratio.* To leading order in the deviation from sphericity, E and $\mathcal{E}$ coincide, in spheres of any given mass. Indeed, the energy loss through shell-crossing is accounted for in both quantities. (Only the gravitational energy exchange due to triaxiality is not accounted for in $\mathcal{E}$ while it is in E.) Consequently, the ratio $E/\mathcal{E}$ is conserved to leading order from t_i to t. This conservation has two consequences.

First, the equality $E = \mathcal{E} + \delta\mathcal{E}$ then implies, to leading order,

$$\frac{\mathcal{E}_\mathrm{h}(r)}{\mathcal{E}_\mathrm{p}(r_\mathrm{p})} = \frac{\delta\mathcal{E}_\mathrm{h}(r)}{\delta\mathcal{E}_\mathrm{p}(r_\mathrm{p})}\,. \tag{3.38}$$

Second, since $\mathcal{E}$ does not depend on the shape of the system, it must be the same in a triaxial as in a spherically symmetric system with identical mass profile. The non-radial motion produced in the non-linear evolution of a triaxial system must thus cause a transfer from the radial to the tangential kinetic energy in parallel to a departure of the gravitational potential from its spherically symmetric counterpart without altering, to leading order, the total energy found in the spherically symmetric system. In other words, the fractional velocity variance transferred from the

radial to the tangential direction (equal to half the fractional 1-D tangential velocity variance generated) must be equal, to leading order, to half the typical fractional deviation of the potential from its spherical average, implying

$$\frac{\sigma_{\rm th}^2(r)}{\sigma_{\rm h}^2(r)} = \left\langle \left(\frac{\delta\Phi_{\rm h}}{\Phi_{\rm h}} \right)^2 \right\rangle^{1/2} (r) \,. \tag{3.39}$$

We stress that the conservation relations ii and iii are only satisfied to leading order. But this is enough to determine the triaxiality and kinematics of the halo to the same order.

3.7 Halo Properties

In the present Section, we derive the properties of halos from those of protohalos, i.e. the unconvolved spherically averaged density and ellipticity and prolateness (or primary and secondary eccentricity) profiles derived in Section 3.5. This derivation makes use of the link between the inner properties of protohalos and halos that arises from ellipsoidal collapse and virialisation. It is independent of how the properties of the protohalo (i.e. the collapsing cloud around a peak) are derived. That is, we do not need the halo to evolve by pure accretion. It may have undergone major mergers as well, provided, of course, the properties of the protohalo can also be inferred in that case from the peak characteristics (see Sec. 3.8).

3.7.1 Spherically Averaged Density Profile

As apocentre loci never cross each other in ellipsoidal collapse and virialisation, when a shell stabilises, it is necessarily located outside all previously stabilised loci.

Taking profit of that growth and of the fact that the turnaround radii of homeoids increase with increasing time, we can *virtually* move one after the other the layers reaching turnaround without any crossing in order to match the corresponding apocentres in the final halo inside any fixed radius r.[8] The spherical total energy profile of this toy object, $\widetilde{\mathcal{E}}_{\rm h}(r)$ will differ, of course, from the real total energy $\mathcal{E}_{\rm h}(r)$ of the halo because the latter includes the energy loss by shell-crossing, while the toy object has been built with no shell-crossing. In fact, $\widetilde{\mathcal{E}}_{\rm h}(r)$ will be equal to the spherical total energy of the corresponding shell at turnaround or directly equal to

[8]By "virtual" motion we mean a motion that preserves the particle energy and angular momentum, but not the real timing of the motion.

that of the sphere with identical mass in the protohalo, $\widetilde{\mathcal{E}}_{\rm h}(r) = \mathcal{E}_{\rm p}(r_{\rm p})$.

Another difference between the toy object and the real halo is that the toy object is not in equilibrium. But this can be arranged. As the quantity $\widetilde{\mathcal{E}}_{\rm h}(r) - \widetilde{\mathcal{W}}_{\rm h}(r)$, with $\widetilde{\mathcal{W}}_{\rm h}(r)$ equal to the potential energy of a homogeneous sphere with identical mass $M_{\rm h}(r)$, is positive,[9] we can virtually expand, one after the other, every homeoid outwards avoiding shell-crossing so as to end up with a uniform density equal to the mean density of the real halo inside r and still have an excess of spherical kinetic energy inside that radius. This kinetic energy can then be re-distributed over the sphere, exchanging the local radial and tangential components of the spherical velocity variance, $\widetilde{s}^2_{\rm h}(r)$, so as to satisfy the spherical virial relation (3.29) with null spherical radial velocity variance. In doing this, we will end up with a steady homogeneous toy object with the same total mass $M_{\rm h}(r)$ as the real halo, but a spherical total energy profile $\widetilde{\mathcal{E}}(r)$ equal to $\mathcal{E}_{\rm p}(r_{\rm p})$ and a null $\widetilde{s}_{\rm rh}(r)$ profile. This uniform toy object will thus satisfy the virial relation (eq. [3.29]) for a spherical homogeneous system, i.e. $\widetilde{\mathcal{W}}_{\rm h}(M_{\rm h}) = -3/5\, GM^2_{\rm h}/r(M_{\rm h})$, with total energy equal to $\mathcal{E}_{\rm p}(r_{\rm p})$ and null spherical surface term $\widetilde{\mathcal{S}}_{\rm h}(r)$ or, equivalently (Salvador-Solé et al. 2012a),

$$r(M_{\rm h}) = -\frac{3}{10}\,\frac{GM^2_{\rm h}}{\mathcal{E}_{\rm p}(M_{\rm h})}\,. \tag{3.40}$$

Note that the inside-out growth of halos leads to the same virial relation as in the simple homogeneous spherical collapse model, the *spherical* total energy being also conserved despite the energy lost by shells during virialisation.

Equation (3.40), satisfied by collisionless systems having undergone ellipsoidal collapse and virialisation regardless of their triaxial shape, fixes the mass profile $M_{\rm h}(r)$ of halos from the spherical total energy $\mathcal{E}_{\rm p}(M_{\rm p} = M_{\rm h})$ of their corresponding protohalos with density profile $\rho_{\rm p}(r) = \bar{\rho}(t_{\rm i})[1+\delta_{\rm p}(r)]$, given in the parametric form by

$$\mathcal{E}_{\rm p}(r_{\rm p}) = 4\pi\int_0^{r_{\rm p}} {\rm d}r\, r^2 \rho_{\rm p}(r)\left\{\frac{[H(t_{\rm i})r - v_{\rm p}(r)]^2}{2} - \frac{GM_{\rm p}(r)}{r}\right\} \tag{3.41}$$

$$M_{\rm p}(r_{\rm p}) = 4\pi\int_0^{r_{\rm p}} {\rm d}r\, r^2\, \rho_{\rm p}(r)\,, \tag{3.42}$$

[9] At turnaround, $\widetilde{\mathcal{E}}_{\rm h}$ is equal to the potential energy of the system less concentrated than the homogeneous toy object.

where $H(t)$ is the Hubble constant and

$$v_{\rm p}(r) = \frac{2G\left[M_{\rm p}(r) - 4\pi r^3 \bar{\rho}(t_{\rm i})/3\right]}{3H(t_{\rm i})r^2} \tag{3.43}$$

is the peculiar velocity caused by the mass excess within r Peebles (1980).[10]

Once $M_{\rm h}(r)$ is known, equation (3.33) leads to the typical spherically averaged halo density profile $\rho_{\rm h}(r)$. On the other hand, as $\rho_{\rm h}(r)$, $s^2_{\rm h}(r)$ and $s^2_{\rm rh}(r)$ do not depend on the shape of the object, we can assume spherical symmetry in order to infer the latter two functions from the former one. In the spherical symmetric case, orbits are purely radial because they collapse and virialise radially, so we have $s^2_{\rm h}(r) = s^2_{\rm rh}(r)$. Then, equations (3.34) and (3.35) lead to a differential equation for $\mathcal{E}_{\rm h}(r)$ that can be readily integrated for the boundary condition $\mathcal{E}_{\rm h} = 0$ at $r = 0$, the result being

$$\mathcal{E}_{\rm h}(r) = -R \int_0^r {\rm d}\tilde{r} \left[4\pi\, \rho_{\rm h}(\tilde{r})\, G M_{\rm h}(\tilde{r}) + \frac{\mathcal{W}_{\rm h}(r)}{2\tilde{r}^2}\right] . \tag{3.44}$$

From equations (3.44) and (3.27)–(3.28), we can compute the dissipation factor by shell-crossing, $\mathcal{D}(M) \equiv \mathcal{E}_{\rm h}(M)/\mathcal{E}_{\rm p}(M)$. The form of the resulting $\mathcal{D}(r)$ profile is such that $\rho_{\rm h}(r)$ is always outwards decreasing (Salvador-Solé et al. 2012a) as a consequence of the energy lost by homeoids during virialisation.

3.7.2 Shape and Kinematic Profiles

Taking into account the relations (B.3), equation (3.37) takes the form

$$\frac{(1-\epsilon^2_{\rm h})(1-\varepsilon^2_{\rm h})}{[1+(1-\epsilon^2_{\rm h})+(1-\varepsilon^2_{\rm h})]^3}(r) = \frac{(1-\epsilon^2_{\rm p})(1-\varepsilon^2_{\rm p})}{[1+(1-\epsilon^2_{\rm p})+(1-\varepsilon^2_{\rm p})]^3}(r_{\rm p}) \,, \tag{3.45}$$

in terms of the eccentricities $e_{\rm p}(r)$ and $e_{\rm s}(r)$. On the other hand, substituting the expressions for $\delta\mathcal{E}$ (eq. [3.28]) in the halo and protohalo into equation (3.38) and differentiating it, we are led to

$$\frac{\Phi_{\rm h}(r)}{\mathcal{D}(r)}\left[\left\langle \frac{\delta\rho_{\rm h}}{\rho_{\rm h}}\frac{\delta\Phi_{\rm h}}{\Phi_{\rm h}}\right\rangle + \frac{\sigma^2_{\rm h}-s^2_{\rm h}}{\Phi_{\rm h}}\right](r) = \Phi_{\rm p}(r_{\rm p})\left\langle \frac{\delta\rho_{\rm p}}{\rho_{\rm p}}\frac{\delta\Phi_{\rm p}}{\Phi_{\rm p}}\right\rangle(r_{\rm p}) \,. \tag{3.46}$$

[10] In equation (3.43), we have taken into account that the cosmic virial factor $f(\Omega) \approx \Omega^{0.1}$ is at $t_{\rm i}$ essentially equal to one. We have also neglected the velocity dispersion of DM particles (see Salvador-Solé et al. (2012a)).

And, taking the mean crossed density-potential fluctuation as a function of the mean squared density fluctuation and the relation between this latter and the eccentricities (see the Appendix B), we arrive at

$$\left\{1-\frac{3[(1-\epsilon_{\rm h}^2)^2(1-\varepsilon_{\rm h}^2)^2+(1-\epsilon_{\rm h}^2)^2+(1-\varepsilon_{\rm h}^2)^2]}{[(1-\epsilon_{\rm h}^2)(1-\varepsilon_{\rm h}^2)+(1-\epsilon_{\rm h}^2)+(1-\varepsilon_{\rm h}^2)]^2}-S_{\rm h}\right\}(r)$$
$$=\frac{1}{U(r)}\left\{1-\frac{3[(1-\epsilon_{\rm p}^2)^2(1-\varepsilon_{\rm p}^2)^2+(1-\epsilon_{\rm p}^2)^2+(1-\varepsilon_{\rm p}^2)^2]}{[(1-\epsilon_{\rm p}^2)(1-\varepsilon_{\rm p}^2)+(1-\epsilon_{\rm p}^2)+(1-\varepsilon_{\rm p}^2)]^2}\right\}(r_{\rm p})\,, \tag{3.47}$$

where

$$U(r)\equiv\frac{\Phi_{\rm h}(r)V_{\rm p}(r_{\rm p})}{\Phi_{\rm p}(r_{\rm p})\mathcal{D}(r)V_{\rm h}(r)} \tag{3.48}$$

$$S_{\rm h}(r)=\frac{5}{2}\frac{\sigma_{\rm h}^2(r)-s_{\rm h}^2(r)}{\Phi_{\rm h}(r)}V_{\rm h}(r) \tag{3.49}$$

with $V(r)=1-\xi(r)\gamma(r)\left\{1-[1+\kappa(r)]\gamma(r)-\frac{{\rm d}\ln\gamma}{{\rm d}\ln r}\right\}$ and $\xi(r)$, $\kappa(r)$ and $\gamma(r)$ being the DM two-point correlation function and the logarithmic derivatives of the mean squared density and mean crossed density-potential fluctuation profiles, respectively.

Equations (3.45) and (3.47) show that the eccentricity profiles of halos, $\epsilon_{\rm h}(r)$ and $\varepsilon_{\rm h}(r)$, arise from those of their protohalos, $\epsilon_{\rm p}(r)$ and $\varepsilon_{\rm p}(r)$, through a relation that involves the halo velocity dispersion $\sigma_{\rm h}^2(r)$ profile (eq. [3.49]). Only at small radii is $S_{\rm h}(r)$ negligible,[11] so that, except for factor $U(r)$, equation (3.47) becomes an identity relation like equation (3.45). Interestingly, the set of algebraic equations (3.47) and (3.45) is solvable only for a very narrow range of $U(r)$ values around unity. Therefore, halo eccentricities at small radii are necessarily close to those of the protohalo at the corresponding radii (Salvador-Solé et al. 2012b). To accurately solve the problem for any r we need the closure relation between $\sigma_{\rm h}^2(r)$ and the shape of the system provided by equation (3.39).

Replacing the anisotropy profile,

$$\beta_{\rm h}(r)=1-\frac{\sigma_{\rm th}^2(r)}{\sigma_{\rm rh}^2(r)}=1-\frac{\sigma_{\rm th}^2(r)}{\sigma_{\rm h}^2(r)}\left[1-2\frac{\sigma_{\rm th}^2(r)}{\sigma_{\rm h}^2(r)}\right]^{-1}\,, \tag{3.50}$$

in the generalised Jeans equation for steady virialised objects to leading order in the

[11] $\sigma_{\rm h}^2(r)$ is always of the order of the squared circular velocity, $GM_{\rm h}(r)/r$, while $|\Phi_{\rm h}(r)|$ is much larger than $GM_{\rm h}(r)/r$ at small radii.

deviation from sphericity (Salvador-Solé et al. 2012b),

$$\frac{\mathrm{d}}{\mathrm{d}r}\left(\frac{\rho_\mathrm{h}\,\sigma_\mathrm{h}^2}{3-2\beta_\mathrm{h}}\right)+\rho_\mathrm{h}(r)\left[\frac{2\beta_\mathrm{h}(r)}{3-2\beta_\mathrm{h}(r)}\frac{\sigma_\mathrm{h}^2(r)}{r}+\frac{GM_\mathrm{h}(r)}{r^2}-\Phi_\mathrm{h}(r)\right]=0, \tag{3.51}$$

and writing the ratio $\sigma_\mathrm{th}^2(r)/\sigma_\mathrm{h}^2(r)$ as a function of the rms potential fluctuation profile (eq. [3.39]) and the latter as a function of its counterpart in the protohalo (as functions of the known typical eccentricity profiles; see the Appendix B) and the halo velocity variance profile (eqs. [3.47] and [3.49]), we arrive at a differential equation for $\sigma_\mathrm{h}^2(r)$, which can be solved for the usual boundary condition of null dispersion at infinity.[12]

The solution so found is such that the pseudo phase-space density profile is very close to the power-law form found by Bertschinger (1985) taking into account shell-crossing in a spherically symmetric system undergoing self-similar collapse. The reason for this is that, in ellipsoidal collapse and virialisation: i) the increase in the coarse-grained phase-space density is due to the phase-mixing produced by shell-crossing; ii) the inside-out growth of accreting halos makes homeoids evolve in a closely self-similar way; and iii) the tangential velocity dispersion develops from the initial radial one at the same time that there is a deviation of the gravitational energy from spherical symmetry, keeping the total spherical energy unaltered, like in spherically symmetric systems where both deviations are null (Salvador-Solé et al. 2012b).

Once $\sigma_\mathrm{h}(r)$ is known, we can compute the crossed density-potential fluctuation profile in the halo from that in the protohalo (eq. [3.46]), then the squared density and squared potential fluctuation profiles (see the Appendix B) and, from the latter, the velocity anisotropy profile, $\beta_\mathrm{h}(r)$ (eqs. [3.50]–[3.39]), as well as the eccentricity profiles, $\epsilon_\mathrm{h}(r)$ and $\varepsilon_\mathrm{h}(r)$ (eqs. [3.45] and [B.7]). As a byproduct, we can also obtain the deviation from sphericity of the gravitational potential in the halo at r.

3.8 Major Mergers

As shown in in Section 3.5, the typical properties of protohalos inferred assuming pure accretion are determined by the typical (mean) $\delta(R)$ trajectory of the associ-

[12] Inside-out growth ensures that the solution is kept unaltered as the radius increases, so we have the right to endorse the boundary condition at infinity, even though current halos do not reach that radius.

ated peaks, so the typical properties of the corresponding halos are determined by the typical (mean) accretion rate, according to their inside-out growth.

But halos often undergo major mergers where the system is brought out of equilibrium and suffers an important rearrangement, in contrast with what happens during accretion. The fact that the predictions of the CUSP formalism assuming pure accretion are in excellent agreement with the results of simulations thus seems to imply that the typical properties of halos with M at t formed in major mergers are identical, despite that rearrangement, to those of halos arising from pure accretion. In the present Section, we show that this is indeed the case and that this is a consequence of the halo-peak one-to-one correspondence in Gaussian filtering without any extra assumption.

3.8.1 Typical Protohalo

As mentioned, the link between protohalos and halos is set by ellipsoidal collapse and virialisation, regardless of the particular past aggregation history of the objects. The only difference in halos formed through pure accretion or major mergers is the properties of their respective unconvolved protohalos. In the former case, there is a smooth mass distribution giving rise to a monolithic collapse while, in the other, there is a more clumpy distribution giving rise to a hierarchical mass assembly. Is that difference compelling for the properties of the final objects?

The deconvolution of peak properties achieved in Section 3.5 for purely accreting halos taking into account the halo-peak one-to-one correspondence was carried out down to $R = 0$. However, such a deconvolution is, of course, meaningful only down to the particle size. DM particles are tiny, but they are not smoothly distributed in the protohalo. There are small-scale mass concentrations that evolve in the substructures detected in halos.[13] Consequently, that deconvolution seems to be justified only down to the size of the biggest clumps.

Actually, the only protohalo properties whose convolution characterise peaks are the *spherically averaged* density profile $\delta_{\rm p}(r)$ and the axis profiles $a_{\rm p}(r)$ (see eqs [3.21] and [3.22]) and these profiles harbour no information on the small-scale clumps present in protohalos, just on the smooth mass distribution around the corre-

[13] In fact, such mass concentrations may even harbour virialised nodes at small enough scales collapsed and virialised before $t_{\rm i}$.

sponding peaks. Indeed, following Salvador-Sole & Solanes (1993), we can scramble the position of particles over the ellipsoidal isodensity contours of the protohalo, which will automatically destroy all its small-scale clumps but conserve the ellipsoidal isodensity contours of the protohalo, and the resulting (convolved) properties of the associated peak will be the same. Therefore, the deconvolution can indeed be carried out down to $R = 0$ (more exaclty down to the size of DM particles) because the protohalo properties we need in order to infer those of halos do not depend on how clumpy the matter is around the peak. (The information on clumps is is only needed provided we want to determine the subhalo abundance.)

In these circumstances, the fact that there is only one main or two main clumps in the protohalo, implying that the final halo has formed either through accreting or through a major merger, is irrelevant for the properties of the final object. What is only needed to find those properties is the spherically averaged density and axes profiles, $\delta_{\rm p}(r)$ and $a_{\rm p,j}(r)$, respectively, of the protohalo, indistinguishable from those of the smooth (or scrambled) mass distribution around the central peak, which would lead to a virialised halo formed by pure accretion. In other words, halos arising from the ellipsoidal collapse and virialisation of peaks have identical shape, spherically averaged density and kinematics profiles, regardless of their aggregation history. (The only imprint of such a history is their substructure, which informs on the halos *assembled*, regardless of whether they have been directly accreted or they have resulted from possible major mergers, the largest objects in those events having disappeared.)

Therefore, if we are interested in the *typical* properties of halos with M at t, we have the right to consider protohalos with the tyical properties (including substructure) of a peak with suited δ and R, having the typical $\delta(R)$ trajectory (and the typical nested peaks).

3.8.2 Memory Loss

The fact that the individual or typical properties of halos with M at t do not depend on whether they have developed by pure accretion or have undergone major mergers is consistent with the idea that "virialisation is a real relaxation yielding the memory loss of the system", as assumed in previous papers. Here we have shown that such a memory loss naturally results from ellipsoidal collapse and virialisation and, since ellipsoidal collapse without shell-crossing does not lose the memory of the protohalo, virialisation (through shell-crossing) is necessarily what causes the memory loss.

We are then led to the following implication. Since halos with M at t are fully equivalent to peaks with δ at R in the density field at t_i filtered with a Gaussian window, the properties of peaks cannot harbour information either on their filtering evolution. Otherwise, we could unveil the past aggregation history of halos by looking at the filtering evolution of their corresponding peaks.

None of the properties characterising peaks at R, namely the height, curvature, ellipticity and prolateness, allows one to assess whether or not there is a peak in its immediate vicinity at an infinitesimally smaller scale. If no second order spatial derivative, $\partial_\mathrm{i}^2\delta(\mathbf{r})$, vanishes at that scale, the peak exists at the smaller scale (and the corresponding halo has formed through accretion), while, if some does, there is a saddle point at the new scale indicative of the existence of two peaks of identical density contrast at similar smaller scales (and the halo has formed in a major merger). To know the answer we would need to know all higher order spatial derivatives of the convolved density field at the peak or, equivalently, all the information on the density field on smaller scales, not just the properties of the peak.

4

Halo Growth and Evolving Density Profiles

I... a universe of atoms, an atom in the universe.
Richard Feynman

In the present Chapter, we use the CUSP formalism to analize halo growth and the evolution of density profile fits. This allows us to confirm that halos evolve inside-out, one crucial ingredient in this formalism.

The spherically averaged density profile for cold dark matter (CDM) halos plays a key role in many cosmological issues. N-body simulations provide with accurate numerical density profiles, well-fit by the multiparametric NFW (Navarro et al. 1995) and Einasto (1965) analytic expressions. However, they cover relatively small volumes with a modest dynamic range, so the validity of those fitting expressions is only ensured in a rather limited domain.

For instance, simulations reach halos with the neutralino free-streaming mass ($\sim 10^{-6}$ $M_\odot$) only at redshifts (z) of about 30 (Diemand et al. 2005; Anderhalden & Diemand 2013; Ishiyama 2014), while the calculation of the CDM annihilation signal requires the density profile of halos with that mass when they were aggregated by current halos. Similarly, galaxy formation models need the density profile of halos with ordinary masses at redshifts higher than covered by current simulations (Bullock et al. 2001; Eke et al. 2001; Neto et al. 2007; Gao et al. 2008; Zhao et al. 2009;

Muñoz-Cuartas et al. 2011; Klypin et al. 2011; Prada et al. 2012; Ludlow et al. 2013; Dutton & Macciò 2014).

On the other hand, simulations do not easily inform on how the inner structure of halos evolves. The radial mapping of particles does not enable one to ascertain to which extent they grow from the inside out because particles orbit within halos (Wang et al. 2011). While the accurate follow-up of density profiles is not conclusive either (Zhao et al. 2009; Muñoz-Cuartas et al. 2011) due to the non-perfect fit of halo density profiles by the analytic expressions above (see Section 4.3.2 for details). Likewise, the possible dependency of density profiles on halo formation time is hard to disentangle from the apparent signal due the usual formation time estimates themselves (Salvador-Solé et al. 2005; Li et al. 2008; Li 2010).

As a consequence, some authors (Manrique et al. 2003; Helmi et al. 2003; Romano-Díaz et al. 2006; Wang et al. 2011; Salvador-Solé et al. 2005, 2007; Salvador-Solé et al. 2012a) claim that, in accretion periods, halos stretch indeed inside-out (see also the recent finding by Ludlow et al. 2013, 2014), while others (Bullock et al. 2001; Wechsler et al. 2002; Zhao et al. 2003; Muñoz-Cuartas et al. 2011) maintain that the whole density profile is changing. Similarly, some authors defend the idea that density profiles depend on whether halos have undergone major mergers (Wechsler et al. 2002; Zhao et al. 2003; Lu et al. 2006; Duffy et al. 2008), while others claim it does not (Huss et al. 1999; Wang & White 2009; Salvador-Solé et al. 2005, 2007; Salvador-Solé et al. 2012a).

Since the halo merger rate or, similarly, the halo formation time seems to depend on environment (e.g. Gottlöber et al. 2001, 2002; Sheth & Tormen 2004; Fakhouri & Ma 2009a, 2009b; Hahn et al. 2009), the latter trend would cause the so-called "assembly bias" that the density profile for halos depends on their environment besides their mass. However, provided that halos grow inside-out during accretion, their density profile will depend on their accretion rate and environment even if major mergers leave no imprint in halo density profiles.

As one can see, in order to be able to make substantial progress within all these questions one cannot simply rely on improvements in N-body simulation performance; greater effort is required to find complementary information and to design more compelling tests to reveal the evolution of halo density profiles. In the following sections we will use the CUSP formalism to make those tests and understand the evolution of halo density profiles in CDM cosmologies.

4.1 The NFW and Einasto Profiles

N-body simulations show that spherically averaged density profiles for virialised halos with ordinary masses at low-z are well fit, down to one hundredth the total radius R, by the two-parameter NFW profile (Navarro et al. 1995)

$$\rho_{\rm h}(r) = \rho_{\rm s} \frac{4r_{\rm s}^3}{r\left(r + r_{\rm s}\right)^2}\,, \tag{4.1}$$

where the scale radius $r_{\rm s}$ (sometimes written r_{-2} to indicate the logarithmic slope of the density profile at this radius) or the concentration $c \equiv R/r_{\rm s}$ correlate with the total mass M or the characteristic density $\rho_{\rm s} \equiv \rho_{\rm h}(r_{\rm s})$ or the mass inside $r_{\rm s}$,

$$M_{\rm s} = 16\pi \left(\ln 2 - \frac{1}{2}\right) \rho_{\rm s}\, r_{\rm s}^3. \tag{4.2}$$

These correlations define an independent relation between typical (usually median) values of the NFW parameters. The most widely used formulations of this relationship are the $M - c$ relation (Navarro et al. 1997; Eke et al. 2001; Bullock et al. 2001; Kuhlen et al. 2005; Neto et al. 2007; Gao et al. 2008; Duffy et al. 2008; Macció et al. 2007; Macciò et al. 2008) and the $M_{\rm s} - r_{\rm s}$ relation (Zhao et al. 2003, 2009; Salvador-Solé et al. 2005, 2007). The fact that c is a decreasing function of M is interpreted as being due to the fact that less massive halos assemble at higher z, when the mean cosmic density is higher (Navarro et al. 1997; Salvador-Solé et al. 1998).

The three-parameter Einasto (1965) profile,

$$\rho_{\rm h}(r) = \rho_{\rm s} \exp\left\{-\frac{2}{\alpha}\left[\left(\frac{r}{r_{\rm s}}\right)^{\alpha} - 1\right]\right\}\,, \tag{4.3}$$

yields slightly better fits at smaller radii, down to 10^{-3}–10^{-4} the radius R (Navarro et al. 2004, 2010; Merritt et al. 2005, 2006; Prada et al. 2006; Gao et al. 2008; Diemand et al. 2008; Salvador-Solé et al. 2007; Stadel et al. 2009; Salvador-Solé et al. 2012a; Dutton & Macciò 2014). At any z, parameters $r_{\rm s}$ or c, defined as in the NFW case, also correlate with $\rho_{\rm s} \equiv \rho_{\rm h}(r_{\rm s})$ or M (Merritt et al. 2005; Gao et al.

2008; Ludlow et al. 2013; Dutton & Macciò 2014) or the mass inside $r_{\rm s}$,

$$M_{\rm s} = 2\pi \left(\frac{2}{\alpha}\right)^{1-\frac{3}{\alpha}} {\rm e}^{\frac{2}{\alpha}} \left[\Gamma\left(\frac{3}{\alpha}\right) - \Gamma\left(\frac{3}{\alpha}, \frac{2}{\alpha}\right)\right] \rho_{\rm s} r_{\rm s}^3 \,, \tag{4.4}$$

where $\Gamma(x)$ and $\Gamma(x, y)$ are the Gamma and incomplete Gamma functions, respectively.

Part of the success of the Einasto profile over the NFW profile is of course due to the extra freedom arising from the shape parameter α. Halo density profiles become increasingly steep as we move outwards. In the NFW case, the inner and outer asymptotic logarithmic slopes take fixed values, respectively equal to -1 and -3, while in the Einasto profile they depend on the value of α: the larger α, the less steep the inner asymptotic profile and the steeper the outer one (being respectively equal to zero and $-\infty$ for the largest possible value of α equal to 2; see Dutton & Macciò 2014). The price to be paid for this extra freedom is the greater number of parameters to be adjusted which causes a greater degeneracy, particularly in parameter α.

For halos with ordinary masses at low redshifts, α takes values from ~ 0.12 to ~ 0.35 (Gao et al. 2008; Ludlow et al. 2013; Dutton & Macciò 2014). The results are however very sensitive to the fitting radial range used. If the NFW and Einasto expressions fit halo density profiles well, the respective values of $r_{\rm s}$, $\rho_{\rm s}$ and $M_{\rm s}$ for halos with given values of M at t should be quite similar. Equations (4.2) and (4.4) then imply the approximate relation

$$\left(\frac{2}{\alpha}\right)^{1-\frac{3}{\alpha}} {\rm e}^{\frac{2}{\alpha}} \left[\Gamma\left(\frac{3}{\alpha}\right) - \Gamma\left(\frac{3}{\alpha}, \frac{2}{\alpha}\right)\right] \approx 8 \left(\ln 2 - \frac{1}{2}\right) \,, \tag{4.5}$$

whose solution is $\alpha = 0.256$. Certainly, as the NFW and Einasto profiles are not identical, α can deviate notably from this value. In particular, it should take values substantially less than 0.256 for halos with steep inner profiles and shallow outer ones and vice versa.

Note that, while the $M_{\rm s} - r_{\rm s}$ and, at a lesser extent, the $M_{\rm s} - \alpha$ relations involve parameters that characterise halo *inner* structure,[1] the $M - c$ and $M - \alpha$ relations

[1]Strictly, parameter α characterises the whole profile; but, since the Einasto profile fits halo density profiles better at very small radii, its value should be mostly determined by the inner structure of halos.

involve *global* properties such as M and R. For this reason, the former relations are hereafter referred to as 'internal', while the latter are referred to as 'global'.

4.2 Mass-Concentration-Shape Relations

4.2.1 Numerical Relations

In N-body simulations, halos are identified at any z by means of some halo-finding algorithm. In the Spherical Overdensity (SO) algorithm, the radius R from a density maximum encompassing a region with fixed overdensity $\Delta(z)$ with respect to the mean cosmic density, $\bar{\rho}(z)$, or the critical density, $\rho_{\rm crit}(z)$, hereafter generically denoted by $\rho_{\rm cos}(z)$, is supposed to delimit a halo with mass M given by

$$\frac{3M}{4\pi R^3} = \Delta(z)\rho_{\rm cos}(z)\,. \tag{4.6}$$

When $\Delta(z)$ is taken equal to the cosmology-dependent virial overdensity, $\Delta_{\rm vir}(z)$ (e.g. Bryan & Norman 1998; Henry 2000) and $\rho_{\rm cos}(z)$ equal to $\bar{\rho}(z)$, halo masses are usually denoted by $M_{\rm vir}$. While if Δ is taken fixed and equal to 200 and $\rho_{\rm cos}(z)$ is $\rho_{\rm crit}(z)$, then masses are usually denoted by M_{200}. In the Friends-of-Friends (FoF) percolation algorithm, halos are identified according to a linking length b in units of the mean interparticle separation, usually taken as equal to 0.2.

For those halos harbouring a large enough number of mass particles (usually $\geq$ 500) and satisfying some virialisation criteria, a discrete spherically averaged mass profile is derived by counting the mass particles in constant logarithmic radial bins around the peak-density, outwards from some fraction (usually one hundredth) of the total radius R. This mass profile or its associated density profile is then fitted to the NFW or Einasto density profiles. The fit is better if all the parameters (two or three) entering the fitting expression are adjusted freely. However, since the fit is never perfect, the mass corresponding to the analytic density profile will differ somewhat from the real mass of the object. Alternatively, one can adjust one fewer parameter by imposing the mass (or the maximum circular velocity, $V_{\rm max}$) of the halo. Another more subtle effect arising from the non-perfect fit is that the adjusted parameter values will depend slightly on the fitting radial range used.

Once the parameters have been adjusted, their median values are calculated for objects in logarithmic mass bins at every z. An alternative justified (Reed et al.

Table 4.1: Cosmological Parameters.

Cosmology	Ω_Λ	Ω_m	h	n_s	σ_8	Ω_b
Planck14	0.71	0.32	0.67	0.96	0.83	0.049
WMAP7	0.73	0.27	0.70	0.95	0.81	0.045
Millennium	0.75	0.25	0.73	1.0	0.90	0.045

2011) procedure is to fit the stacked profiles directly for halos in every logarithmic mass bin, which rather leads to the values of the parameters fitting the average density profile of halos in the mass bin. Lastly, the sampled values of the parameters are fitted by some guessed parametric function of M and z. The result is a toy model that allows one to calculate the parameter values for any desired M and z.

For the NFW profile, we will consider the toy models by Zhao et al. (2009), Muñoz-Cuartas et al. (2011) and Klypin et al. (2011), available for the same *WMAP7* cosmology (Komatsu et al. 2011) or close to it[2] (see Table 4.1), the same SO(Δ_vir) halo-finding algorithm, the same M_vir masses and the same minimum number (500) of particles in halos. The most recent toy models by Prada et al. (2012) and Dutton & Macciò (2014) give essentially the same results as those by Klypin et al. (2011) and Muñoz-Cuartas et al. (2011), respectively, but use distinct cosmologies or parametrisations (see Sec. 4.5). The only difference between those toy models arises from the different characteristics of the simulations and the virialisation criteria used and the fact that Zhao et al. (2009) and Muñoz-Cuartas et al. (2011) adjust two parameters, while Klypin et al. (2011) impose the V_max and adjust only one parameter. In all cases the fits are performed down to $R/100$.

For the Einasto profile, the only toy models available are those by Gao et al. (2008) and Dutton & Macciò (2014). They refer to the *Millennium* (Springel et al. 2005) and Planck14 (Planck Collaboration et al. 2014) cosmologies, respectively (see Table 4.1) and, even though halos are identified by means of the FoF(0.2) and the SO(Δ_vir), respectively, the masses adopted in both studies are M_{200}. In both cases, the fitting is unconstrained and it is performed on stacked density profiles of halos with at least 3000 particles, down to $5\times10^{-2}R$ in Gao et al. (2008) and on individual profiles of halos with a number of particles of the order of 10000 (the exact number depends on z; at $z=0$ it is as large as 63000), in the range $R/100$ to $1.2R_\mathrm{vir}$

[2]Klypin et al. (2011) use the *Bolshoi* cosmology and Muñoz-Cuartas et al. 2011 the *WMAP5* cosmology (Dunkley et al. 2009).

in Dutton & Macciò (2014). Ludlow et al. (2013) recently repeated the study by Gao et al. (2008) for the same cosmology, but fitting the stacked density profiles of halos with at least 6000 particles, down to $10^{-2.5}R$, and focusing on $z = 0$ where the results by Gao et al. (2008) are confirmed. Note the much higher minimum number of particles in halos adopted by these authors than that used in the NFW case with the purpose of balancing the degeneracy in the results due to the extra parameter. In any event, parameter α is poorly determined, so that Dutton & Macciò (2014) rely on the $M - \alpha$ relation reported by Gao et al. (2008).

In all figures throughout this Chapter, the mass-concentration-shape relations arising from these toy models are drawn in thick solid lines over the mass ranges covered by the original simulations and in thin dashed lines outside those ranges.

4.2.2 Theoretical Relations

As we have already seen, there is a one-to-one correspondence between peaks in the primordial density field and halos that can be described using equations (3.9), (3.10) and the values found on Table 3.1[3].

Halo density profiles, $\rho_{\rm h}(r)$, predicted trough the procedure detailed in the last chapter, can be fitted to the NFW or Einasto profiles, in the same fashion that numerical ones are. The only difference is that, once the parameters are adjusted, we do not need neither to take their median (or mean) value in halo mass bins at any z nor to guess any toy model fitting them. The theoretical profiles are, by construction, typical (mean) profiles for halos with M at z, so they coincide with the stacked profile of such halos. Furthermore, the fits can be achieved for halos with any desired M and z, so there is no need to interpolate discrete values.

To facilitate the comparison between the theoretical and numerical parameters, in the NFW case, we adopt the same cosmology and mass definition ($M_{\rm vir}$) as in the corresponding toy models, while, in the Einasto case, we adopt M_{200} masses as in all the corresponding toy models, but we also include $M_{\rm vir}$ masses as in the NFW case.

Regarding the use of mass-constrained or unconstrained fits, each procedure

[3]We use a BBKS CDM spectrum with Sugiyama (1995) shape parameter. In Section 4.5, we also consider the same power spectrum exponentially cut at the neutralino free-streaming scale (Green et al. 2004).

has its pros and cons. Unconstrained fits yield density profiles closer to, but total masses farther from, the real ones. While the converse is true for mass-constrained fits. Since the toy models here considered use both fits and the difference between the two kinds of values relative to their mean is small ($< 3\%$ at $10^{-4}M_{\rm cr}(t)$ and up to about 12% at $M = 10^4 M_{\rm cr}(t)$, where $M_{\rm cr}(t)$ is the critical mass for ellipsoidal collapse at t, defined through the equality $\sigma_0[M_{\rm cr}(t), t] = \delta_{\rm cr}(t)$), when dealing with $M_{\rm vir}$ masses, we take the mean values of the constrained and unconstrained fits.[4] While, in the Einasto case, we also consider unconstrained fits as in all the corresponding toy models.

As a guide, in all Figures throughout this section, the theoretical curves are drawn in thick solid lines for $M \leq 10^4 M_{\rm cr}(t)$) and in thin dashed lines beyond this limit.

4.3 Characterisation of Halo Growth

As we have already mentioned, the CUSP formalism assumes that i) accreting halos grow inside-out and ii) that their density profiles are representative of all halos, that is that major mergers lead to the same typical density profile as pure accretion. Therefore, the comparison between the theoretical and numerical relations should reveal *whether or not these two growth conditions are met in simulations*. More specifically, for at least one of these conditions to be rejected, the theoretical relations should deviate from the numerical ones more markedly than the numerical relations deviate from themselves.

4.3.1 Global Relations

In Figure 4.1, we show the theoretical and numerical NFW $M - c$ relations. Even though the theoretical curves refer to mean parameter values while the numerical ones refer, in this case, to median values, they are very similar at $z = 0$. More specifically, the theoretical curve is very close to, just slightly higher than, the numerical one given by Zhao et al. (2009) (Fig. 4.2). They only deviate at very large masses ($M \gtrsim 10^{15}$ M$_\odot$) where the theoretical curve continues to decrease at the same accelerated rate, while the curve given by Zhao et al. (2009) suddenly levels off. In fact, all the curves differ from each other at $M \gtrsim 10^{15}$ M$_\odot$; in particular,

[4] In the case of c, we take the mean *logarithmic* value because of the lognormal distribution of halo concentrations (Reed et al. 2011).

those in Muñoz-Cuartas et al. (2011) and Klypin et al. (2011) continue to evolve at a constant or decelerated rate, respectively, the latter even bending upwards at masses beyond the range in the Figure. But all the numerical curves behave strangely at the high mass end: their smooth trend with halo mass changes at $M \sim 10^{15}$ $M_\odot$, while there is no reason for this change.

The same strange behaviour is shown by the numerical curves at any other z but at progressively smaller masses. This causes the agreement between the theoretical and numerical curves at $z = 0$ to deteriorate as z increases. While there is nothing special with regard to $z = 0$ in the CUSP formalism, there is a small effect varying with z in the numerical curves: halos in the fixed mass range analysed have ordinary masses relative to $M_{\rm cr}$ at $z = 0$, while they become increasingly massive relative to $M_{\rm cr}(z)$ at higher z's. Thus, there seems to be something wrong with simulations at very large masses at every z.

The Einasto $M - c$ relations shown in Figure 4.3 behave similarly to the NFW ones (Fig. 4.1), so the numerical curves are likely also affected by the same bias above. Indeed, Ludlow et al. (2012) noticed that some fraction of massive halos are non fully virialised. Ludlow et al. (2013) state: a number of "massive halos that pass the virialisation criteria are actually out of equilibrium". According to these authors, the Einasto profile does not correctly fit their density profiles and their values of c and α are higher-than-average. This explains the progressive departure of the theoretical curves from the numerical ones at increasingly smaller masses as z increases. In contrast, at $z = 0$, there is good agreement between the theoretical and numerical curves, despite the disparity in cosmologies and numbers of parameters adjusted.

The theoretical $M - \alpha$ relations shown in Figure 4.4 are very different from the numerical ones. In the former, the values of α decrease with increasing mass, while, in the latter, they increase. The main difference is at large masses and starts at increasingly lower M as z increases. Thus, the discrepancy seems to be due to the same bias mentioned above. This suspicion is confirmed by Ludlow et al. (2013) who state that, at $z = 0$, unbiased "halos of average concentration have approximately the same shape parameter α ($\alpha \approx 0.18$), regardless of mass". Note that $\alpha \sim 0.18$ corresponding to unbiased halos agrees with the predicted value of α for halos with masses$10^{12} M_\odot \lesssim M \lesssim 10^{15} M_\odot$.

The theoretical curves in panels a of Figures 4.3 and 4.4 are very similar to those in panels d, but shifted towards lower z's, an effect that tends to decrease with

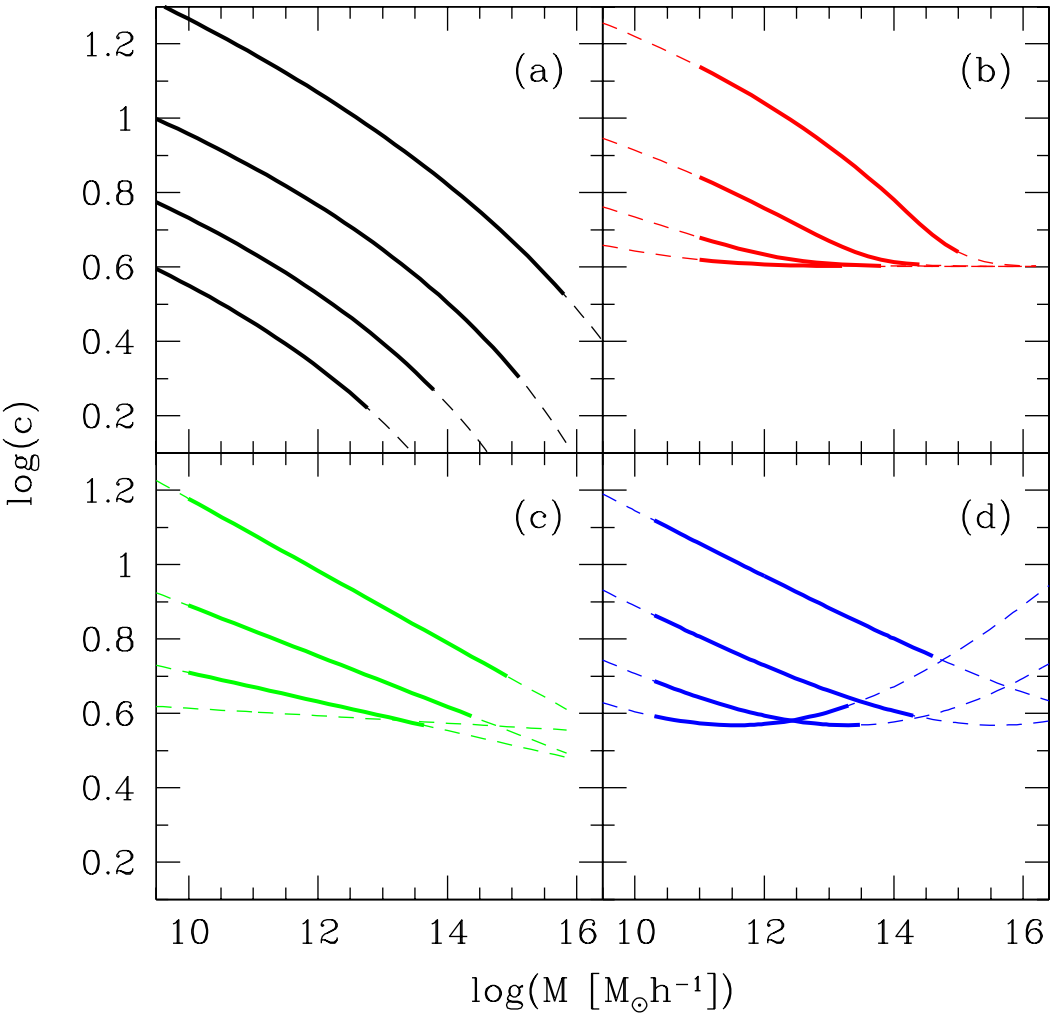

Figure 4.1: NFW $M - c$ relation derived from the CUSP formalism (black lines in panel a) and the numerical relations drawn from the toy models by Zhao et al. (2009) (red lines in panel b), Muñoz-Cuartas et al. (2011) (green lines, in panel c) and Klypin et al. (2011) (blue lines in panel e) at $z = 0$, 1, 2 and 3 (from top to bottom) for essentially the same cosmology and $M_{\rm vir}$ masses.

increasing z. This is also expected from inside-out growth since, in the cosmology considered, the overdensities at $z = 0$ with respect to $\bar{\rho}(z)$ for $M_{\rm vir}$ and M_{200} halos are 359 and 740, respectively, and equal to 181 and 208, respectively, at $z = 3$. Thus, M_{200} objects are much like $M_{\rm vir}$ ones at a higher z (but see Sec. 4.5).

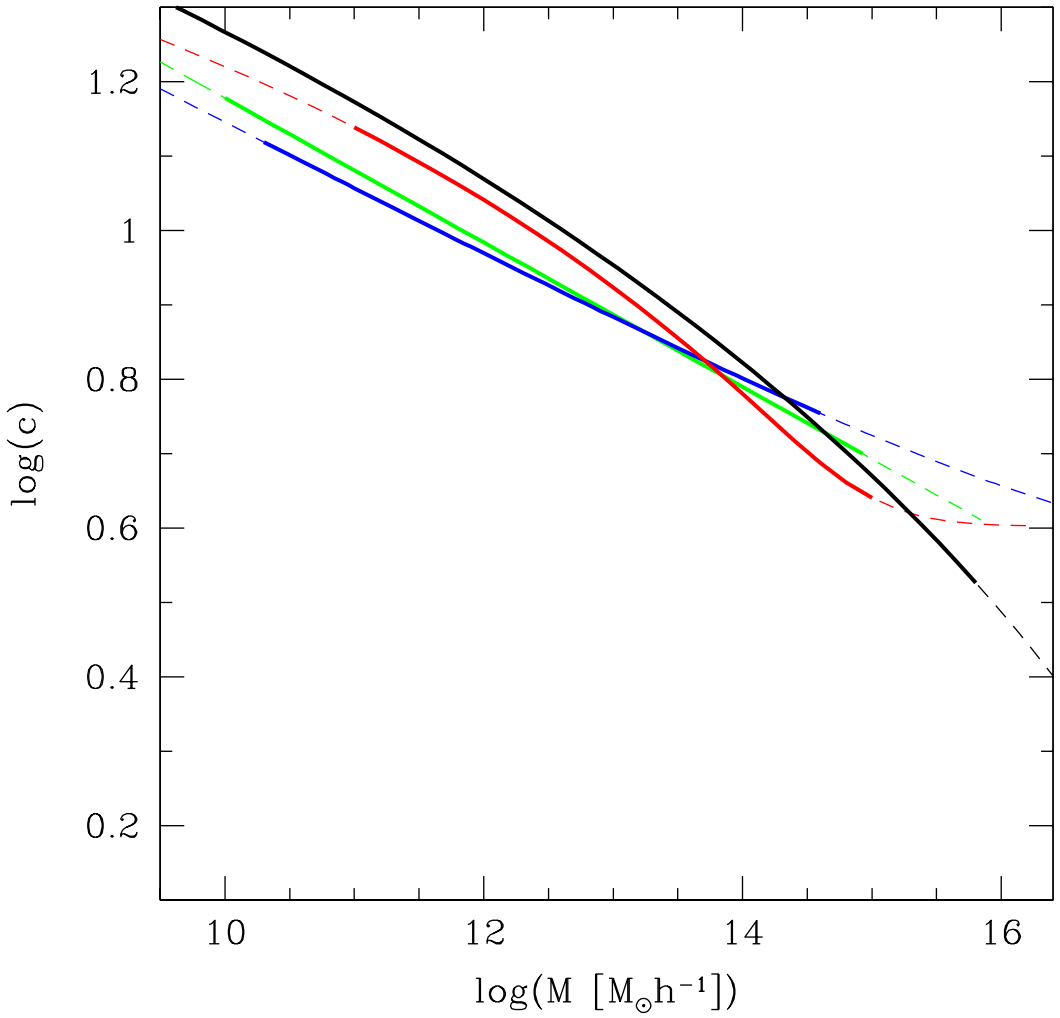

Figure 4.2: Same as Figure 4.1 but restricted to the curves at $z = 0$, superimposed in one panel.

4.3.2 Internal Relations

As mentioned in Section 4.2.2, if the CUSP formalism is right, the $M_s - r_s$ relation should be close to a power-law. Furthermore, it should not depend on z because, given the inside-out growth of accreting halos, the values of r_s and M_s (and, at a lesser extent α) should remain unchanged. Of course, such a time invariance could be blurred by major mergers; but, if the density profiles emerging from such events

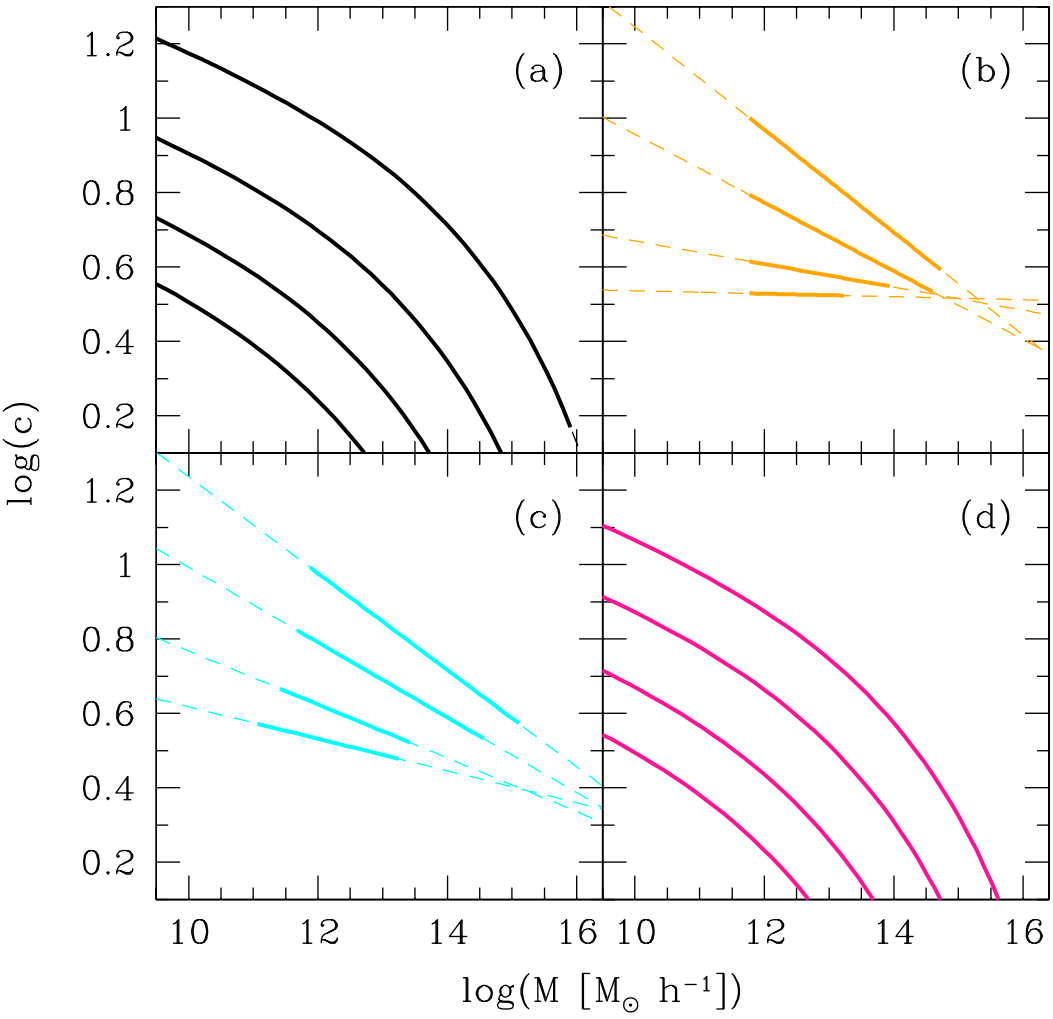

Figure 4.3: Einasto $M - c$ relations derived from the CUSP formalism for $M_{\rm vir}$ masses (black lines in panel a) and M_{200} masses (pink lines in panel d) in the same cosmology as in Figure 4.1 and from the toy models by Gao et al. (2008) (orange lines in panel b), Dutton & Macciò (2014) (cyan lines in panel c), both for M_{200} masses but somewhat different cosmologies, at $z = 0$, 1, 2 and 3.

are indistinguishable from those resulting from pure accretion, this should not happen. Since the density profiles are not perfect NFW and Einasto profiles, the values of $r_{\rm s}$ and $M_{\rm s}$ can slightly vary with z due to the varying fitting radial range. But this effect can be readily shown up: fitting the density profiles at different z's over

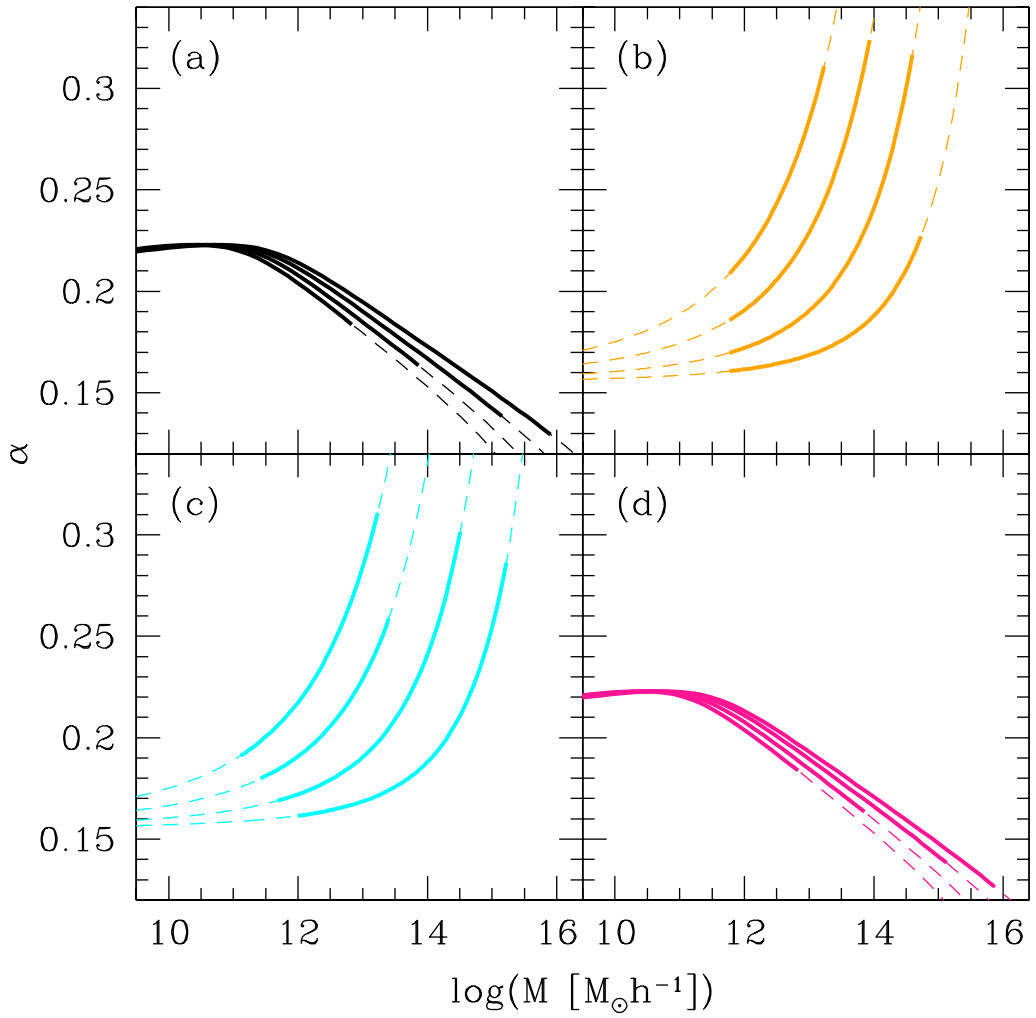

Figure 4.4: Same as Figure 4.3 but for the corresponding $M - \alpha$ relations for redshifts 0, 1, 2 and 3 (from bottom to top; on the left in panels a and d).

the same fixed radial range, any dependency on z should automatically disappear.

The chance of the $M_s - r_s$ relation being time-invariant and essentially scale-free for any other reason is highly unlikely, so confirmation (or rejection) of those properties are a very compelling test of the validity (or not) of the two growth conditions included in the CUSP formalism.

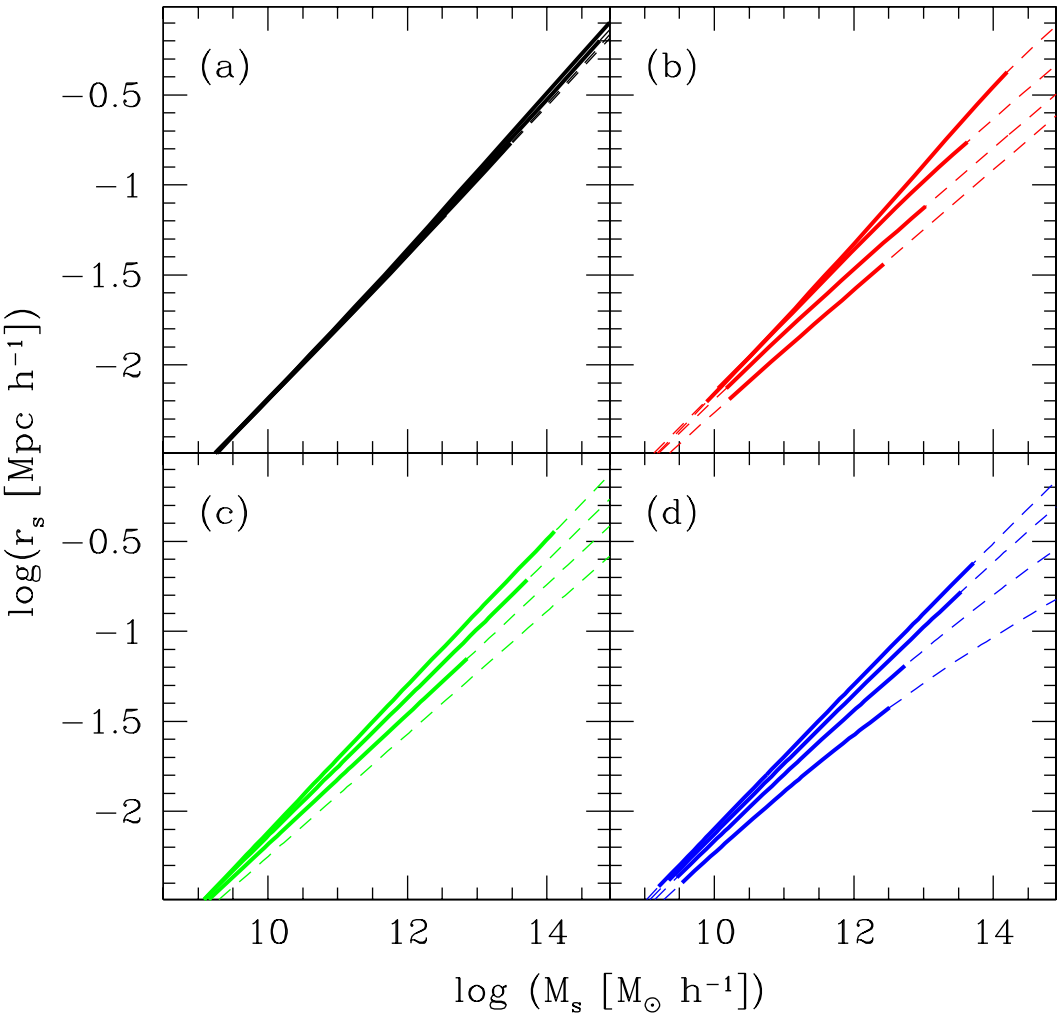

Figure 4.5: NFW $M_{\rm s} - r_{\rm s}$ relations (same lines and colours as in Figure 4.1). In all panels, the curves corresponding to redshifts 0, 1, 2 and 3 spin clockwise.

Figure 4.5 shows the NFW $M_{\rm s} - r_{\rm s}$ relations. All the curves are much more similar to each other than in the $M - c$ case. In fact, at $z = 0$ where the toy models are unbiased, all the curves essentially overlap (Fig. 4.6). Moreover, they are close to power-laws as predicted by the CUSP formalism, although their logarithmic slope varies slightly with z. This effect is negligible in the theoretical curves and completely disappears when fits are carried out over the same fixed radial range, while it is quite marked in the numerical curves and shows significant differences between

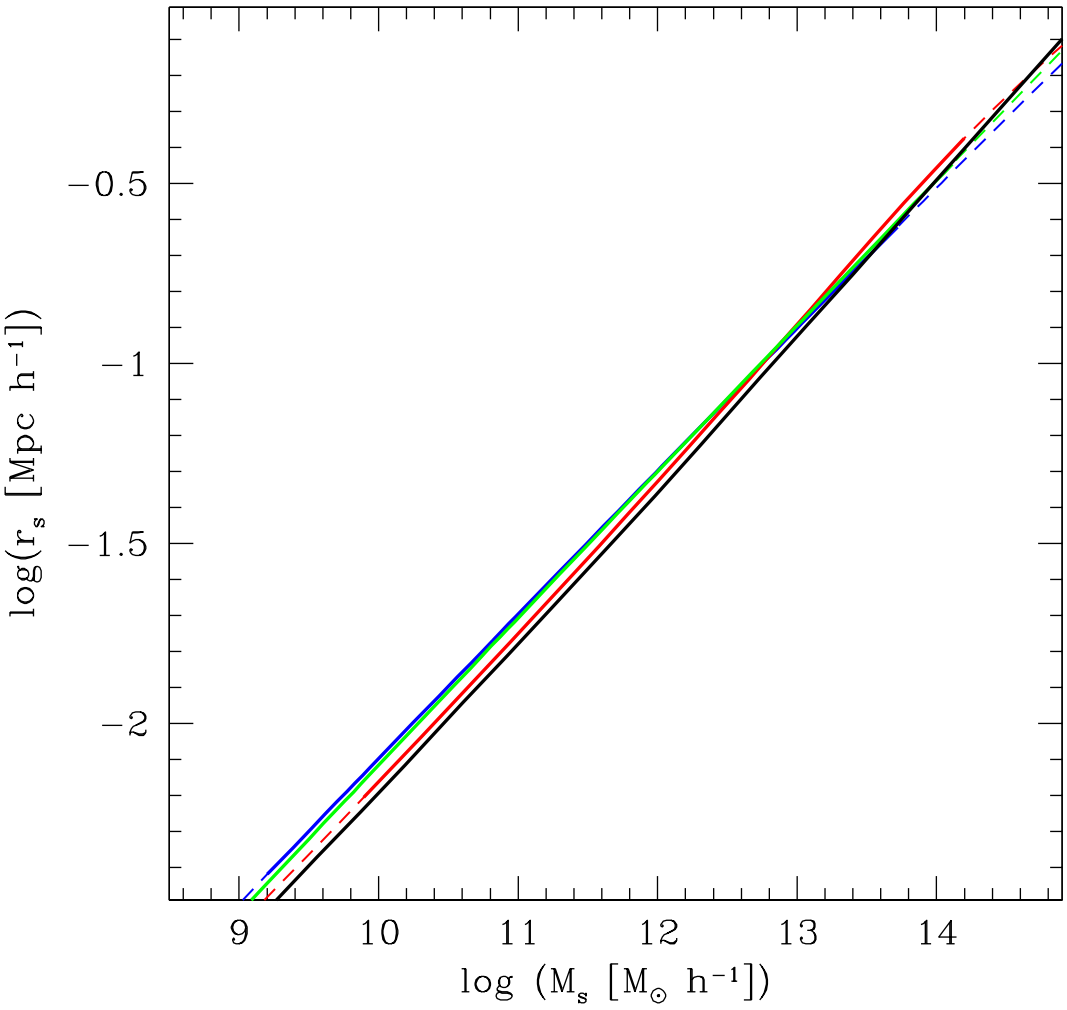

Figure 4.6: Same as Figure 4.5 but restricted to the curves at $z = 0$, superimposed in one only panel.

the results of different authors, as for the $M - c$ curves. This indicates that such a light dependency on z of the numerical curves is due to the bias affecting massive halos.

The Einasto $M_{\rm s} - r_{\rm s}$ relations shown in Figure 4.7 are even more similar to the NFW ones than in the $M - c$ case. The theoretical curves at different values of z now almost fully overlap and coincide in panels a and d. The $M_{\rm s} - \alpha$ relations,

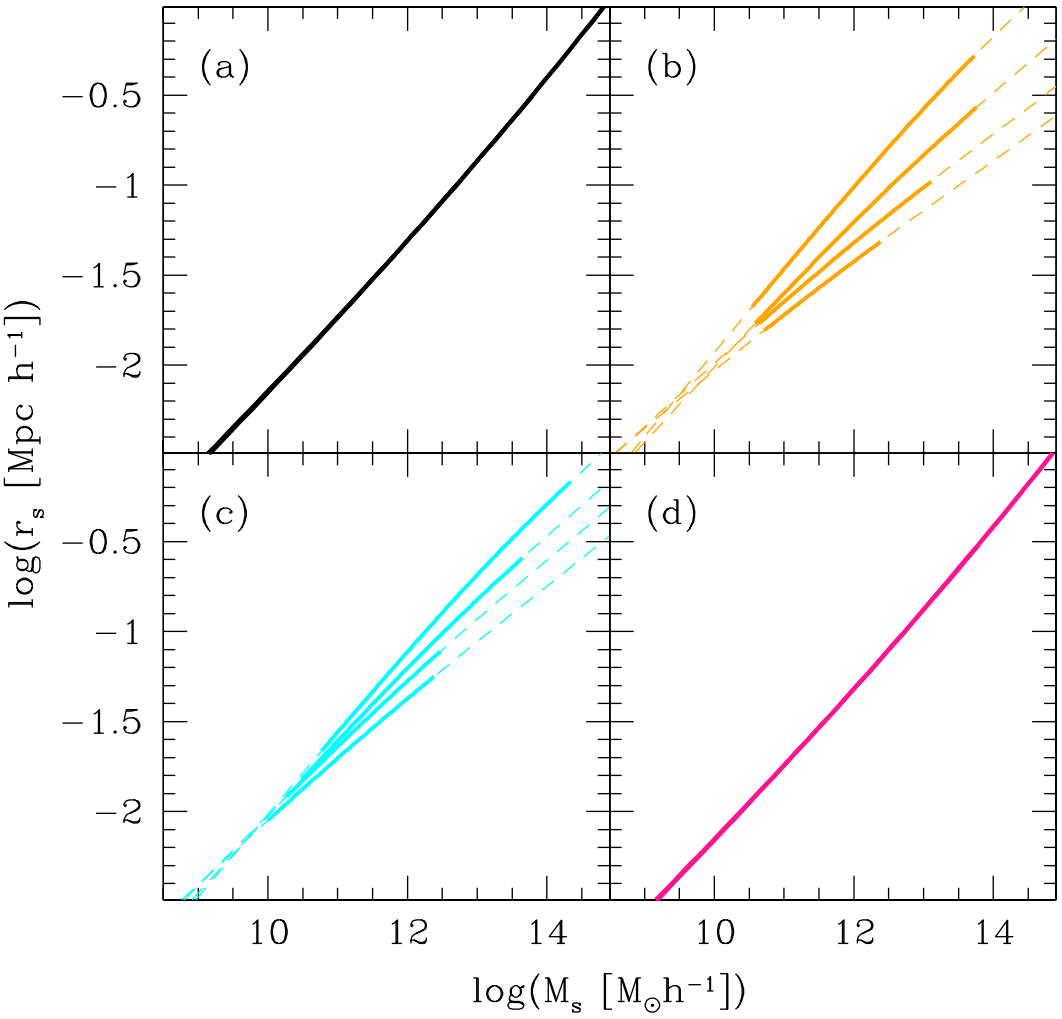

Figure 4.7: Einasto $M_{\rm s} - r_{\rm s}$ relations (same lines and colours as in Figure 4.3).

shown in Figure 4.8, also behave similarly to the $M - \alpha$ relations (Fig. 4.4). Again, the variation of α with z disappears when the fit is carried out over a fixed radial range.

4.4 Analytic Approximations

Thus, not only cannot the growth conditions checked be rejected, but they are strongly favoured. But the CUSP formalism is hard to implement. For this reason, we provide practical analytic expressions for the theoretical mass-concentration-shape relations, more reliable than the toy models affected by the bias. We emphasise that these analytic expressions are not toy models: they are physically motivated. Moreover, since the CUSP formalism does not privilege any particular mass or redshift range, they should be valid for halos well beyond the usual ranges covered by simulations.

The NFW and Einasto $M_{\rm s} - r_{\rm s}$ relations at a given z predicted by the CUSP formalism are approximately of the power-law form with a small torsion with $M_{\rm s}$ and a slight spinning with z, so they are well-fitted by the expression

$$r_{\rm s} = r_0 \left(\frac{M_{\rm s}}{M_0}\right)^{\tau}, \tag{4.7}$$

$$\tau = \tau_0 \left[1 + t_1(1+z)^{t_2} + t_3 \left(\frac{M_{\rm s}}{M_0}\right)^{t_4}\right], \tag{4.8}$$

where M_0 and r_0 are the values of $M_{\rm s}$ and $r_{\rm s}$ around which the $M_{\rm s} - r_{\rm s}$ relation spins as z varies. For similar rerasons, the Einasto $M_{\rm s} - \alpha$ relations are well-fitted by the expression

$$\alpha = \alpha_0 \left[1 + a_1 \left[\frac{M_{\rm s}}{M_{\rm s}+M_1}\right]^{a_2} + \left[\frac{M_{\rm s}+M_1}{M_1}\right]^{a_3}\right], \tag{4.9}$$

The best fitting values of the coefficients are given in Tables 4.2 and 4.3.

The $c(M,z)$ values follow from the identity $c \equiv R/r_{\rm s}$ and the functions $R(M,z)$ and $r_{\rm s}(M,z)$ given by equations (4.6) and (4.7), respectively, for $M = M_{\rm s}/f(c)$ with $f(c) = \ln(1+c) - c/(1+c)$ in the NFW case (eqs. [4.1]–[4.2]) and $f(c) = \Gamma(3/\alpha) - \Gamma(3/\alpha, 2c^{\alpha}/\alpha)$ in the Einasto case (eqs. [4.3]–[4.4]). Likewise, the $\alpha(M,z)$ values follow from equation (4.9) for $M = M_{\rm s}/f(c,\alpha)$.

As shown in Figures 4.9, 4.10 and 4.11, these analytic approximations give very good fits to the relations predicted by the CUSP formalism over the whole relevant range: $10^{-6}\ M_\odot \lesssim M \lesssim 10^{16}\ M_\odot$ and $40 \lesssim z \leq 0$. There is just a small deviation in the NFW case for very low masses at $z \lesssim 2$. In principle, the fit could be improved by taking a more complicated analytic expression, but the simple one proposed is

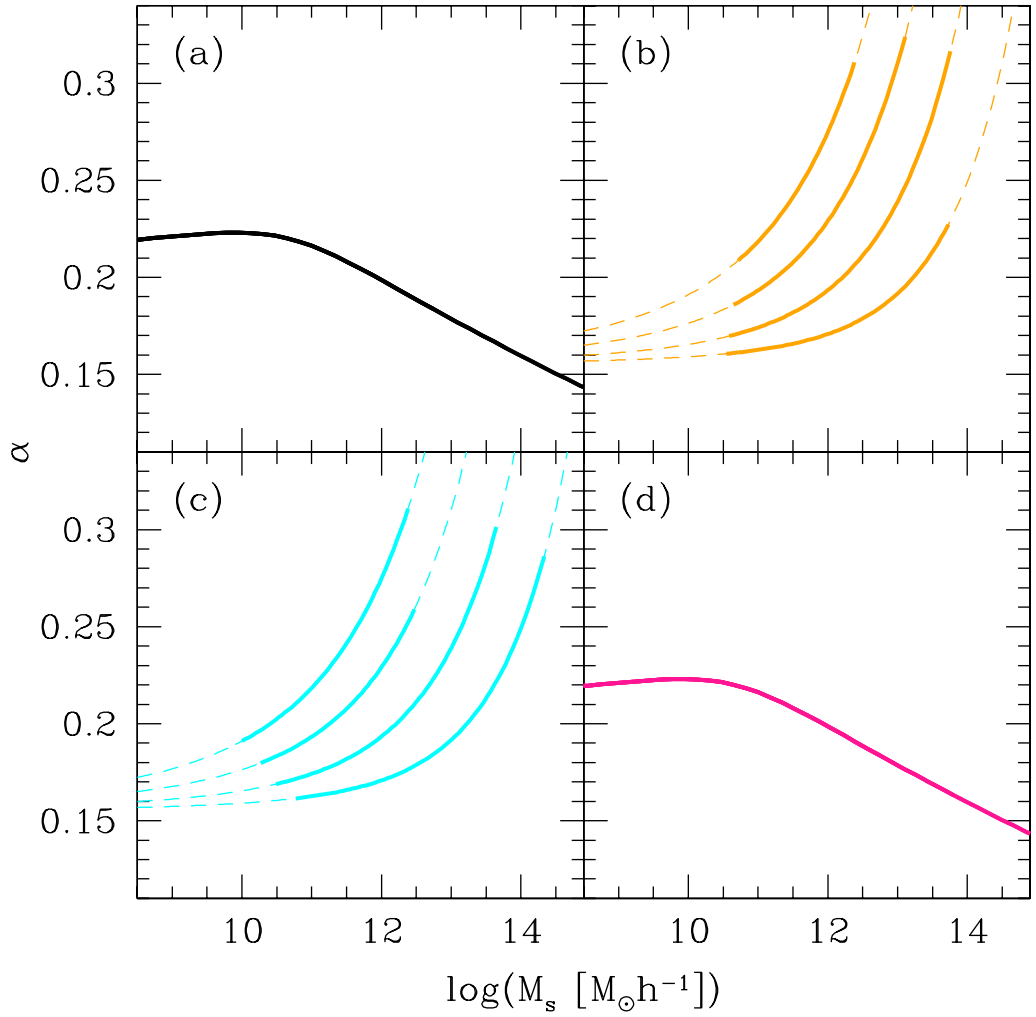

Figure 4.8: Same as Figure 4.7 but for the $M_s - \alpha$ relations.

enough because, as shown below, the NFW profile does not yield acceptable fits in that particular region of the M vs. z plain.

Table 4.2: Coefficients in the NFW and Einasto $M_{\rm s} - r_{\rm s}$ relations.

Cosmol.	Mass	Profile	r_0 (Mpc)	M_0 ($\mathrm{M}_\odot$)	τ_0	t_1	t_2	t_3	t_4
Planck14	$M_{\rm vir}$	NFW	.069	2.09×10^{12}	.264	.0526	−1.381	.548	.00876
		Einasto	.026	1.63×10^{11}	.353	-.00344	1.0	.175	.0316
	M_{200}	NFW	.062	2.31×10^{12}	.229	.117	−.141	.631	.00603
		Einasto	.022	1.12×10^{12}	.354	−.00330	1.0	.172	.0325
WMAP7	$M_{\rm vir}$	NFW	.071	2.01×10^{12}	.313	.224	−.116	.134	.0453
		Einasto	.076	1.74×10^{12}	.384	−.00394	1.0	.140	.0631
	M_{200}	NFW	.030	2.51×10^{11}	.308	0.140	−.175	.219	.0141
		Einasto	.048	6.31×10^{11}	.382	−.00404	1.0	.125	.0631

Table 4.3: Coefficients in the Einasto $M_{\rm s} - \alpha$ relation, identical for all mass definitions.

Cosmology	M_1 (Mpc)	a_0	a_1	a_2	a_3
Planck14	1.44×10^{12}	0.238	−1.068	−0.00336	−0.0341
WMAP7	7.08×10^{10}	0.364	−1.375	−0.00316	−0.0272

4.5 Acceptability Domain of the NFW and Einasto Profiles

The estimates of c for halos of very low masses and redshifts is important for the calculation of the CDM annihilation signal. Unfortunately, those halos cannot be reached by current simulations. Assuming $c(M, z)$ a power-law of M for fixed z, one can estimate the concentration of halos with the neutralino free-streaming mass from that of halos with ordinary masses at $z = 0$. Alternatively, one can use (Sánchez-Conde & Prada 2014) the functionality $c(M, z) \propto (1 + z)^{-1}$ for halos with fixed M to convert the concentration of halos with the neutralino free-streaming mass found at $z \sim 30$ (Diemand et al. 2005; Anderhalden & Diemand 2013; Ishiyama 2014) to $z = 0$. Are those procedures justified?

The approximate functionality $c(M, z) \propto (1 + z)^{-1}$ (Bullock et al. 2001) arises from the assumption that $r_{\rm s}$ is roughly constant, i.e. $r_{\rm s}(M, z) = r_{\rm s}(M, 0)$, which leads to[5]

[5]At high redshifts, $\Delta_{\rm vir}(z)$ also tends to the fixed value 186 and $\rho_{\rm crit}(z)$ to $\bar{\rho}(z)$, implying

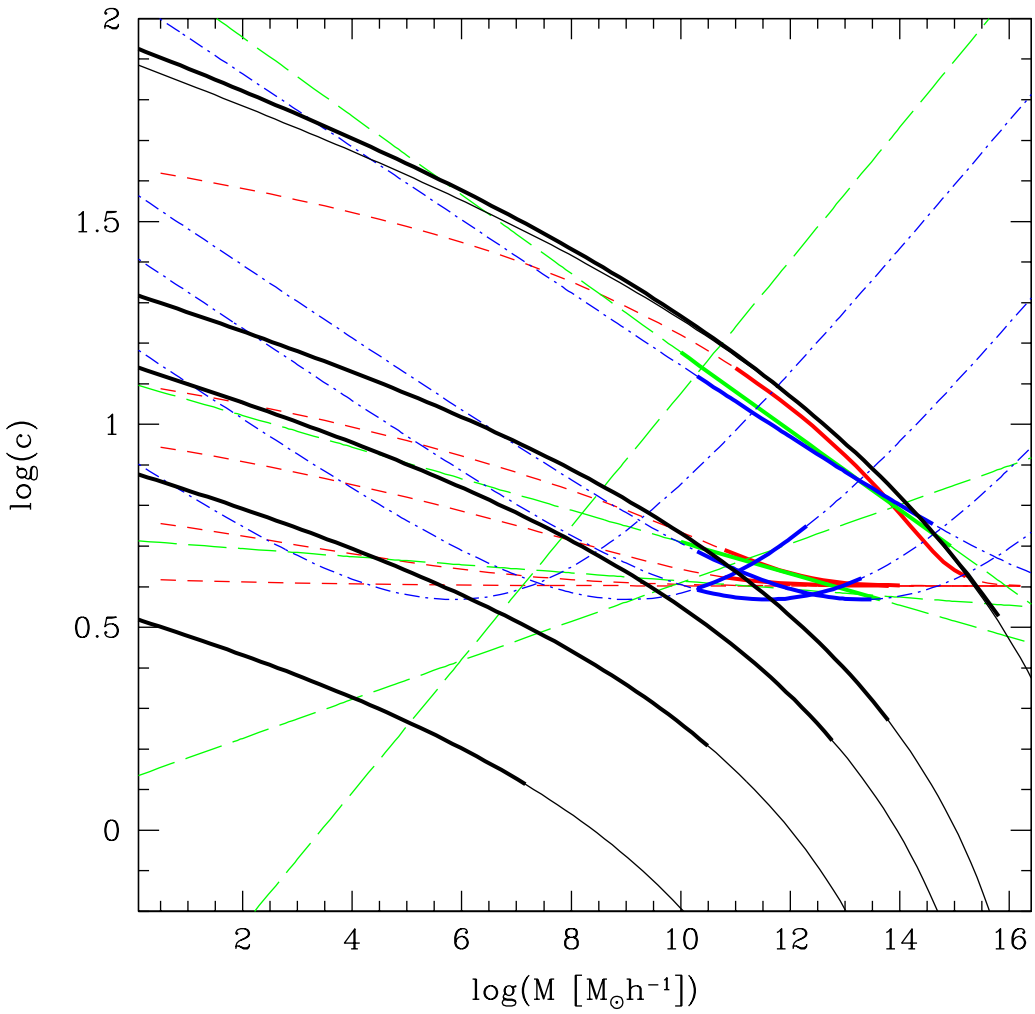

Figure 4.9: Same $M - c$ relations for the NFW profile as in Figure 4.1 but in one single panel across a much wider mass range and z equal to 0, 2, 3, 5 and 9, now including the analytic approximations to the theoretical curves (thin black lines).

$$c(M,z) \equiv \frac{R(M,z)}{r_\mathrm{s}(M,z)} \approx \frac{R(M,0)(1+z)^{-1}}{r_\mathrm{s}(M,0)} = \frac{c(M,0)}{1+z}\,. \tag{4.10}$$

Unfortunately, r_s varies with z and the exact functionality of c on z differs from equation (4.10) by the extra factor $r_0/r_\mathrm{s} = [M_0 f(c)/M]^\tau$. Consequently, $c(M,z)$ is

$R(M,z) \approx R(M,0)(1+z)^{-1}$.

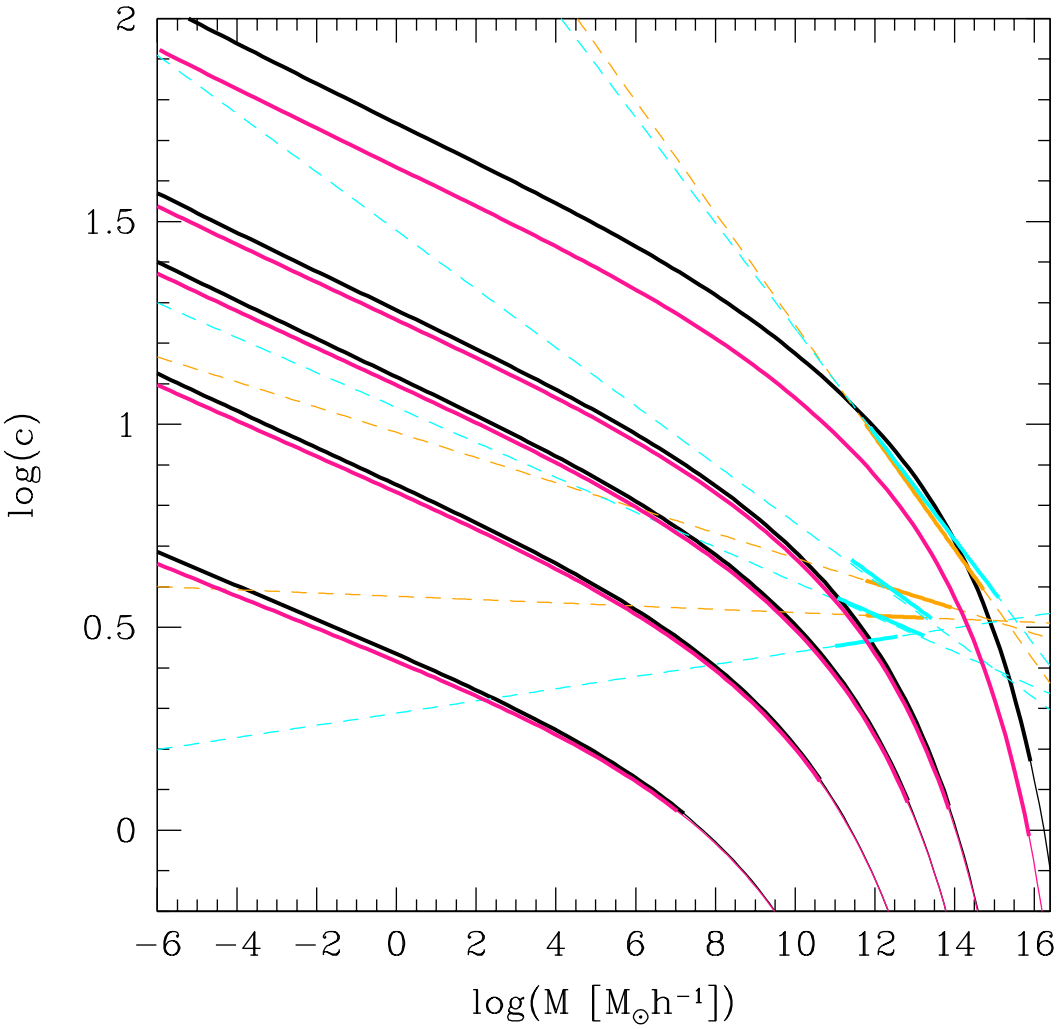

Figure 4.10: Same as Figure 4.9 but for the Einasto profile as in Figure 4.3. To avoid crowding, the analytic approximations (thin solid lines) are for the theoretical relations corresponding to $M_{\rm vir}$ (black lines) only, not to M_{200} (pink lines).

not proportional to $(1+z)^{-1}$ (see Fig. 4.12). The dependency of $r_{\rm s}$ on z is not only due to the varying fitting radial range, but also to an intrinsic effect. Indeed, the inside-out growth ensures that the values of $r_{\rm s}$ and $M_{\rm s}$ remain unaltered only for accreting halos; in major mergers, they both increase, keeping the $M_{\rm s} - r_{\rm s}$ relation unchanged. Since major mergers also increase the relative abundance of massive

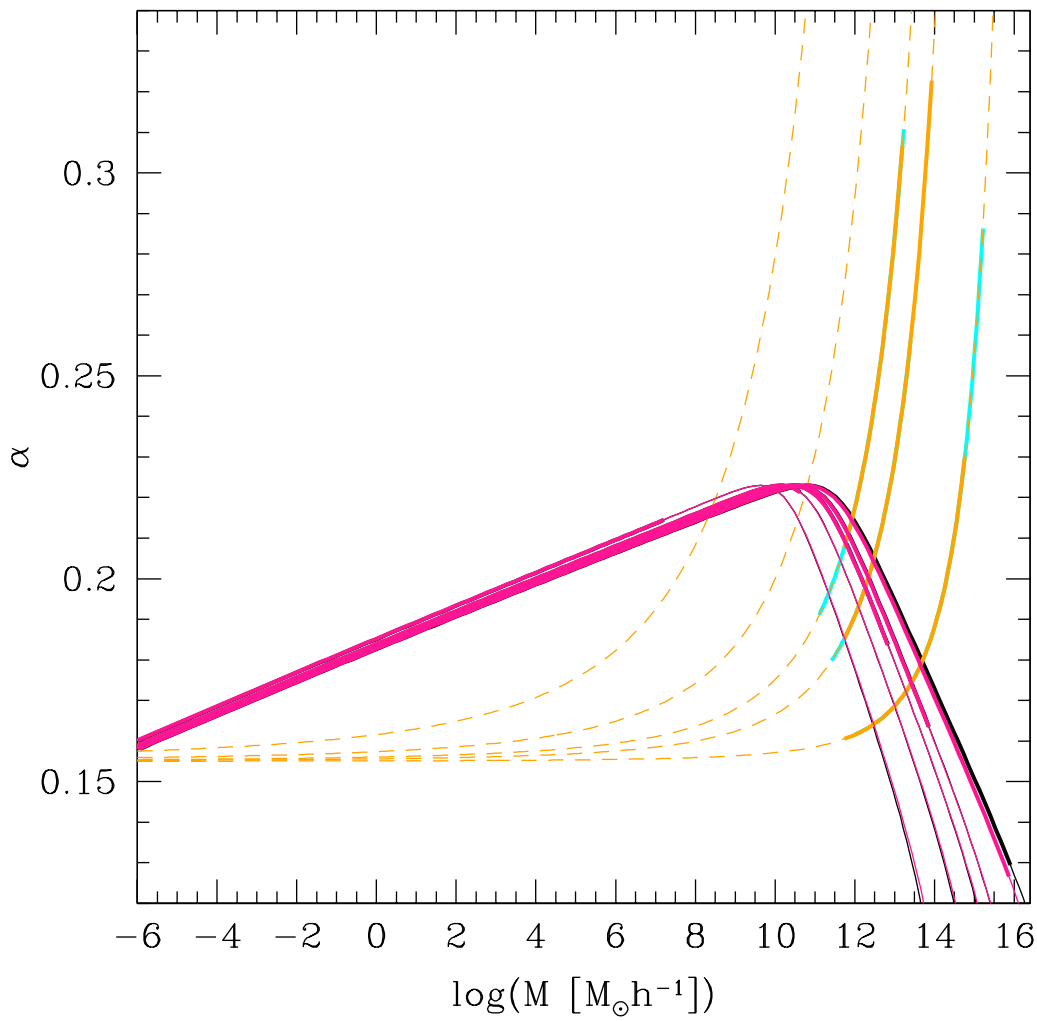

Figure 4.11: Same as Figure 4.10 but for the $M - \alpha$ relations.

halos, the average value of $r_{\rm s}$ (and of $M_{\rm s}$) increases with decreasing z.[6] However, at fixed M, $r_{\rm s}$ slightly decreases with decreasing z (see Fig. 4.13), causing $c(M, z)$ to decrease with increasing z more rapidly than $(1 + z)^{-1}$.

Likewise, $c(M, z)$ is not a power-law of M but it becomes shallower at low masses. This trend predicted by the CUSP formalism agrees with that found by Prada

[6]This slight trend prevents the $M - c$ relations for different mass definitions from *exactly* coinciding with a change in z (see panels a and d in Fig. 4.3).

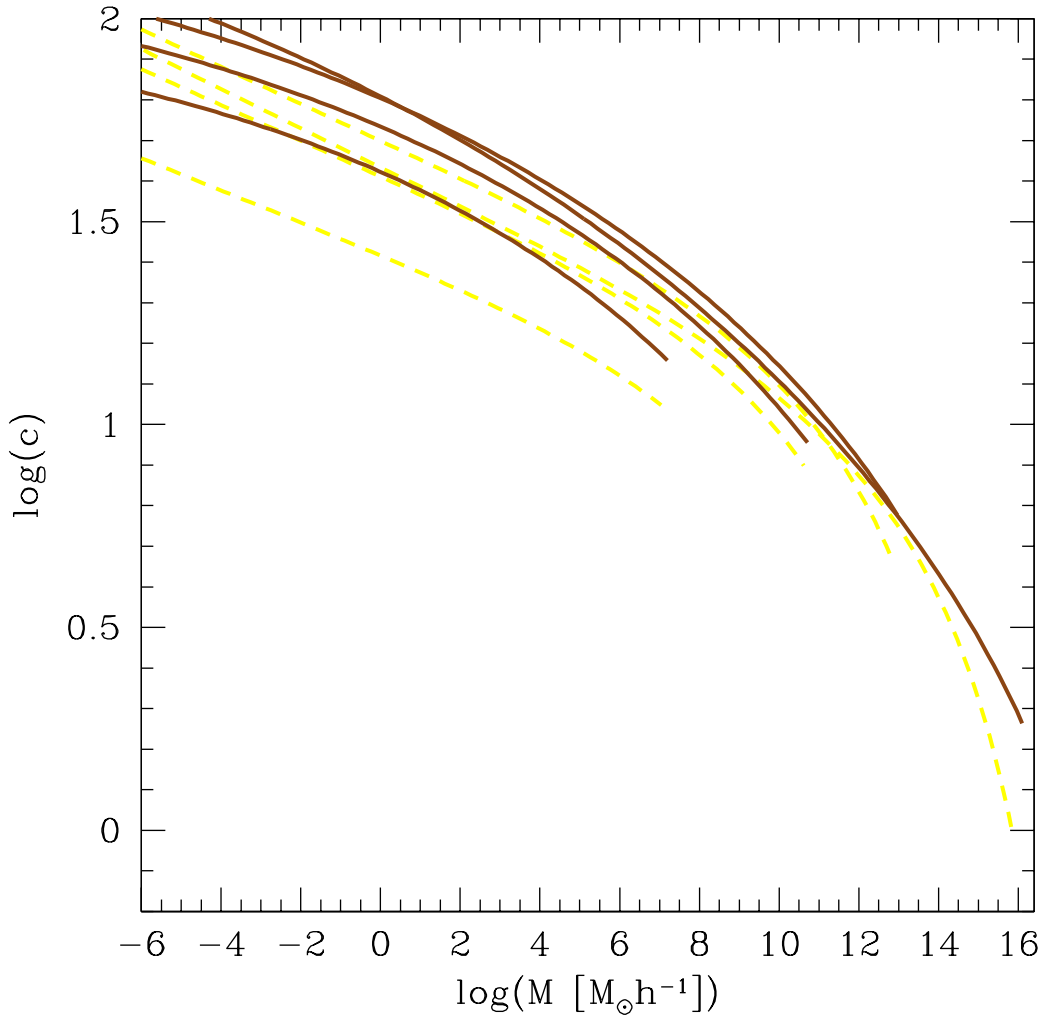

Figure 4.12: $M - c$ relations for halos with M_{200} masses at redshifts 0, 3, 5 and 9 (from top to bottom) predicted by the CUSP formalism in the NFW (solid brown lines) or Einasto (dashed yellow lines) cases, shifted by a factor of $1 + z$.

et al. (2012) by means of the sophisticated toy model for $M_{\rm vir}$ masses, parametrised through $\sigma^{\rm th}(M, z)$. Such a parametrisation yields very good results, indeed, because the function $c(\sigma_0^{\rm th})$ appears to be roughly universal, i.e. time- and cosmology-invariant (Prada et al. 2012), so that we can adjust it by taking simultaneously into account the ordinary mass range at $z = 0$ and masses around 10^{-6} $M_\odot$ at $z \sim 30$. The reason for such a rough universality is the same as for the rough universality of

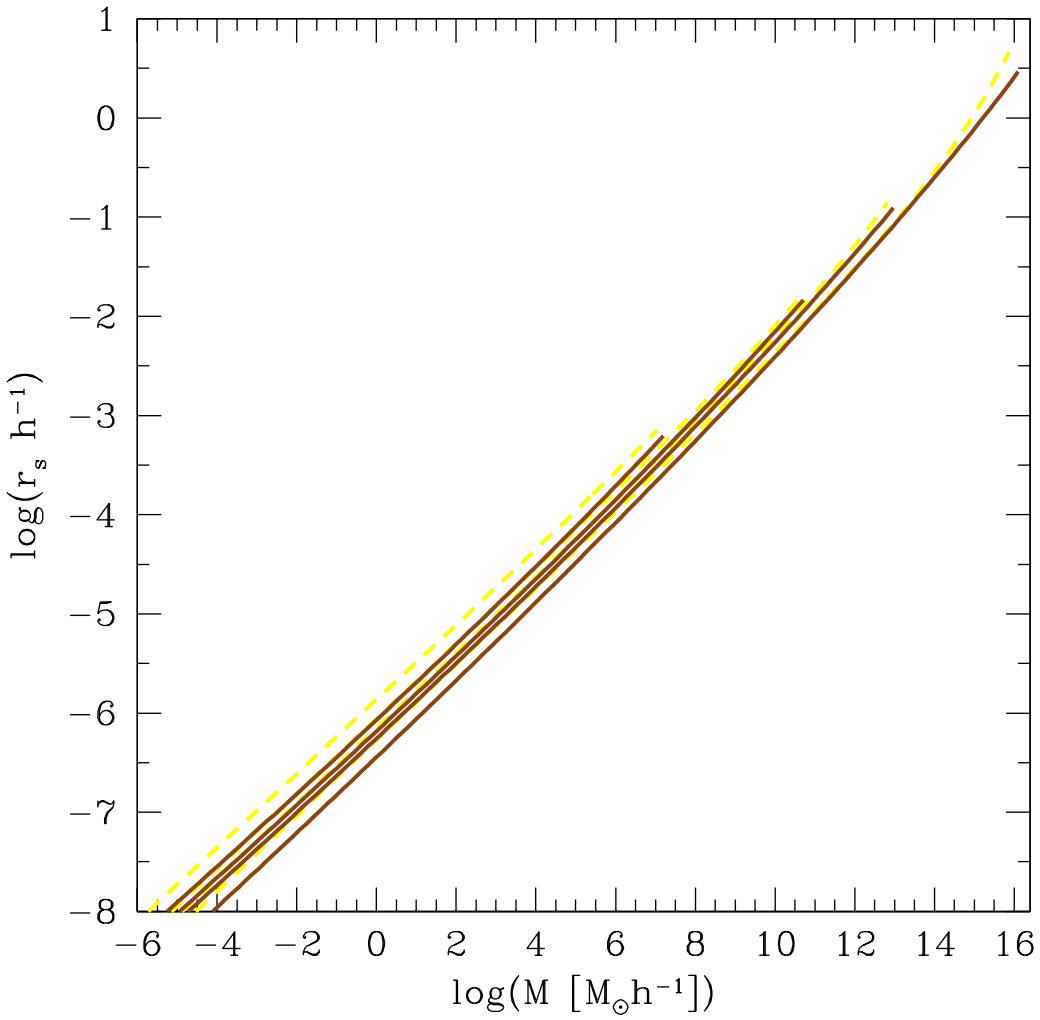

Figure 4.13: Same as Figure 4.12 but for the $M - r_{\rm s}$ relations. The curves at redshifts 0, 3, 5 and 9 are from bottom to top.

the halo multiplicity function for $M_{\rm vir}$ mases (see the next Chapter and Juan et al. 2014b): the relation (3.10) between the filtering scale of peaks and halo masses in ellipsoidal collapse.

And what about the acceptability domain of the NFW and Einasto fitting expressions in general. Halo concentration increases towards high-z and small M. In particular, $c(M, z)$ approaches one at high-z, implying that $r_{\rm s}$ approaches R or,

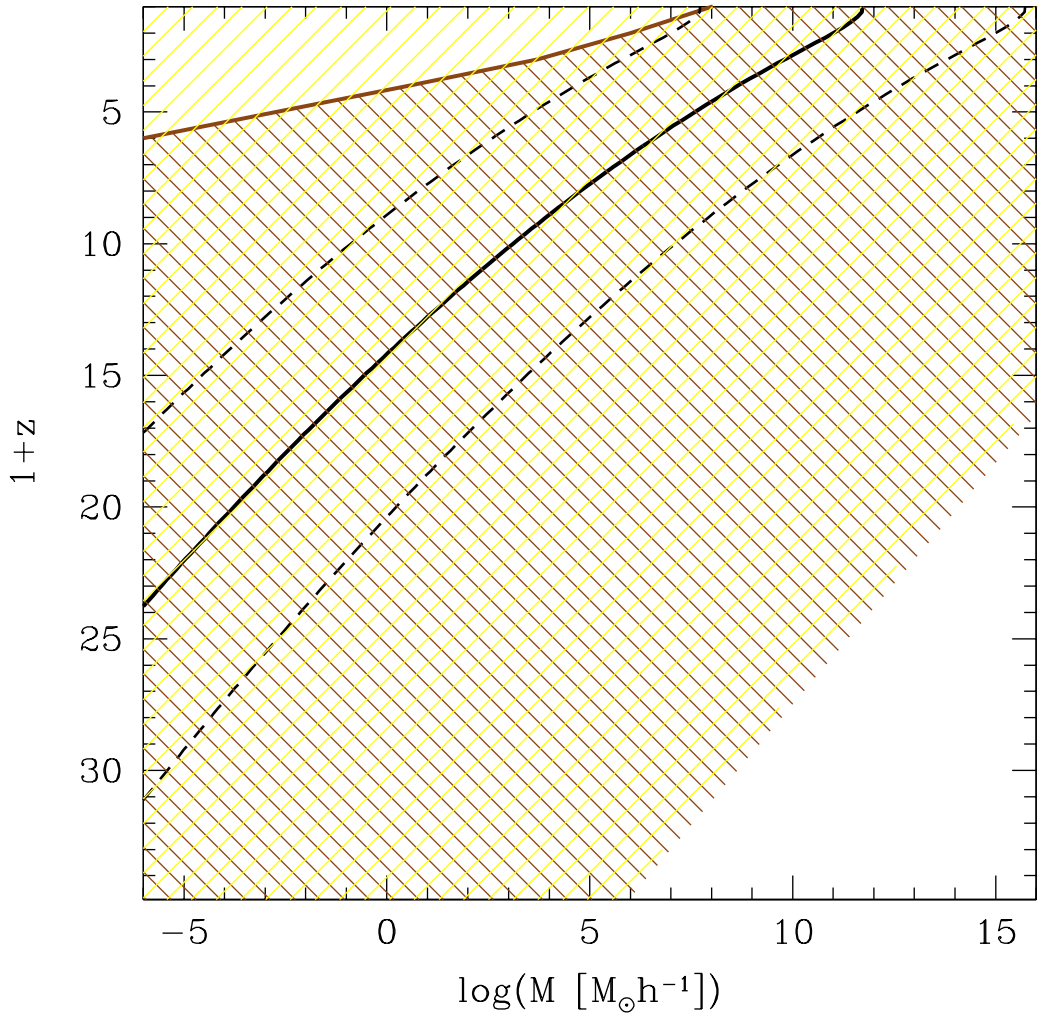

Figure 4.14: Acceptability domains of the NFW (brown hatched area) and Einasto (yellow hatched area) best analytic fits to the density profiles for halos with M_{200} masses in the WMAP7 cosmology (without exponential cut-off at the neutralino free-streaming mass) over the whole relevant mass and redshift ranges according to the CUSP formalism. The region of ordinary masses, $10^{-4} \leq M/M_{\rm cr}(z) \leq 10^{4}$, is that between the two dashed black lines around the $M_{\rm cr}(z)$ curve, in thick solid black line. The region explored at every z is limited to $M \lesssim 10^{11} M_{\rm cr}(z)$.

equivalently, that the outer logarithmic slope approaches -2 (the value defining $r_{\rm s}$). This means that the profile becomes shallower. If the inner slope became greater than -1, it would be impossible to fit the profile with the NFW analytic expression,

while this should not be a problem for the Einasto profile, able to reach arbitrarily shallow inner profiles for α close to 2 (and large values of $r_{\rm s}$). On the other hand, $c(M,z)$ increases towards 100 at small M, implying that $r_{\rm s}$ approaches $R/100$ or, equivalently, that the inner slope approaches -2. This means that the profile becomes very steep. If the outer slope became smaller than -3, it would be impossible to fit the profile with the NFW analytic expression, while this should not be a problem for the Einasto profile, able to reach arbitrarily small outer slopes for α close to 2 (and small values of $r_{\rm s}$). And, at large M, the situation is similar to that found at high-z.

This discussion suggests that the acceptability of the NFW profile may be bounded for small enough and large enough halo masses at any given z, contrarily to the Einasto profile which should be acceptable in a much wider range of masses and redshifts. In Figure 4.14, we show the acceptability domains of the two fitting expressions for halos with M_{200} masses in the *WMAP7* cosmology according to the CUSP predictions. As can be seen, the NFW profile gives acceptable fits over ordinary masses, but not for extremely low ones at any given z. In particular, the NFW profile is not acceptable for halos with the neutralino free-streaming mass at $z = 0$, which have steeper inner density profiles. (For $M_{\rm vir}$ masses reaching larger total radii, this restriction is slightly more severe. On the other hand, when the CDM power spectrum includes an exponential cut-off at the neutralino free-streaming mass, the density profiles near that mass limit are slightly more cuspy, in agreement with the results by Ishiyama 2014.) No similar restriction is found, however, at the large mass up to masses as high as $10^{11}M_{\rm cr}(z)$ and redshits up to 35. In contrast, the Einasto profile yields acceptable fits over the whole relevant region. It is worth noting that, according to the CUSP formalism that accounts for ellipsoidal collapse, the mass of 10^{-6} $M_\odot$ is reached as an ordinary mass, $M \lesssim 10^4 M_{\rm cr}(z)$, at $z = 31$, in agreement with the results of simulations (Diemand et al. 2005; Anderhalden & Diemand 2013; Ishiyama 2014),[7] which confirms once again the validity of the CUSP formalism.

[7] In contrast, the same mass would be reached at $z \sim 25$ if $M_{\rm cr}(z)$ were defined according to spherical collapse.

5

Halo Mass and Multiplicity Function

When you look into the abyss, the abyss also looks back at you.
Friedrich Nietzsche

In this Chapter, we use the CUSP formalism to have a deeper insight on the halo mass and multiplicity functions and the role of the halo mass definition used.

5.1 Halo mass

As already mentioned, the boundary of a virialized halo is a fuzzy concept. There are several mass definitions found in the literature, usually arising from the halo finders used in simulations (Klypin et al. 2011). The halo mass function depends on the mass definition used. In this chapter we will use the CUSP formalism to study how these properties change depending on the mass definition used, comparing our results with those obtained using the excursion set formalism.

The various halo mass definitions found in the literature arise from the different halo finders used in simulations (Klypin et al. 2011). For instance, in the Spherical Overdensity (SO) definition (Lacey & Cole 1994), the mass of a halo at the time t is that leading to a total mean density $\bar{\rho}_{\rm h}(R_{\rm h})$ equal to a fixed, constant or time-

varying, overdensity Δ times the mean cosmic density $\bar{\rho}(t)$,

$$\bar{\rho}_{\rm h}(R_{\rm h}) = \Delta\bar{\rho}(t)\,. \tag{5.1}$$

While in the Friends-of-Friends (FoF) definition (Davis et al. 1985), the mass of a halo is the total mass of its particles, identified by means of a percolation algorithm with fixed linking length b in units of the mean inter-particle separation.

The main drawback of the FoF definition is that, for large values of b, it tends to over-link haloes. Its main advantage is that it can be applied without caring about the symmetry and dynamical state of haloes. Haloes are, indeed, triaxial rather than spherically symmetric, harbour substantial substructure and may be undergoing a merger, which complicates the use of the SO definition. However, one can focus on virialised objects and consider the spherically averaged density profile $\rho_{\rm h}(r)$ and mass profile $M(r)$ around the peak-density, in which case the FoF mass coincides with the mass inside the radius $R_{\rm h}$ where spheres of radius b harbour two particles in average (Lacey & Cole 1994),

$$\rho_{\rm h}(R) = \frac{3}{2\pi}\,b^{-3}\bar{\rho}(t)\,. \tag{5.2}$$

Equations (5.1) and (5.2) imply the relation

$$\Delta = \frac{3F(c)}{2\pi}\,b^{-3}\,, \tag{5.3}$$

between Δ and b for haloes of a given mass M, where $F(c) \equiv \bar{\rho}_{\rm h}(R_{\rm h})/\rho_{\rm h}(R_{\rm h})$ is a function of halo concentration c.

As c depends on M, there is no pair of Δ and b values satisfying equation (5.3) for all M at the same time. Consequently, there is strictly no equivalent SO and FoF mass definitions (Muñoz-Cuartas et al. 2011). Yet, numerical simulations show that, at least in the Standard Cold Dark Matter (SCDM) cosmology, FoF masses with $b = 0.2$, tightly correlate with SO masses with overdensity Δ equal to the so-called virial value, $\Delta_{\rm vir} \approx 178$, from now on SO($\Delta_{\rm vir}$) (Cole & Lacey 1996). This correlation is often interpreted as due to the fact that haloes are close to isothermal spheres, for which $F(c)$ is equal to 3, so equation (5.3) for $b = 0.2$ implies $\Delta \approx 178$.

Simulations also show that, in any cold dark matter (CDM) cosmology, FoF(0.2) haloes have a multiplicity function that, expressed as a function of the top-hat height

for spherical collapse, is approximately universal (Jenkins et al. 2001; White 2002; Warren et al. 2006; Lukić et al. 2007; Tinker et al. 2008; Crocce et al. 2010) and very similar to that found for SO($\Delta_{\rm vir}$) haloes (Jenkins et al. 2001; White 2002). As $\Delta_{\rm vir}$ may substantially deviate from 178 depending on the cosmology, such a similarity cannot be due to the roughly isothermal structure of haloes as suggested by the SCDM case. Moreover, the universality of this multiplicity function is hard to reconcile with the dependence on cosmology of halo density profile (Courtin et al. 2011). On the other hand, haloes do not form through spherical collapse but through ellipsoidal collapse. For all theses reasons, the origin of such properties is unknown. Having a reliable theoretical model of the halo MF would be very useful for trying to clarify these issues.

Assuming the spherical collapse of halo seeds, Press & Schechter (1974) derived a MF that is in fair agreement with the results of numerical simulations (e.g. Efstathiou et al. 1988; White et al. 1993; Lacey & Cole 1994; Bond & Myers 1996), although with substantial deviations at both mass ends (Lacey & Cole 1994; Gross et al. 1998; Jenkins et al. 2001; White 2002; Reed et al. 2003; Heitmann et al. 2006). An outstanding characteristic of the associated multiplicity function is its universal shape as a function of the height of density fluctuations. Whether this characteristic is connected with the approximately universal multiplicity function of simulated haloes for FoF(0.2) masses is however hard to tell.

In an alternative approach, the extension to peaks was directly attempted from the original Press-Schechter MF (Bond 1989; Colafrancesco et al. 1989; Peacock & Heavens 1990; Appel & Jones 1990; Bond & Myers 1996; Hanami 2001). As we have already seen, the most rigorous derivation along this line was by Manrique & Salvador-Solé (1995, hereafter MSS; see also Manrique et al. 1998) through the CUSP formalism.

A common feature of all these derivations is that they assume monolithic collapse or pure accretion. While in hierarchical cosmologies there are certainly periods in which haloes evolve by accretion, major mergers are also frequent and cannot be neglected. We will comeback to this point at the end of the paper. A second and more important issue in connection with the problem mentioned above is that none of these theoretical MFs makes any explicit statement on the halo mass definition presumed, so the specific empirical MF they are to be compared with is unknown.

5.2 Mass Function

All derivations of the halo MF proceed by first identifying the seeds of haloes with mass M at the time t in the density field at an arbitrary small enough cosmic time $t_{\rm i}$ and then counting those seeds.

5.2.1 The Excursion Set Formalism

In this approach, halo seeds are assumed to be spherical overdense regions in the initial density field smoothed with a *top-hat* filter that undergo spherical collapse.

The time of spherical collapse (neglecting shell-crossing) of a seed depends only on its density contrast, so there is a one-to-one correspondence between haloes with M at t and density perturbations with fixed density contrast $\delta_{\rm cr}$ at the filtering radii R satisfying the relations

$$\delta_{\rm cr}(t) = \delta_{\rm c}(t)\frac{D(t_{\rm i})}{D(t)} \tag{5.4}$$

$$R(M) = \left[\frac{3M}{4\pi\bar{\rho}_{\rm i}}\right]^{1/3} . \tag{5.5}$$

In equations (5.4) and (5.5), $\bar{\rho}_{\rm i}$ is the mean cosmic density at $t = t_{\rm i}$, $\delta_{\rm c}(t)$ is the almost universal density contrast for spherical collapse at t linearly extrapolated to that time and $D(t)$ is the cosmic growth factor. In the Einstein-de Sitter universe, $D(t)$ is equal to the cosmic scale factor $a(t)$ and $\delta_{\rm c}(t)$ is equal to $3(12\pi)^{2/3}/20 \approx 1.686$. While, in the concordant model and the present time t_0, $D(t_0)$ is a factor 0.760 smaller than $a(t_0)$ and $\delta_{\rm c}(t_0)$ is equal to ≈ 1.674 (e.g. Henry 2000).

Equation (5.5) is valid to leading order in the perturbation, the exact relation between R and M being

$$R(M,t) = \left\{\frac{3M}{4\pi\bar{\rho}_{\rm i}[1+\delta_{\rm cr}(t)]}\right\}^{1/3} . \tag{5.6}$$

The interest of adopting the approx relation (5.5) is that the filtering radius then depends only on M. This greatly simplifies the mathematical treatment.

Following Press & Schechter (1974), every region with density contrast greater than or equal to $\delta_{\rm cr}(t)$ at the scale $R(M)$ will give rise at t to a halo with mass

greater than or equal to M. Consequently, the MF, i.e. the comoving number density of haloes per infinitesimal mass around M at t, is simply the M-derivative of the volume fraction occupied by those regions, equal in Gaussian random density fields to

$$V(M,t) = \frac{1}{2}\,\mathrm{erfc}\left[\frac{1}{\sqrt{2}}\,\frac{\delta_{\rm cr}(t)}{\sigma_0^{\rm th}(M,t_{\rm i})}\right], \tag{5.7}$$

divided by the volume $M/\bar{\rho}(t)$ of one single seed,

$$\frac{\partial n_{\rm PS}(M,t)}{\partial M} = \frac{\bar{\rho}(t)}{M}\,\frac{\partial V(M,t)}{\partial M}\,. \tag{5.8}$$

In equation (5.7), $\sigma_0^{\rm th}(M,t_{\rm i})$ is the top-hat rms density fluctuation of scale M at $t_{\rm i}$.

But this derivation does not take into account that overdense regions of a given scale may lie within larger scale overdense regions, which translates into a wrong normalisation[1] of the MF (5.7)–(5.8). To correct for this effect, Bond et al. (1991) introduced the excursion set formalism. The density contrast δ at any fixed point tends to decrease as the smoothing radius R increases, so, using a sharp k-space filter, δ traces a Brownian random walk, easy to monitor statistically. In particular, one can estimate the number of haloes reaching M at t by counting the excursion sets $\delta(R)$ intersecting $\delta_{\rm cr}(t)$ at any scale $R(M)$. The important novelty of this approach is that, whenever a halo undergoes a major merger, δ increases instead of decreasing, so every trajectory $\delta(R)$ can intersect $\delta_{\rm cr}(t)$ at more than one radius R, meaning that there will be haloes appearing within other more massive ones. Therefore, to correct for cloud-in-cloud configurations, one must simply count the excursion sets intersecting $\delta_{\rm cr}(t)$ for the first time as R decreases from infinity (or $\sigma_0^{\rm th}$ increases from zero), as if they were absorbed at such a barrier. The MF so obtained has identical form as the Press-Schechter one (eqs. [5.8]-[5.7]) but with an *additional factor two*,

$$\frac{\partial n_{\rm es}(M,t)}{\partial M} = 2\frac{\partial n_{\rm PS}(M,t)}{\partial M}\,, \tag{5.9}$$

yielding the right normalisation of the excursion set MF.

Note that, as the height of a density fluctuation, defined as the density contrast normalised to the rms value at the same scale, is constant with time, the volume $V(M,t)$ (eq. [5.7]) can be written as a function of $\nu_{\rm es} = \delta_{\rm cr}(t)/\sigma_0^{\rm th}(M,t_{\rm i}) = \delta_{\rm c}(t)/\sigma_0^{\rm th}(M,t) = \delta_{\rm c0}(t)/\sigma_0^{\rm th}(M,t)$, where $\delta_{\rm c0}(t)$ is $\delta_{\rm c}(t)D(t_0)/D(t)$ and $\sigma_0^{\rm th}(M,t)$

[1]The normalisation condition reflects the fact that all the matter in the universe must be in the form of virialised haloes.

stands for the 0th order spectral moment at the current time t_0. Thus, the resulting MF (eq. [5.8]) is independent of the arbitrary initial time $t_{\rm i}$.

5.2.2 The CUSP Formalism

Given the one-to-one correspondence between haloes and non-nested peaks, the counting of haloes with M at t reduces to count non-nested peaks with that scale at $t_{\rm i}$. In the original version of the CUSP formalism (MSS), such a counting did not take into account the correlation between peaks at different scales. However, the more accurate version later developed (Manrique et al. 1998) yielded essentially the same result, so we will follow here that simple version (see the Appendix [C] for the more accurate one). For simplicity, we will omit hereafter any subindex in the Gaussian rms density fluctuation σ_0 and in the CUSP height $\nu \equiv \delta_{\rm pk}/\sigma_0(M,t_{\rm i}) = \delta_c(t)/\sigma_0(M,t) = \delta_{\rm c0}(t)/\sigma_0$, where $\delta_{\rm c0}(t)$ is $\delta_{\rm c}(t)D(t_0)/D(t)$ and σ_0 stands for the 0th order spectral moment at t_0. The subindexes "th" and "es" in the excursion set counterparts are enough to tell between the two sets of variables.

As we have already seen, the number density of peaks with $\delta_{\rm pk}$ per infinitesimal $\ln \sigma_0^{-1}(M,t_{\rm i})$ at $t_{\rm i}$ or, equivalently, with $\delta_{\rm c0}$ per infinitesimal $\ln \sigma_0^{-1}$ at t_0 can be readily calculated from the density of peaks per infinitesimal height around ν, derived by BBKS. The result is

$$N(\sigma_0,\delta_{\rm c0}) = \frac{\langle x\rangle(\sigma_0,\delta_{\rm c0})}{(2\pi)^2\, R_\star^3\, \gamma}\ {\rm e}^{-\frac{\nu^2}{2}}\,, \tag{5.10}$$

where $R_\star$ and γ are respectively defined as $\sqrt{3}\sigma_1/\sigma_2$ and $\sigma_1^2/(\sigma_0\sigma_2)$, being σ_j the j-th order (Gaussian) spectral moment, and $\langle x\rangle(\sigma_0,\delta_{\rm c0})$ is the average curvature (i.e. minus the Laplacian scaled to the mean value σ_2) of peaks with $\delta_{\rm c0}$ and σ_0, well-fitted by the analytic expression (BBKS)

$$\langle x\rangle(\nu) = \gamma\nu + \frac{3(1-\gamma^2) + (1.216-0.9\gamma^4){\rm e}^{-\frac{\gamma}{2}\left(\frac{\gamma\nu}{2}\right)^2}}{\left[3(1-\gamma^2)+0.45+(\gamma\nu/2)^2\right]^{1/2}+\gamma\nu/2}\,. \tag{5.11}$$

But this number density is not enough for our purposes because we are interested in counting *non-nested* peaks only. The homologous number density of non-nested

peaks, $N^{\rm nest}(\sigma_0,\delta_{\rm c0})$, can be obtained by solving the Volterra integral equation

$$N^{\rm nest}(\sigma_0,\delta_{\rm c0}) = N(\sigma_0,\delta_{\rm c0}) - \int_{\ln\sigma_0^{-1}}^{\infty} {\rm d}\ln {\sigma'_0}^{-1} \times N(\sigma_0,\delta_{\rm c0}|\sigma'_0,\delta_{\rm c0}) \frac{M(\sigma'_0,\delta_{\rm c0})}{\bar{\rho}} N^{\rm nest}(\sigma'_0,\delta_{\rm c0}), \tag{5.12}$$

where the second term on the right gives the density of peaks with $\delta_{\rm c0}$ per infinitesimal $\ln\sigma_0^{-1}$ nested into peaks with identical density contrast at larger scales, $\ln {\sigma'_0}^{-1}$. The conditional number density $N(\sigma_0,\delta_{\rm c0}|\sigma'_0,\delta_{\rm c0})$ of peaks with $\delta_{\rm c0}$ per infinitesimal $\ln\sigma_0^{-1}$ subject to lying in backgrounds with $\delta_{\rm c0}$ at $\sigma'_0<\sigma_0$ can also be calculated from the conditional number density per infinitesimal ν in backgrounds with ν' derived by BBKS. The result is

$$N(\sigma_0,\delta_{\rm c0}|\sigma'_0,\delta_{\rm c0}) = \frac{\langle x\rangle(\tilde{\sigma}_0,\delta_{\rm c0})}{(2\pi)^2\, R_\star^3\,\gamma\,\sqrt{1-\epsilon^2}}\, {\rm e}^{-\frac{(\nu-\epsilon\,\nu')^2}{2(1-\epsilon^2)}}\,, \tag{5.13}$$

where ν' and ϵ are respectively defined as $\delta_{\rm c0}/\sigma'_0$ and $\sigma_0^2(R_{\rm m})/[\sigma_0\sigma'_0]$, being $R_{\rm m}^2$ equal to the arithmetic mean of the squared filtering radii corresponding to σ_0 and σ'_0, and where $\langle x\rangle(\tilde{\sigma}_0,\delta_{\rm c0})$ takes the same form (5.11) as $\langle x\rangle(\sigma_0,\delta_{\rm c0})$ in equation (5.10) but as a function of $\tilde{\gamma}\tilde{\nu}$ instead of $\gamma\nu$, being

$$\tilde{\gamma}^2 = \gamma^2\left[1+\epsilon^2\,\frac{(1-r_1)^2}{1-\epsilon^2}\right] \tag{5.14}$$

$$\tilde{\nu}(r) = \frac{\gamma}{\tilde{\gamma}}\,\frac{1-r_1}{1-\epsilon^2}\left[\nu\left(\frac{1-\epsilon^2 r_1}{1-r_1}\right) - \epsilon\nu'\right], \tag{5.15}$$

with r_1 equal to $[\sigma_0(R)\sigma_1(R_{\rm m})/(\sigma_1(R)\sigma_0(R_{\rm m}))]^2$.

Thus, the MF of haloes at t is then

$$\frac{\partial n(M,t)}{\partial M} = N^{\rm nest}[\sigma_0,\delta_c]\,\frac{\partial\ln\sigma_0^{-1}}{\partial M}\,. \tag{5.16}$$

Note that this expression of the MF is also independent of the (arbitrary) initial time $t_{\rm i}$.

The CUSP formalism thus solves all the problems met in the excursion set formalism: it deals with triaxial peaks that undergo ellipsoidal collapse and virialisation, conveniently corrected for nesting, and the smoothing of the initial density field is always carried out with the same Gaussian filter. The only drawback of this ap-

proach is the need to solve the Volterra equation (5.12), which prevents from having an analytic expression for the resulting MF.

5.3 Implicit Halo Mass Definition

For any theoretical MF to be complete, the mass definition it refers to must be specified. In other words, one must state the condition defining the total radius $R_{\rm h}$ or, equivalently, the spherically averaged density profile for haloes with different masses at t that result from the specific halo seeds and dynamics of collapse assumed.

5.3.1 The Excursion Set Formalism

In the excursion set formalism, halo seeds are arbitrary overdense regions with no definite inner structure, so their typical (mean) density and peculiar velocity fields are uniform. As a consequence, the density distribution in the corresponding final virialised objects is also uniform[2]. In addition, the system is supposed to undergo spherical collapse. Therefore, halo formation follows the simple spherical top-hat model, in which case the typical radii $R_{\rm h}$ of haloes with different masses at t can be readily inferred (Peebles 1980).

As we have seen in section 3.7 the virial relation, holds for the final uniform object[3] together with energy conservation[4]. This implies that $R_{\rm h}$ is half the radius of the uniform system at turnaround.

we are lead to

$$E_{\rm p}(r) = -\frac{20\pi}{3}\int_0^r {\rm d}\tilde{r}\,\tilde{r}\,\rho_{\rm p}(\tilde{r})\,G\,\delta M(\tilde{r})\,. \tag{5.17}$$

Taking into account that the total energy $\mathcal{E}_{\rm p}(M_{\rm h})$ is, to leading order in the

[2]As shown in SVMS, what causes the outwards decreasing density profile of virialised objects is the fact that, for seeds with outwards decreasing density profiles, virialisation progresses from the centre of the system outwards. In the case of homogeneous spheres in Hubble expansion, all the shells cross at the same time at the origin of the system, so the final object does not have an outwards decreasing density profile.

[3]The effects of the cosmological constant at halo scales can be neglected.

[4]In the top-hat spherical model, energy cannot be evacuated outwards like in the virialisation of haloes formed by the collapse of seeds with outwards decreasing density profiles (SVMS), so the total energy is conserved.

perturbation, equal to $-\delta_{\rm cr}(t)GM^2/R$, equation (3.40) takes the form

$$R_{\rm h} = \left[\frac{3M}{4\pi\Delta_{\rm vir}(t)\bar{\rho}(t)}\right]^{1/3} \tag{5.18}$$

or, equivalently,

$$\bar{\rho}_{\rm h}(R_{\rm h}) = \Delta_{\rm vir}(t)\,\bar{\rho}(t)\,, \tag{5.19}$$

where we have introduced the so-called virial overdensity corresponding to the spherical top-hat model,

$$\Delta_{\rm vir}(t) \equiv \left[\frac{10\,\delta_{\rm c}^{th}(t)a(t)}{3\,D(t)}\right]^3 . \tag{5.20}$$

Comparing equations (5.1) and (5.19), we see that the halo mass definition implicitly presumed in the excursion set formalism is the SO($\Delta_{\rm vir}$) one, with $\Delta_{\rm vir}$ dependent on time and cosmology. In the Einstein-de Sitter universe, where $\delta_{\rm c}(t)$ is equal to $3(12\pi)^{2/3}/20$ and $D(t) = a(t)$, $\Delta_{\rm vir}(t)$ takes the constant value $18\pi^2 \approx 178$. While, at t_0 in the concordant model, where $\delta_{\rm c}(t_0)$ and $D(t_0)$ are respectively equal to ≈ 1.674 and ≈ 0.760, $\Delta_{\rm vir}(t_0)$ takes the value ≈ 359 (Henry 2000)[5].

5.3.2 The CUSP Formalism

As we have already seen, the CUSP MF is more general than the excursion set one in the sense that it does not presume any particular mass definition; it holds for any arbitrary one, adapting to it through the functions $\delta_{\rm c}(t)$ and the relation between top-hat and Gaussian spectral moments.

5.4 Similarity of SO and FoF Masses

The fact that the CUSP formalism distinguishes between different mass definitions can be used to try to understand the origin of the similarity between SO and FoF masses and their respective mass and multiplicity functions.

[5]According to equation (5.20), $\Delta_{\rm vir}(t_0) = 359$ and $D(t_0) = 0.760$ imply $\delta_{\rm c}(t_0) = 1.621$ rather than 1.674. This 3.5% error arises from the neglect of the cosmological constant in equation (5.20).

Equations (3.42) and (5.17) imply

$$\frac{\mathrm{d}E_\mathrm{p}}{\mathrm{d}M} = -\frac{5G\,\delta M(R_\mathrm{p})}{3R_\mathrm{p}} = -\frac{5}{3}\left[\frac{4\pi\bar{\rho}_\mathrm{i}}{3}\right]^{1/3} GM^{2/3}\delta_c^\mathrm{th}(M,t)\,, \tag{5.21}$$

where we have taken into account that the radius R_p of the protohalo is equal to $q_\mathrm{p}R$ (see Section 3.2). Comparing with the M-derivative of equation (3.40) and taking into account the identity $M = 4\pi\bar{\rho}_\mathrm{h}(R_\mathrm{h})R_\mathrm{h}^3/3$, equation (5.21) leads to the relation

$$\frac{5}{9}\left[\frac{\bar{\rho}_\mathrm{i}}{\bar{\rho}(t)}\right]^{1/3}\delta_c^\mathrm{th}(M,t) = \left[\frac{\bar{\rho}_\mathrm{h}(R_\mathrm{h})}{\bar{\rho}(t)}\right]^{1/3}\left[1-\frac{\bar{\rho}_\mathrm{h}(R_\mathrm{h})}{6\,\rho_\mathrm{h}(R_\mathrm{h})}\right], \tag{5.22}$$

which, making use of the definition of $F(c)$, can be rewritten in the two following forms

$$\bar{\rho}_\mathrm{h}(R) = \bar{\rho}(t)\left[\frac{5\,\delta_c^\mathrm{th}(M,t)a(t)}{9\,a(t_\mathrm{i})}\right]^3\left[1-\frac{F(c)}{6}\right]^{-3} \tag{5.23}$$

and

$$\rho_\mathrm{h}(R) = \bar{\rho}(t)\left[\frac{5\,\delta_c^\mathrm{th}(M,t)a(t)}{9\,a(t_\mathrm{i})]}\right]^3\left[1-\frac{F(c)}{6}\right]^{-3}\frac{1}{F(c)}\,. \tag{5.24}$$

For SO and FoF masses, these expressions therefore imply

$$\Delta = \left[\frac{5\,\delta_c^\mathrm{th}(M,t)a(t)}{9\,a(t_\mathrm{i})}\right]^3\left[1-\frac{F(c)}{6}\right]^{-3} \tag{5.25}$$

and

$$b = \left[\frac{2\pi}{3F(c)}\right]^{-1/3}\left[\frac{5\,\delta_c^\mathrm{th}(M,t)a(t)}{9\,a(t_\mathrm{i})}\right]^{-1}\left[1-\frac{F(c)}{6}\right]\,, \tag{5.26}$$

respectively.

Equation (5.25) seems to indicate that, in the SO case, *the mass dependence* of δ_c^th must cancel with that coming from $F(c)$. But equation (5.1) implies $R_\mathrm{h} \propto M^{1/3}$, which, replaced into equation (3.40) at $r = R_\mathrm{h}$, leads to $E_\mathrm{p}(M) \propto M^{5/3}$ and, hence, to $\mathrm{d}E_\mathrm{p}/\mathrm{d}M \propto M^{2/3}$, implying (see eq. [5.21]) that δ_c^th is *a function of* t *alone*. The solution to this paradox is that, to leading order in the perturbation as used in the derivation of the density profile (see eq. [3.43]), δ_c^th and $F(c)$ are, in the SO case, independent of M. (Likewise, eq. [5.26] multiplied by the cubic root of $F(c)$ leads in the FoF case to a similar paradox, with identical solution.) Consequently, to such an order of approximation, the SO and FoF mass definitions with Δ and b satisfying equation (5.3) are equivalent to each other.

We thus see that the origin of this approx equivalence is the inside-out growth of accreting haloes, crucial to obtain equation (3.40) setting the typical spherically averaged density profile for haloes arising from peaks that undergo ellipsoidal collapse and virialisation. But this is not all. We can go a step further and infer the value of b leading to FoF masses equivalent to SO($\Delta_{\rm vir}$) ones.

The relation between the two functions (of t) $\delta_c^{\rm th}$ and $1 - F(c)/6$ can be readily derived for the particular case of SO($\Delta_{\rm vir}$) haloes. Through equation (3.40), we have that haloes arising from ellipsoidal collapse of peaks with δ_c in the density field at $t_{\rm i}$ smoothed with a Gaussian filter of radius R, could have formed according to the spherical top-hat model from the same seeds with $\delta_c^{\rm th}$ when the density field is smoothed with a top-hat filter of radius qR.[6] Equations (5.20) and (5.25), the latter for $\Delta = \Delta_{\rm vir}$, then imply

$$\delta_c^{\rm th}(t) = \delta_{\rm cr}(t)\, 6 \left[1 - \frac{F(c)}{6}\right] . \tag{5.27}$$

The typical value of $F(c)$ for SO($\Delta_{\rm vir}$) haloes can be inferred from equation (5.27) for $\delta_{\rm cr}(t)$ given by equation (5.4) and $\delta_c^{\rm th}$ given by

$$\delta_c^{\rm th}(M,t) = \frac{3}{R_{\rm p}^3} \int_0^{R_{\rm p}} {\rm d}r\, r^2\, \delta_{\rm p}(r) . \tag{5.28}$$

for seeds of any arbitrary mass. However, the density profile $\delta_{\rm p}(r)$ of protohaloes is not accurate enough (owing to the inverse Laplace transform of eq. [3.21]) for $\delta_c^{\rm th}$ to be inferred with the required precision. Therefore, as the CUSP formalism recovers, to leading order in the perturbation, the typical spherically averaged density profile for simulated haloes, we can estimate $F(c)$ directly from such empirical profiles. As well-known these profiles are of the NFW form (Navarro et al. 1997) and, hence, satisfy the relation

$$F(c) \equiv \frac{\bar{\rho}_{\rm h}(R_{\rm h})}{\rho_{\rm h}(R_{\rm h})} = 3\, \frac{(1+c)^2}{c^2} \left[\ln(1+c) - \frac{c}{1+c}\right] . \tag{5.29}$$

For c spanning from ~ 5 to ~ 15 as found in simulations of the concordant cosmol-

[6]The outwards decreasing density profile of seeds for *purely accreting haloes* ensures the possibility to use any spherical window to define the one-to-one correspondence between haloes and peaks. The use of a Gaussian window is only mandatory, as mentioned, if haloes can also undergo major mergers (see MSS and SVMS).

ogy for SO($\Delta_{\rm vir}$) haloes at t_0 (and approximately at any other time and cosmology), we find $F(c) \sim 5.1 \pm 0.1$. And, bringing this value of $F(c)$ and $\Delta = \Delta_{\rm vir} \approx 359$ into equation (5.3), we arrive at $b \sim 0.19$, in full agreement with the results of numerical simulations. Of course, the exact typical value of $F(c)$ varies with time and cosmology (see Chapter 4). But, according to the results of numerical simulations, we do not expect any substantial variation in this sense, so we have that FoF(0.2) masses are approximately equivalent to SO($\Delta_{\rm vir}$) ones, in general.

As a byproduct we have that equation (5.27) for $F(c) \approx 5.1 \pm 0.1$ implies the relation $\delta_{\rm c}^{\rm th}(t) \sim 0.9\,\delta_{\rm c}(t)$. In other words, in the case of SO($\Delta_{\rm vir}$) or FoF(0.2) masses, the top-hat density contrast for ellipsoidal collapse and virialisation would take an almost universal value independent of M, just a little smaller than the almost universal value $\delta_{\rm c}(t)$ for spherical collapse. This result thus suggests that it should be possible to modify the excursion set formalism in order to account for ellipsoidal collapse and virialisation by simply decreasing the usual density contrast for spherical collapse by a factor ~ 0.9. We will comeback to this interesting prediction below.

5.5 Multiplicity Function

The multiplicity function associated with any given MF, $\partial n(M,t)/\partial M$, is defined as

$$f(\sigma_0^{\rm th}, t) = \frac{M}{\bar{\rho}} \frac{\partial n[M(\sigma_0^{\rm th}), t]}{\partial \ln[(\sigma_0^{\rm th})^{-1}]} \,. \tag{5.30}$$

In the excursion set case, this leads to a function of the simple form

$$f_{\rm es}(\sigma_0^{\rm th}, \delta_{\rm c0}) = \left(\frac{2}{\pi}\right)^{1/2} \nu_{\rm es}\, {\rm e}^{-\frac{\nu_{\rm es}^2}{2}} \,, \tag{5.31}$$

while, in the CUSP case, it leads to (see eqs. [5.16] and [5.30])

$$f_{\rm CUSP}(\sigma_0, \delta_{\rm c0}) = \frac{M(\sigma_0, \delta_{\rm c0})}{\bar{\rho}}\, N^{\rm nest}(\sigma_0, \delta_{\rm c0}) \,. \tag{5.32}$$

To obtain equation (5.32) we have taken the partial derivative of $n_{\rm CUSP}$ with respect to σ_0 instead of $\sigma_o^{\rm th}$ as prescribed in equation (5.30). But this is irrelevant for SO($\Delta_{\rm vir}$) or FoF(0.19) masses in the concordant cosmology as hereafter assumed, given the relation (3.10) between the two 0th order spectral moments.

5.5.1 Comparison with Simulations

In Figure 5.1 we compare these two multiplicity functions at t_0 to the Warren et al. (2006) analytic expression, of the Sheth & Tormen (2002) form,

$$f_{\rm W}(\nu_{\rm es}) = 0.3303 \left(\nu_{\rm es}^{1.625} + 0.5558\right) \, {\rm e}^{-0.4565\nu_{\rm es}^2} \, , \tag{5.33}$$

fitting the multiplicity function of simulated haloes with FoF(0.2) masses at t_0 in all CDM cosmologies. $f_{\rm W}$ is usually expressed as a function of $\sigma_0^{\rm th}$ instead of $\nu_{\rm es}$; the expression (5.33) has been obtained from that usual expression assuming $\delta_{\rm c}(t_0) = 1.674$ (taking the value 1.686 would make no significant difference). In Figure 5.1, all the multiplicity functions are expressed as functions of the Gaussian height for ellipsoidal collapse and virialisation, ν, instead of the top-hat height for spherical collapse, $\nu_{\rm es}$. The change of variable from $\nu_{\rm es}$ to ν has been carried out using the relation 3.10. This is a mere change of variable; it does not presume any modification in the assumptions entering the derivation of the different multiplicity functions.

As can be seen, while $f_{\rm es}$ shows significant deviations from $f_{\rm W}$ at both mass ends, $f_{\rm CUSP}$ is in excellent agreement with $f_{\rm W}$ all over the mass range covered by simulations. This is true regardless of whether we consider the approximate or more accurate versions of $f_{\rm CUSP}$. The deviation (of opposite sign in both cases) is less than 6.5%. We stress that there is no free parameter in the CUSP formalism, so this agreement is really remarkable.

It might be argued that $f_{\rm CUSP}$ cannot be trusted at small ν's because peaks with those heights have big chances to be destroyed by the gravitational tides of neighbouring massive peaks. Although this possibility exists, peaks suffering strong tides are expected to be nested within such neighbours and, hence, they should not be counted in the MF corrected for nesting. The correction for nesting becomes increasingly important, indeed, towards the small ν end. On the other hand, $f_{\rm CUSP}$ is well-normalised[7] and still predicts the right abundance of massive haloes, which would hardly be the case if $f_{\rm CUSP}$ overestimated the abundance of low-mass objects. Therefore, we do not actually expect any major effect of that kind.

It is thus worth seeing how $f_{\rm CUSP}$ compares to $f_{\rm W}$ outside the mass range covered by simulations. In Figure 5.2 we represent the same multiplicity functions as in Figure 5.1 over a much wider range. Surprisingly, the agreement between $f_{\rm CUSP}$ and

[7]The CUSP MF is well-normalised by construction as this is one of the conditions imposed to obtain the functions $\delta_{\rm c}(t)$ and $q(M,t)$.

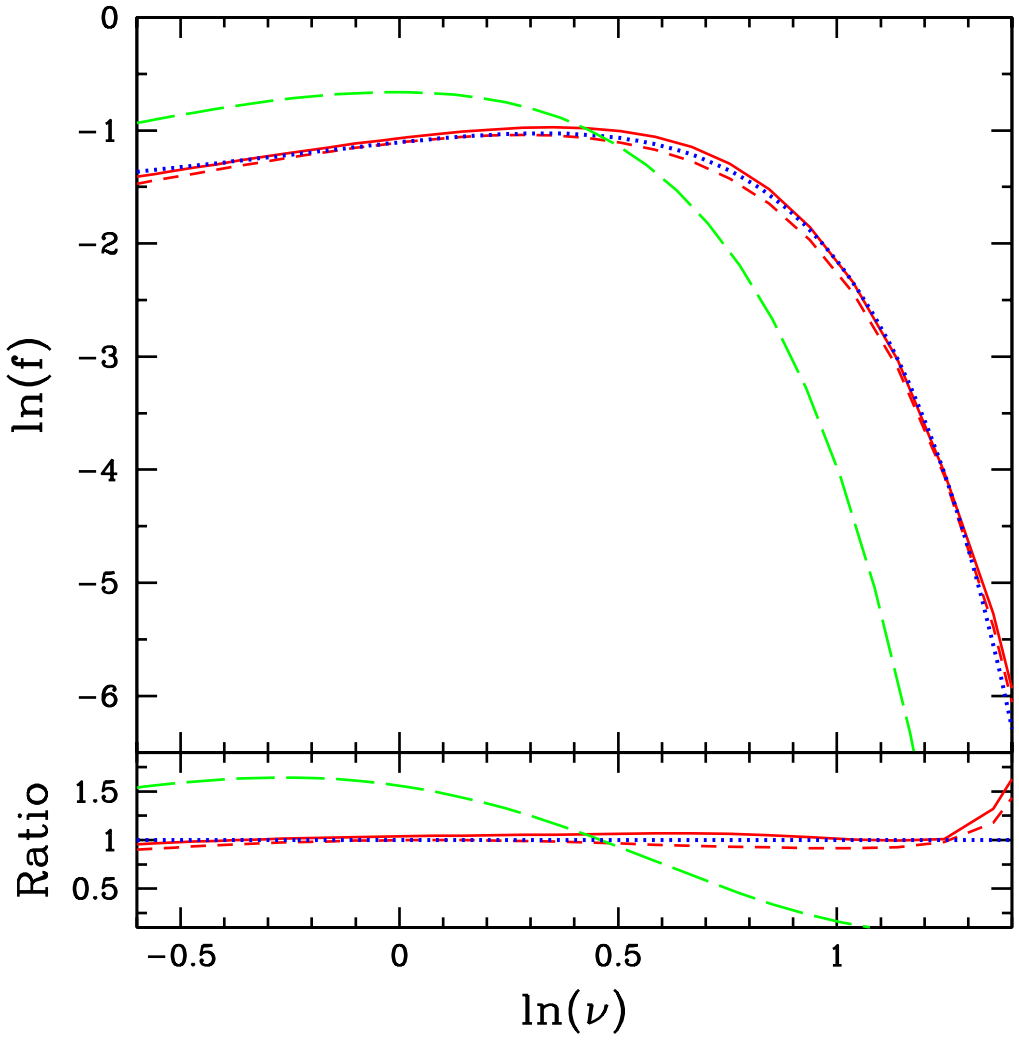

Figure 5.1: Multiplicity function at t_0 derived from the CUSP (red lines) and excursion set (green long-dashed line) formalisms, compared to Warren et al. (2006) analytic fit to the multiplicity function of simulated haloes (blue dotted line) over the maximum mass range (2×10^{10} $M_\odot$, 2×10^{15} $M_\odot$) covered by simulations. For the CUSP case, we plot both the the approximate solution not accounting for the correlation between peaks of different scales (dashed line) and the more accurate solution given in Appendix C (solid line). Ratios in the bottom panel are with respect to f_W.

f_W is still very good. At very small ν's, f_W shows a slight trend to underestimate

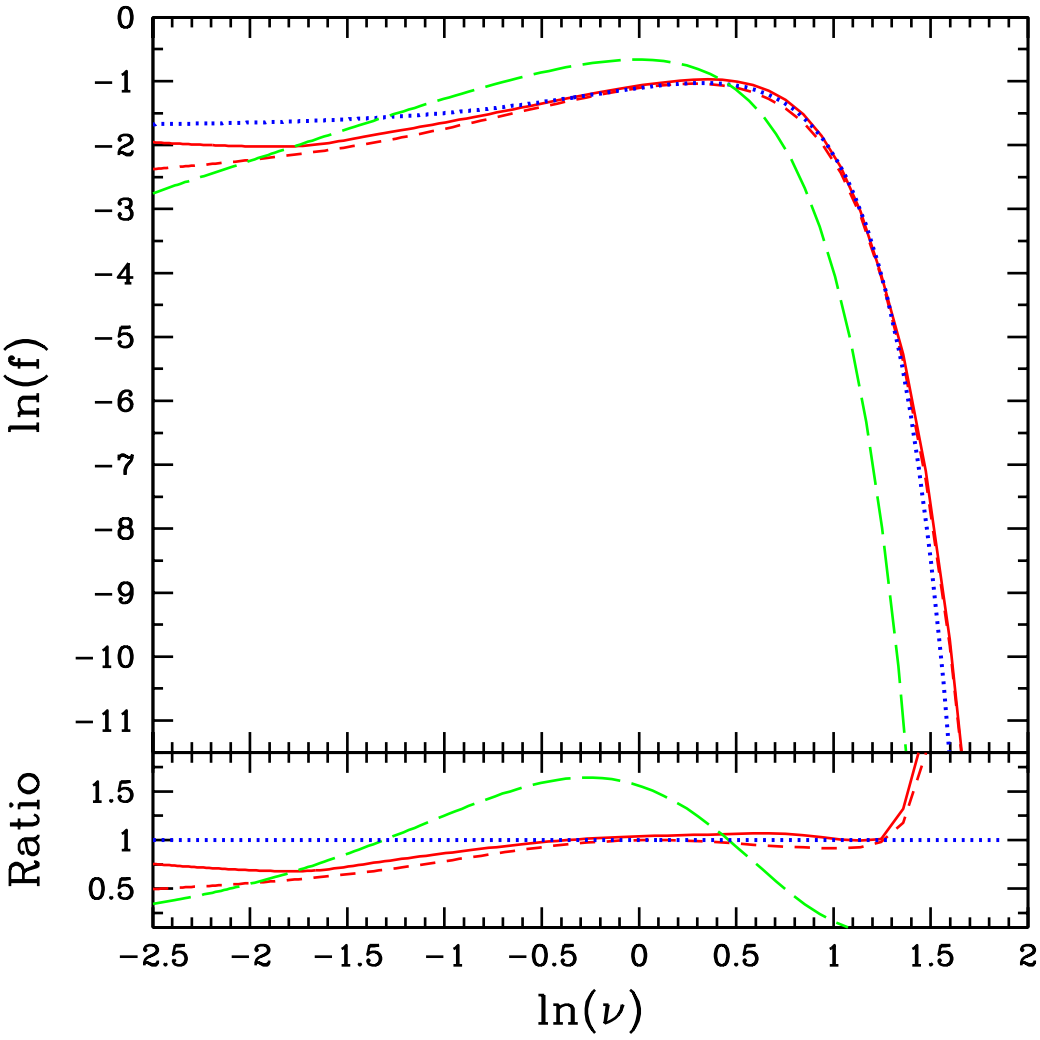

Figure 5.2: Same as Figure 5.1 but in a much wider mass range, corresponding to current haloes with masses from 1 $M_\odot$to 3×10^{16} $M_\odot$.

the abundance of haloes predicted by $f_{\rm CUSP}$, but the difference is small. It increases monotonously until reaching, in the case of the accurate version of $f_{\rm CUSP}$, a ratio of ~ 0.70 ($\sim 30\%$ deviation) at $M \sim 5 \times 10^4$ $M_\odot$.

5.5.2 Approx Universality

The excursion set multiplicity function expressed as a function of $\nu_{\rm es}$, $f_{\rm es}(\nu_{\rm es})$, is cosmology-independent (it takes the same form [5.31] in all cosmologies) and time-invariant (the height is constant). Hence, it is universal in a strict sense. Such a universality is in fact what has motivated the use of the multiplicity function defined in equation (5.30) instead of the (non-universal) MF. Unfortunately, $f_{\rm es}$ does not properly recover the multiplicity function of simulated haloes.

But $f_{\rm CUSP}$ does, so the question rises: is $f_{\rm CUSP}$ also universal? Certainly, since the CUSP MF (as well as the real MF of simulated haloes) depends on the particular halo mass definition while $\sigma_0^{\rm th}$ does not, $f_{\rm CUSP}$ will necessarily depend on the mass definition adopted.(like the multiplicity function of simulated haloes; see e.g. Tinker et al. 2008). Thus, we will focus on the SO($\Delta_{\rm vir}$) or FoF(0.2) mass definitions, as suggested by the results of simulations (see the form [5.33] of $f_{\rm W}(\nu_{\rm es})$).

By construction, the unconditioned and conditional peak number densities, $N(\sigma_0, \delta_{\rm c})$ and $N(\sigma_0, \delta_{\rm c}|\sigma_0', \delta_{\rm c})$ entering the Volterra equation (5.12) take the same form of σ_0, σ_0' and $\delta_{\rm c0}$, through the heights ν and ν', in all cosmologies (see eqs. [5.10], [5.13] and [5.11])[8]. Certainly, these number densities also depend on γ, γ' and $R_\star$ that involve spectral moments of different orders and, hence, depend on the cosmology through the exact shape of the (linear) power spectrum. However, in all CDM cosmologies, the effective spectral index n takes essentially the same fixed value, with less than 20% error over the whole mass range (2×10^{10} M$_\odot$, 2×10^{15} M$_\odot$) of interest, implying that $\gamma\approx\gamma'$ and $R_\star/R[3(1-\gamma^2)]^{1/2}$ takes almost "universal" values respectively equal to 0.6 ± 0.1 and 1.4 ± 0.1. Thus, those number densities are indeed very approximately universal functions of ν and ν' *but for a factor* R^{-3}. Moreover, if we multiply the Volterra equation (5.12) by $M/\bar\rho = 4\pi\bar\rho_{\rm i}(qR)^3/(3\bar\rho)$ so that its solution is directly $f_{\rm CUSP}$ (see eq. [5.32]), then the factor R^{-3} in the two number densities cancels with the factor R^3 coming from the mass. Therefore, the solution $f_{\rm CUSP}$ of such a Volterra equation will have very approximately the same expression of ν in all CDM cosmologies, provided only the function $q(M,t)$ does.

But, according to equations (3.11)–(3.10) holding for SO($\Delta_{\rm vir}$) and FoF(0.19) haloes, $q(M,t)$ involves the ratio $\sigma_0^{\rm th}/\sigma_0$ which is not a function of ν alone, but also depends on t through the cosmology-dependent relation 3.10. Nevertheless,

[8] ϵ takes the form $2^{(n+3)/2}(\nu/\nu')[1+(\nu/\nu')^{4/(n+3)}]^{-(n+3)/2}$, where n is the effective spectral index in the relevant mass range.

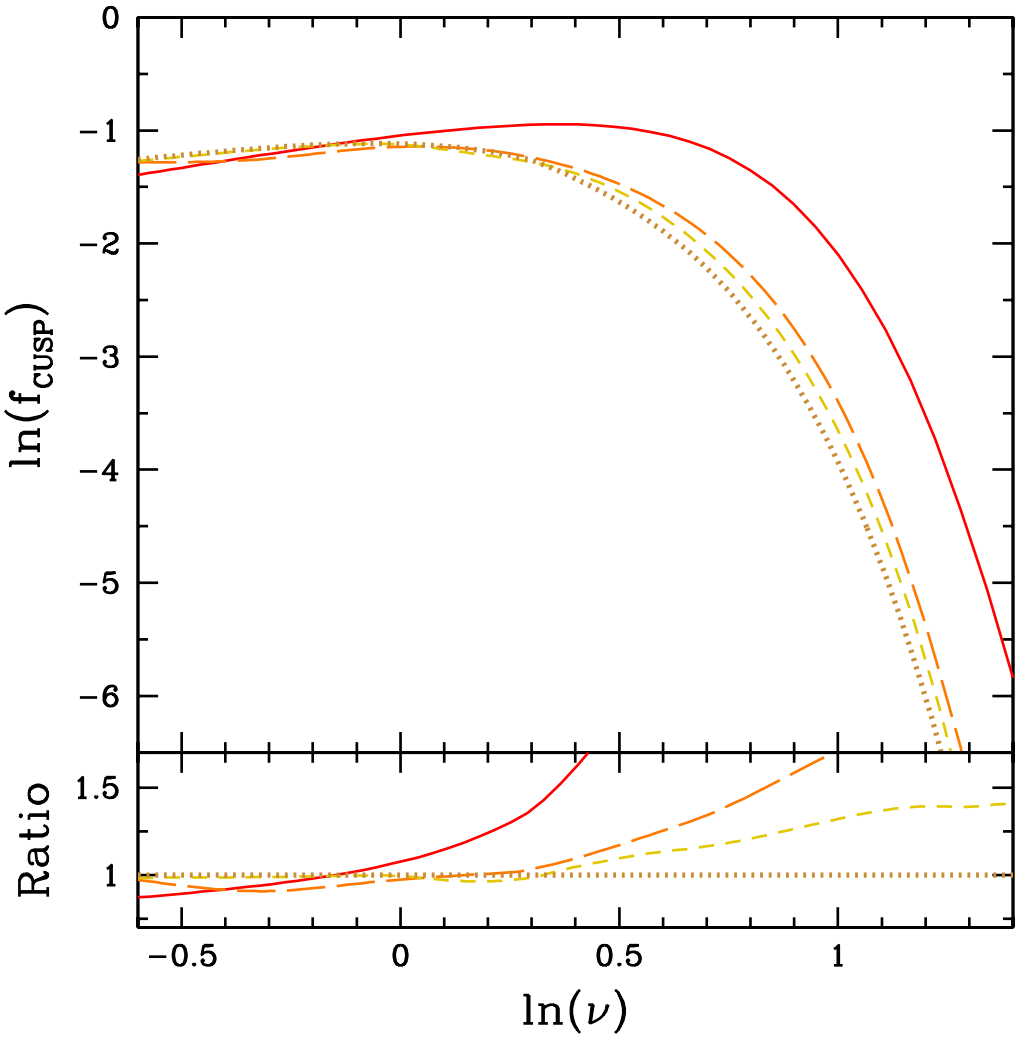

Figure 5.3: CUSP multiplicity functions at $z = 0$, 5, 10 and 20, from left to right, in red (solid line), orange (long-dashed line), gold (dashed line) and brown (dotted line), respectively. Ratios in the bottom panel are with respect to the multiplicity function at $z = 20$.

the term with the ratio $\sigma_0^{\rm th}/\sigma_0$ responsible of the undesired functionality of $q(M,t)$ is small in general (except for large ν's), particularly at high-z where $D(t)/D(t_0)$ becomes increasingly small. There, $q(M,t)$ becomes constant (equal to $Q^{-2/(n+3)}$) and $f_{\rm CUSP}(\nu)$ becomes essentially universal. However, at low-z this is only true for small enough ν's.

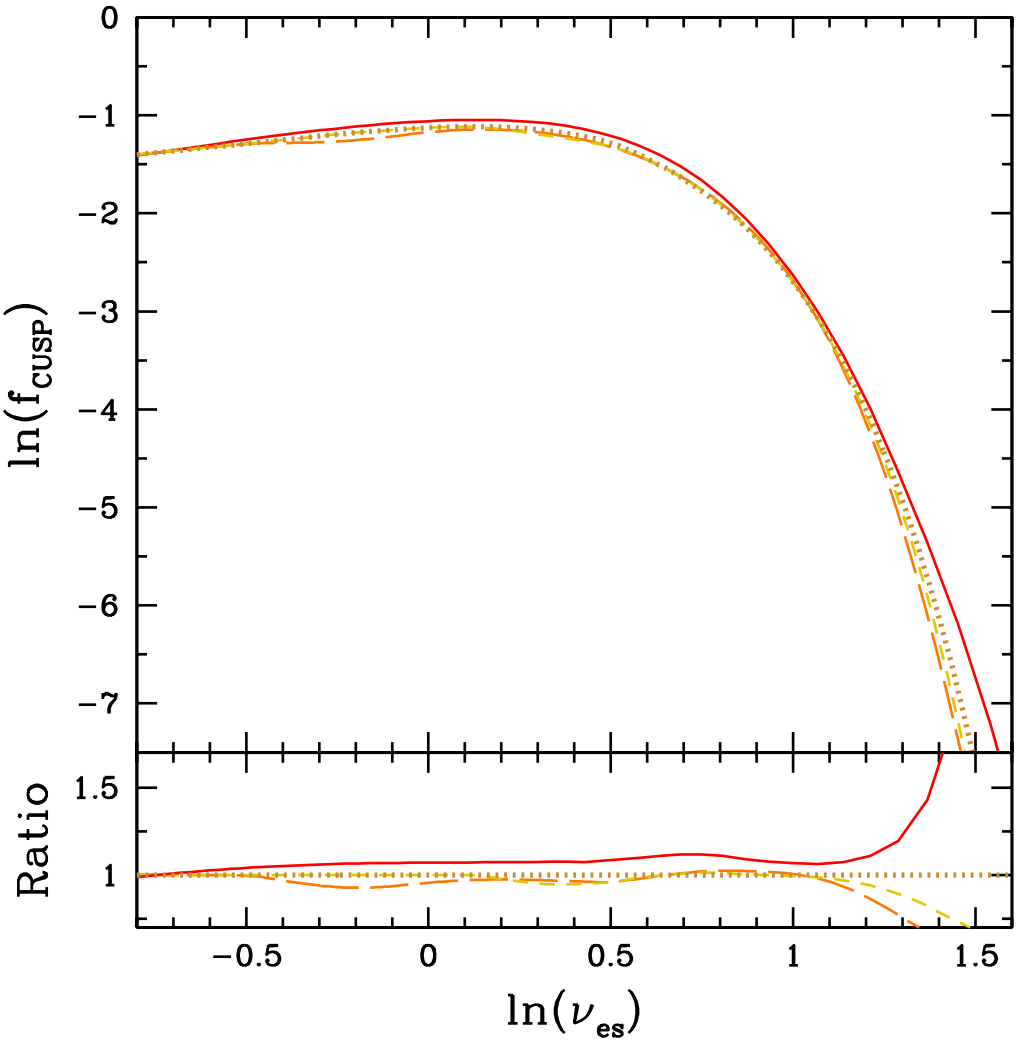

Figure 5.4: Same as Figure 5.3 but for $f_{\rm CUSP}$ expressed as a function of variable $\nu_{\rm es}$ instead of ν. The green long-dashed line represents the multiplicity function that would be obtained from the excursion set formalism taking a density contrast for spherical collapse equal to 0.89 times the usual value.

In Figure 5.3 we show $f_{\rm CUSP}(\nu)$ in the concordant model for various redshifts (see 3.4 for the corresponding MFs, in full agreement with the results of simulations). The deviations from universality or, more exactly, from time-invariance at high-z are small as expected, but at low-z they are very marked. Thus, $f_{\rm CUSP}(\nu)$ is far

from universal.

But this result was not unexpected. Given the relation between ν and $\nu_{\rm es}$, we cannot pretend that $f_{\rm CUSP}(\nu)$ is universal as a function of both arguments at the same time. Inspired by the universality of $f_{\rm es}(\nu_{\rm es})$, most efforts in the literature have been done in trying to find one mass definition rendering the multiplicity function of simulated haloes approximately universal *as a function of the top-height for spherical collapse*, not as a function of the (unknown) Gaussian height for ellipsoidal collapse and virialisation. Therefore, what we should actually check is whether $f_{\rm CUSP}$ is universal as a function of $\nu_{\rm es}$ and not of ν. As shown in Figure 5.4, when the change of variable from ν to $\nu_{\rm es}$ is made, $f_{\rm CUSP}$ becomes indeed almost fully time-invariant. Strictly, it still shows slight deviations from universality at large $\nu_{\rm es}$, but these deviations are in full agreement with those found in simulations (see Fig. 14 in Lukić et al. 2007).

Thanks to the CUSP formalism, we can determine the Gaussian height for ellipsoidal collapse and virialisation corresponding to any desired mass definition. Thus, we can seek the halo mass definition for which $f_{\rm CUSP}$ expressed as a function of ν takes a universal form. According to the reasoning above, for this to be possible the ratio $\sigma_0^{\rm th}/\sigma_0$ should be equal to $1 + c\,\nu$, with c equal to an arbitrary universal constant. This would ensure both that the partial derivative of $n_{\rm CUSP}$ with respect to σ_0 coincides with the partial derivative with respect to $\sigma_0^{\rm th}$ and that the function $q(M,t)$ is a function of ν alone: $q(\nu) \approx [Q\ (1 + c\,\nu)]^{-2/(n+3)}$. Consequently, following the procedure given in Section 5.3.2, we can infer, from such a function $q(\nu)$ and any arbitrary function $\delta_{\rm c}(t)$, the desired halo mass definition. Unfortunately, despite the freedom left in those two functions, the mass definition so obtained will hardly coincide with any of the practical SO and FoF ones. Thus, it is actually preferable to keep on requiring the universality of the multiplicity function in terms of $\nu_{\rm es}$ as usual.

But this does not explain why the FoF mass definition with linking length ~ 0.2 is successful in giving rise to a universal multiplicity function expressed as a function of $\nu_{\rm es}$. Clearly, what makes this mass definition special is that, for the reasons explained in Section 5.4, it coincides with the SO($\Delta_{\rm vir}$) definition. In fact, as mentioned there, the exact value of the linking length may somewhat vary with time and cosmology, so the canonical mass definition would be the SO($\Delta_{\rm vir}$) definition rather than the FoF(0.2) one. But why should a mass definition that involves the virial overdensity $\Delta_{\rm vir}$ arising from the formal *spherical top-hat model* successfully lead to a universal multiplicity function expressed as a function of $\nu_{\rm es}$ if haloes actually form

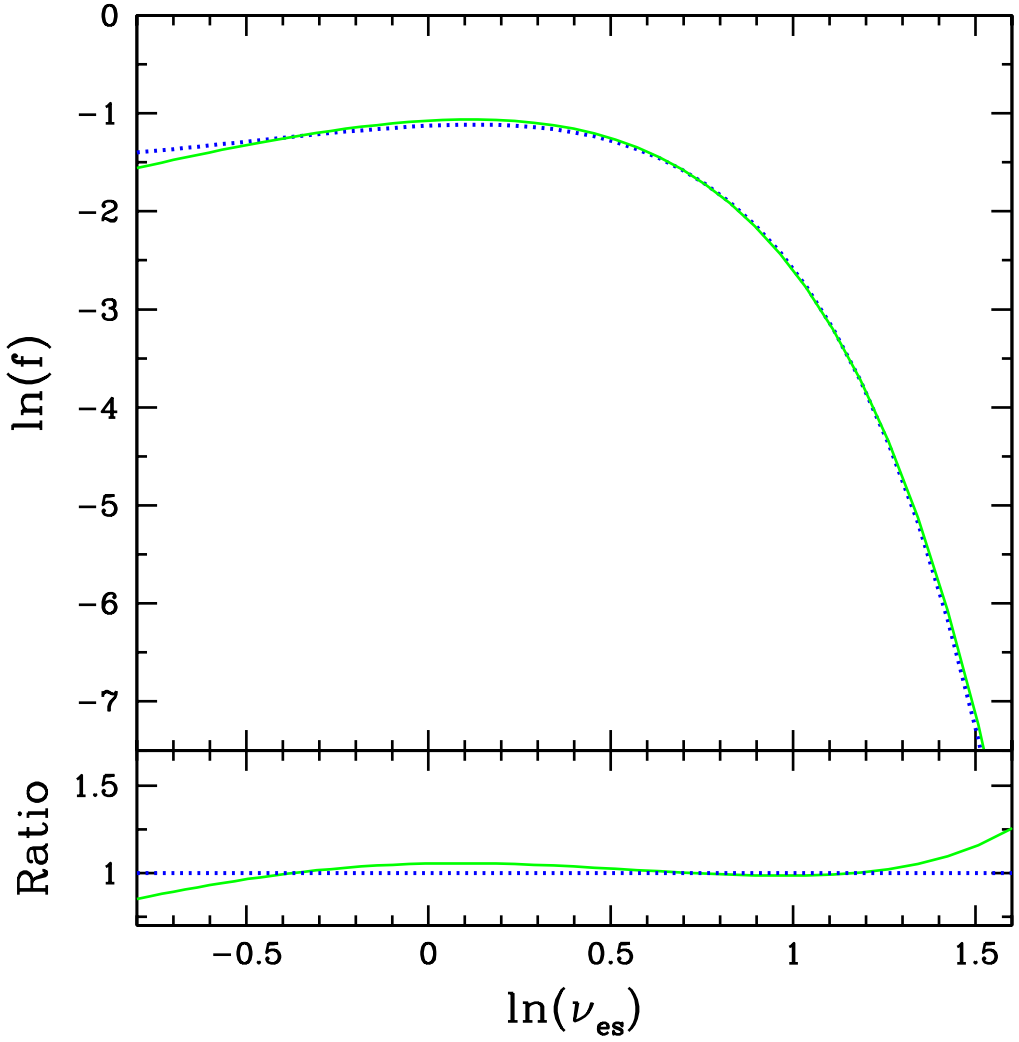

Figure 5.5: Modified excursion set multiplicity function resulting from a density contrast for collapse equal to 0.889 times the usual value (solid green line), compared to $f_{\rm W}$ for FoF(0.2) haloes (dotted blue line). Both multiplicity functions are strictly universal, so the two curves hold for any arbitrary redshift.

from peaks that undergo *ellipsoidal collapse and virialisation*? The reason for this is that, as a consequence of the inside-out growth of haloes formed from ellipsoidal collapse and virialisation, they satisfy the relation (3.40), also satisfied by objects formed in the spherical top-hat model.

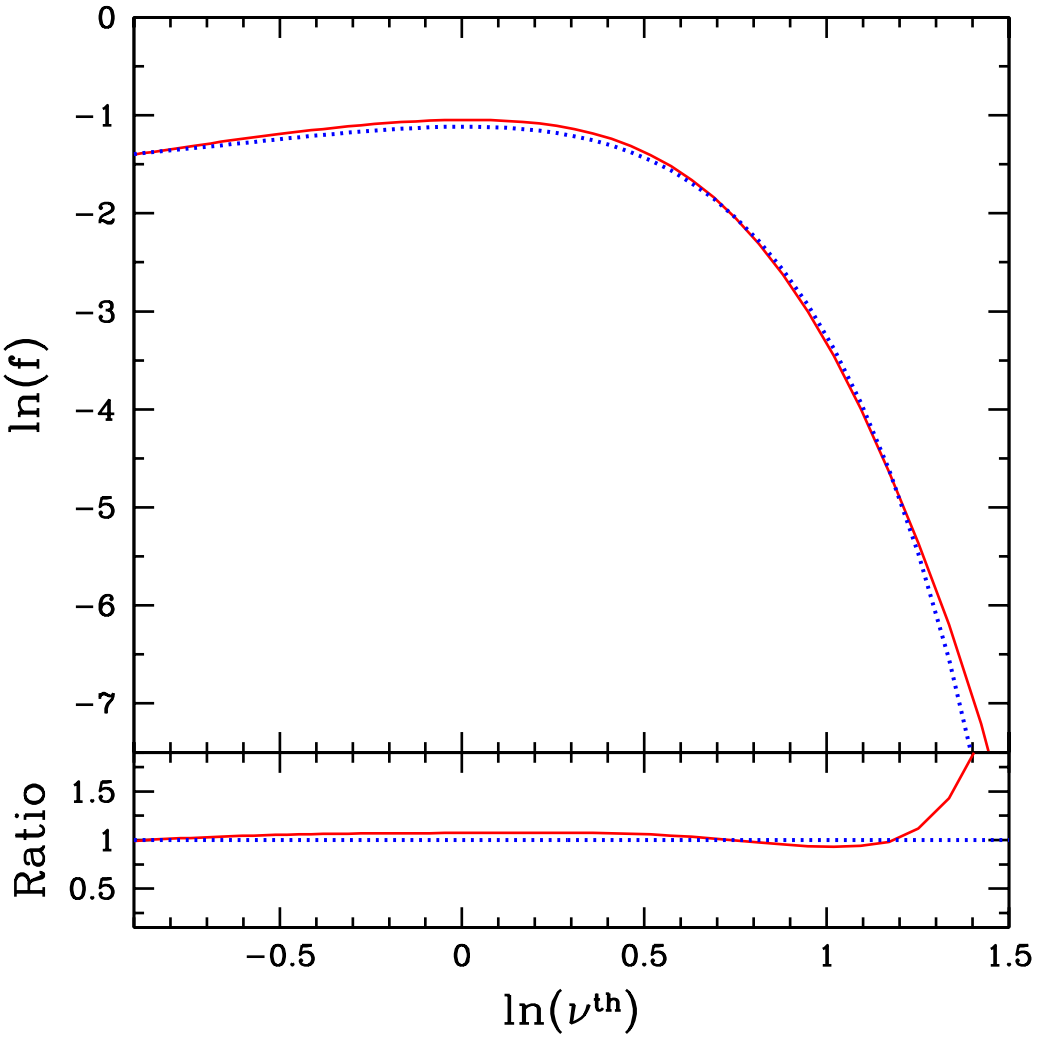

Figure 5.6: Same as Figures 5.3 and 5.4 but for $f_{\rm CUSP}$ expressed as a function of the top-hat height for ellipsoidal collapse and virialisation, $\nu^{\rm th}$, as suggested by the CUSP formalism. This multiplicity function would be strictly universal, so the curves for the different redshifts fully overlap. For comparison we also plot the function $f_{\rm W}$ (blue dotted curve) expressed with the same argument.

As mentioned, an interesting consequence of this "coincidence" is that the top-hat density contrast for ellipsoidal collapse and virialisation for SO($\Delta_{\rm vir}$) masses, $\delta_{\rm c}^{\rm th}$, takes a universal value, independent of M, approximately equal to 0.9 times the top-hat density contrast for spherical collapse, $\delta_{\rm c}(t)$. Given this relation, changing

the latter density contrast by the former in the excursion set formalism, $f_{\rm es}(\nu_{\rm es})$ should keep on being universal and, in addition, recover the real multiplicity function of haloes formed by ellipsoidal collapse and virialisation. As shown in Figure 5.5, this is fully confirmed. One must just renormalise the resulting modified excursion set multiplicity function in the relevant mass range by multiplying it by 0.714. But this is simply due to the fact that the correction for nesting achieved in the excursion set formalism is inconsistent with top-hat smoothing, which yields an increasing deviation of the predicted function at low-masses, the most affected by such a correction. (The right normalisation should naturally result if we could implement the excursion set correction for nesting with top-hat smoothing.)

Therefore, the ultimate reason for the success of the SO($\Delta_{\rm vir}$) mass definition, and by extension of the FoF(0.2) one, is that, as a consequence of the inside-out-growth of accreting haloes, the corresponding top-hat density contrast for ellipsoidal collapse and virialisation is essentially proportional to the formal top-hat density contrast for spherical collapse.

To end up we want to mention that the previous result suggests what is actually the most natural argument for the halo multiplicity function to take a universal form: *the top-hat height for ellipsoidal collapse and virialisation*, $\nu^{\rm th}$, defined as $\delta_{\rm c0}^{\rm th}(t_0)/\sigma_0^{\rm th} \approx 0.889\,\delta_{\rm c0}(t_0)/\sigma_0^{\rm th}$. This expression holds for the current time and the concordant cosmology. The exact dependence of $\delta_{\rm c}^{\rm th}(t)$ (or, more exactly, of the ratio $\delta_{\rm c}^{\rm th}(t)/\delta_{\rm c}(t)$) on time and cosmology is hard to tell owing to the insufficient precision of the inverse Laplace transform of equation (3.21) or, alternatively, the unknown range of c values of simulated haloes with SO($\Delta_{\rm vir}$) masses at other times and cosmologies. But a reasonable guess is that such a dependence should make $f_{\rm CUSP}(\nu^{\rm th})$ be strictly universal and equal to the multiplicity function represented in Figure 5.6. The reason for this guess is the full consistency, at any time and cosmology, between the SO($\Delta_{\rm vir}$) mass definition and the real dynamics of collapse and virialisation of halo seeds. A similar full consistency is what causes $f_{\rm es}(\nu_{\rm es})$ to be also strictly universal. The difference between the two cases is that, while the excursion set formalism assumes a non-realistic dynamics of collapse (unless it is modified as prescribed above), the CUSP formalism assumes the right dynamics.

6
Summary and Conclusions

Maybe all the schemes of the devil were nothing
compared to what man could think up.
Joe Hill

Throughout this Thesis we have completed an accurate analytic treatment of non-linear structure formation by means of the filtering of the primordial density field. This formalism is able to accurately recover the results of N-body simulations for any desired halo mass definition and cosmology (Salvador-Solé et al. 2012a,b) and allows one to shed light on their ultimate origin.

We have given a general overview of this formalism, explaining its theoretical grounds and how it can be used to derive the typical properties of relaxed dark matter halos. In this overwiew:

1. We have proven the existence of a one-to-one correspondence between halos and peaks despite the ellipsoidal collapse of peaks.
2. We have shown that halos formed through major mergers and accretion have the same properties, dependent on the properties of the respective progenitor peaks at the largest scale.
3. As a consequence, we have explained why the typical properties of halos depend only on their mass and time, regardless of whether and when they have

suffered major mergers.

We have also applied this analytic formalism to analyze halo growth. In particular:

1. We have shown that accreting halos grow inside-out, which is a crucial ingredient in the CUSP formalism.
2. We have derived practical analytical expressions for the mass-concentration-shape NFW (Navarro et al. 1995) and Einasto (1965) relations over the whole mass and redshift ranges.
3. We have stablished the validity domains of the above mentioned relations.

Finally, we have applied the CUSP formalism to study the halo mass and multiplicity functions, and their dependence on the exact mass definition used. In particular:

1. We have shown that the FoF(0.2) halo finding algorithm is equivalent to the SO($\Delta_{\rm vir}$) one, which explains the privileged linking length equal to 0.2
2. We have shown why the virial radii of halos are close to the top-hat radii described by the spherical collapse model, and why the halo mass function is so close to the Press-Shechter form.
3. We have explained why the halo multiplicity function is closely universal in the two equivalent cases of FoF (0.19) and SO(Δ_{vir}).

Although not included in this Thesis, the CUSP formalism also allows one to accurately deal with halo substructure. Work along this particular line is currently in progress (Salvador-Solé et al. 2016b).

The only limitations of this formalism arise from the neglect of the gravitational pull between nearby objects, which yield tidal torques between them, causing their small angular momenta (Doroshkevich 1970; White 1984) and tidally-supported elongations (Salvador-Sole & Solanes 1993), and of the gravitational drag of baryons (Gnedin & Ostriker 1999; Gnedin & Zhao 2002; Governato et al. 2012). These effects should nonetheless be easier to address analytically from the sound basis presented here dealing with self-gravitating, though non-interacting, pure DM halos.

6.1 Further Work

Making use of the CUSP formalism, it should be possible to calculate such important issues as:

- Halo substructure and kinematics, explaining why the later are approximately universal.
- The scatter in halo properties.
- The halo assembly bias
- The spatial correlation between halos of different masses
- Filamentary large-scale structure formation
- The properties of stellar streams and stellar spheroids at the centre of dark matter halos.

Appendices

A

The Number Density of Peaks

A.1 Evaluating the Maximum Constraint

The notation used in this Chapter follows the one introduced by BBKS. Therefore, $\mathcal{N}_{pk}(\nu)d\nu$, with $\nu = \delta/\sigma_0(R)$, refers to the number density of peaks per infinitesimal range of height, and $n_{pk}(\nu_c)$ refers to the number density of peaks with height above the value ν_c. Both quantities also depend on the scale R, which works as a parameter. In some case we will include it as an argument, to explicitly stress the dependence.

In order to evaluate the joint probability function $P(\delta, \boldsymbol{\eta}, \zeta)$, we need the correlations between the different fields evaluated at a given point, say at $\mathbf{r} = \mathbf{0}$. Even though correlations between variables are strictly convolution products, owing to ergodicity, they can be also calculated as ensemble averages over different realisations of the field. Therefore, it is convenient to perform these calculations in the Fourier space, in which the smoothed field $\delta(\mathbf{r}, R)$, its gradient $\eta_i(\mathbf{r}, R)$, and its second-order Cartesian derivatives $\zeta_{ij}(\mathbf{r}, R)$ have the form

$$\delta(\mathbf{r},R) = \frac{1}{(2\pi)^3}\int \mathrm{d}^3\mathbf{k}\,\delta(\mathbf{k})\,W(kR)\,e^{-i\mathbf{k}\cdot\mathbf{r}}\,,$$
$$\eta_i(\mathbf{r},R) = \frac{1}{(2\pi)^3}\int \mathrm{d}^3\mathbf{k}\,(-ik_i)\delta(\mathbf{k})\;W(kR)\,e^{-i\mathbf{k}\cdot\mathbf{r}}\,, \tag{A.1}$$
$$\zeta_{ij}(\mathbf{r},R) = \frac{1}{(2\pi)^3}\int \mathrm{d}^3\mathbf{k}\,(-k_ik_j)\,\delta(\mathbf{k})\,W(kR)\,e^{-i\mathbf{k}\cdot\mathbf{r}}\,.$$

To simplify the notation, from now on, we do not show explicitly the dependence on the point and scale in the field variables. From the definitions of the power spectrum (eq. [2.83]) and the spectral momenta (eq. [2.88]), it can be shown that

$$\langle\delta\,\delta\rangle = \sigma_0^2\,, \qquad \langle\eta_i\,\eta_j\rangle = \frac{\sigma_1^2}{3}\,\delta_{ij}\,,$$
$$\langle\delta\,\eta_i\rangle = 0\,, \qquad \langle\eta_i,\zeta_{jk}\rangle = 0\,, \tag{A.2}$$
$$\langle\delta\,\zeta_{ij}\rangle = -\frac{\sigma_1^2}{3}\,\delta_{ij}\,, \qquad \langle\zeta_{ij}\,\zeta_{kl}\rangle = \frac{\sigma_2^2}{15}\,(\delta_{ij}\delta_{kl}+\delta_{ik}\delta_{jl}+\delta_{il}\delta_{jk})\,.$$

The covariance matrix $\mathbf{M}$ has dimension 10 since it includes correlations between the field, its three first derivatives and its six independent second derivatives. It is almost diagonal apart from one 3×3 box involving the second-order derivatives. We label them ζ_A, where subscript A ranging from 1 to 6 refers to ij = 11, 22, 33, 12, 13, 23. The Gaussian joint probability P does not depend on the form of the variables chosen to characterise the random field. By using variables x, y, and z, defined as

$$\sigma_2 x = -\nabla^2\delta = -(\zeta_1+\zeta_2+\zeta_3)\,, \qquad \sigma_2 y = -\frac{1}{2}(\zeta_1-\zeta_3)\,,$$
$$\sigma_2 z = -\frac{1}{2}(\zeta_1-2\zeta_2+\zeta_3)\,, \tag{A.3}$$

instead of ζ_1, ζ_2, and ζ_3 one obtains a diagonal covariance matrix. Then, by introducing the variable $\nu=\delta/\sigma_0$ the corresponding non-zero correlations adopt the simple form

$$\langle \nu^2 \rangle = 1\,, \quad \langle x^2 \rangle = 1\,, \quad \langle \nu\, x \rangle = \gamma\,, \quad \langle y^2 \rangle = \frac{1}{15}\,, \quad \langle z^2 \rangle = \frac{1}{5}\,, \tag{A.4}$$

where $\gamma = \sigma_1^2/(\sigma_0\sigma_2)$ is a measure of the bandwidth of the power spectrum. From the covariance matrix $\mathbf{M}$ it is possible to calculate the quadratic form Q

$$2Q = \nu^2 + \frac{(x - x_*)^2}{1-\gamma^2} + 15\, y^2 + 5\, z^2 + 3\, \frac{\boldsymbol{\eta}\cdot\boldsymbol{\eta}}{\sigma_1^2} + \sum_{A=4}^{6} \frac{15\zeta_A^2}{\sigma_2^2}. \tag{A.5}$$

with $x_* = \gamma\,\nu$.

The next step is aimed to simplify the calculations and consists of selecting a suitable reference frame. This procedure is always allowed because the correlations given by (A.4) are independent of this choice. Since the matrix ζ_{ij} is symmetric, there is a rotation which diagonalises it: $\mathrm{diag}(\lambda_1, \lambda_2, \lambda_3) = -R\,\zeta\,R^\dagger$, where λ_i ($i =$ 1, 2, 3) are the eigenvalues of the matrix $-\zeta_{ij}$, and R and $R^\dagger$ are the rotation matrix and its transpose respectively. One can select the principal axes along the direction of the eigenvalues λ_i; thus $\zeta_A = -\lambda_A$ ($A =$ 1, 2, 3). In this way, we have used up three degrees of freedom. The other available three permit to fix the orientation of the orthonormal eigenvectors of the matrix by means of the Euler angles α_1, α_2, α_3.

All these choices introduce changes in the volume element associated with the space defined by the second-order derivatives

$$\begin{aligned} \prod_{A=1}^{6} \mathrm{d}\zeta_A &= |(\lambda_1-\lambda_2)(\lambda_2-\lambda_3)(\lambda_1-\lambda_3)|\,\mathrm{d}\lambda_1\,\mathrm{d}\lambda_2\,\mathrm{d}\lambda_3\,\frac{\mathrm{d}\Omega_{S^3}}{6}\,, \\ \mathrm{d}\Omega_{S^3} &= \sin\alpha_2\,\mathrm{d}\alpha_2\,\mathrm{d}\alpha_1\,\mathrm{d}\alpha_3\,, \\ \prod_{A=1}^{3} \mathrm{d}\lambda_A &= \frac{2}{3}\,\sigma_2^3\,\mathrm{d}x\,\mathrm{d}y\,\mathrm{d}z\,, \end{aligned} \tag{A.6}$$

where $d\Omega_{S^3}$ is the volume element on the surface of the three-sphere. Since the whole space is available (there is no constraint on the Euler angles), then its integration yields $2\pi^2$. The factor 6 dividing the first of equations (A.6) arises because the eigenvalues are not ordered. In the new variables, the joint probability function becomes

$$P(\nu, \boldsymbol{\eta}, x, y, z)\,\mathrm{d}\nu\,\mathrm{d}^3\boldsymbol{\eta}\,\mathrm{d}x\,\mathrm{d}y\,\mathrm{d}z = F\,|2y\,(y^2-z^2)|e^{-Q}\mathrm{d}\nu\,\mathrm{d}x\,\mathrm{d}y\,\mathrm{d}z\,\frac{\mathrm{d}^3\boldsymbol{\eta}}{\sigma_0^3}\,,$$

$$F = \frac{15^{5/2}}{32\pi^3}\,\frac{\sigma_0^3}{\sigma_1^3\,(1-\gamma^2)^{1/2}}\,. \tag{A.7}$$

To ensure that the matrix ζ_{ij} is negative definite the eigenvalues have to be ordered in the form

$$\lambda_1 \geq \lambda_2 \geq \lambda_3\,, \tag{A.8}$$

and impose $\lambda_3 > 0$. In this case the factor $1/6$ in the first of equations (A.6) disappears. The eigenvalue ordering causes the variables x, y, and z to be constrained in such a way that the integration only picks out positive values for the λ's. The solution of the inequation system leads to two different domains

$$\begin{aligned} &0 < x\,, \qquad 0 \leq y \leq \frac{x}{4}\,, \qquad -y \leq z \leq y\,; \\ &0 < x\,, \qquad \frac{x}{4} \leq y \leq \frac{x}{2}\,, \qquad 3y - x \leq z \leq y\,. \end{aligned} \tag{A.9}$$

The peak density of maxima of height ν_0 is given by the average

$$\mathcal{N}_{pk}(\nu_0)\,\mathrm{d}\nu = \langle |\lambda_1\lambda_2\lambda_3|\,\theta(\lambda_3)\,\delta^{(3)}(\boldsymbol{\eta})\,\delta(\nu-\nu_0)\rangle\,\mathrm{d}\nu\,, \tag{A.10}$$

which involves the integration of the joint probability function over the variables η_i and λ_i (or x, y, z) taking into account the corresponding constraints. It is valuable to consider the number density of peaks with parameters ν and x [1] per infinitesimal range. This is done by introducing additional δ-functions in equation (A.10). The result is

$$\mathcal{N}_{pk}(\nu,x)\,\mathrm{d}\nu\,\mathrm{d}x = \frac{e^{-\nu^2/2}}{(2\pi)^2 R_*^3}\,\frac{f(x)}{[2\pi\,(1-\gamma^2)]^{1/2}}\,\exp\left[-\frac{(x-x_*)^2}{2(1-\gamma^2)}\right]\mathrm{d}\nu\,\mathrm{d}x\,, \tag{A.11}$$

where $R_* = \sqrt{3}\,\sigma_1/\sigma_2$ is a measure of the characteristic coherence length of the field, and $f(x)$ contains the outcome of integrating the joint probability function over the variables z and y

[1] Notice that in this case we cannot strictly say that these points are peaks since the variable x can be positive or negative. We refer to them as peaks because, eventually, we impose the condition $x > 0$.

$$f(x) = \left(\frac{x^3 - 3x}{2}\right)\left\{\mathrm{erf}\left[x\sqrt{\frac{5}{2}}\right] + \mathrm{erf}\left[\frac{x}{2}\sqrt{\frac{5}{2}}\right]\right\} + \\ + \sqrt{\frac{2}{5\pi}}\left[\left(\frac{31x^2}{4} + \frac{8}{5}\right)e^{-5x^2/8} + \left(\frac{x^2}{2} - \frac{8}{5}\right)e^{-5x^2/2}\right]. \qquad \text{(A.12)}$$

Taking into account the asymptotic behaviour of $f(x)$ for the limits $x \to 0$ and $x \to \infty$, this function can be reasonably approximated by

$$f_{app}(x) = \frac{x^8}{13.2\,(1 + 5x^2/8)} \qquad \text{for } x < 1.5\,,$$

$$f_{app}(x) = x^3 - 3x + \frac{4.08}{x^2} \qquad \text{for } x \geq 1.5\,.$$

Finally, the integration over the variable x (for $x > 0$) leads to the number density of peaks with height in the interval ν to $\nu + \mathrm{d}\nu$

$$\mathcal{N}_{pk}(\nu)\,\mathrm{d}\nu = \frac{e^{-\nu^2/2}}{(2\pi)^2 R_*^3}\,G(\gamma, x_*)\,\mathrm{d}\nu\,, \qquad \text{(A.13)}$$

where the numerical function

$$G(\gamma, x_*) = \frac{1}{[2\pi\,(1-\gamma^2)]^{1/2}}\int_0^\infty \mathrm{d}x\,f(x)\,\exp\left[-\frac{(x - x_*)^2}{2(1-\gamma^2)}\right], \qquad \text{(A.14)}$$

has been accurately fitted by BBKS (see their equations [4.4] and [4.5]) in the range $0.3 < \gamma < 0.7$ and $x_* > 1$.

In the biased formation model, it is assumed that collapsed objects arise from peaks of the smoothed density field (on a fixed scale) with height *above* a specific threshold. Thus, we can compute the number density of these objects by integrating the differential density (A.13) over the variable ν constrained in the interval (ν_c, ∞)

$$n_{pk}(\nu_c) = \int_{\nu_c}^\infty \mathcal{N}_{pk}(\nu)\,\mathrm{d}\nu\,. \qquad \text{(A.15)}$$

A.2 The conditional number density

In hierarchical scenarios the evolution of density fluctuations on a given scale can be altered by the presence of fluctuations on larger scales. The most notable ex-

ample is the aforementioned cloud-in-cloud problem. Furthermore, it is well-known that some regions of the space are almost devoided of galaxies (voids), while others have a galaxy density much greater than that of the background. This fact can be interpreted in the peak model framework. Since relaxed objects are supposed to arise from peaks of the density field above a global critical height, the presence of a background field is able to boost the object formation in those sites where the background density is higher than the average (due to the decrease of the local threshold) and suppress it in those sites where the background density is lower than the average (because the local threshold is increased). In practice, the peak and the background fields are generated by smoothing the same random density field $\delta(\mathbf{r})$ on two different scales that we denote R_s and R_b respectively. Instead of writing explicitly the scale dependence, we will use subscripts s and b to refer to quantities concerning the peak and the background fields.

To quantify the influence of the background field on the peak evolution it is necessary to calculate the number density of peaks on backgrounds with a specific height. Let us begin with the calculation of the conditional probability $P(\nu_b|\nu_s, x)\,\mathrm{d}\nu_b$, which gives the probability that the background field has height $\nu_b = \delta_b/\sigma_{0b}$ in an infinitesimal range subject to the constraint that there is a peak with $\nu_s = \delta_s/\sigma_{0s}$ and scaled Laplacian x [2]. According to BBKS, conditional probabilities involving Gaussian variables adopt a Gaussian form with mean equal to

$$\langle Y_B \otimes Y_A\rangle \langle Y_A \otimes Y_A\rangle^{-1} Y_A^{\dagger}\,, \tag{A.16}$$

and dispersion equal to

$$\langle Y_B \otimes Y_B\rangle - \langle Y_B \otimes Y_A\rangle \langle Y_A \otimes Y_A\rangle^{-1} \langle Y_A \otimes Y_B\rangle\,. \tag{A.17}$$

The angular brackets indicate ensemble averages. The tensor product notation $Y_B \otimes Y_A$ just builds a $m \times n$ matrix out of the vectors Y_B, of dimension m, and Y_A, of dimension n. In this particular case $Y_B = \nu_b$ and $Y_A = (\nu_s, x)$. We have already found the correlation between the peak variables $\langle \nu\, x\rangle = \gamma$. The other non-vanishing correlations appearing in the calculations are

$$\langle \nu_b^2\rangle = 1\,, \qquad \langle \nu_b \nu_s\rangle = \frac{\sigma_{0h}^2}{\sigma_{0s}\sigma_{0b}} \equiv \epsilon\,, \qquad \langle \nu_b\, x\rangle = \frac{\sigma_{1h}^2}{\sigma_{2s}\sigma_{0b}} = \gamma_s \epsilon r_1\,, \tag{A.18}$$

with the cross-momenta defined as

[2] It is not necessary to introduce more variables to characterise the peak because the background variable ν_b does not correlate with y, z, and ζ_A, $A = 4, 5, 6$.

$$\sigma_{jh}^2 = \int_0^\infty \frac{\mathrm{d}k\, k^{2j+1}}{2\pi^2} P(k)\, W(kR_s)\, W(kR_b)\,. \tag{A.19}$$

The parameters ϵ and $r_1 = \sigma_{1h}^2\,\sigma_{0s}^2/(\sigma_{0h}^2\,\sigma_{1s}^2)$ account for the correlations between the peak and background fields resulting from the fact that both are obtained by smoothing the same random field on two different scales. For physically interesting power spectra and filtering functions, this kind of correlations decreases asymptotically to zero as the background smoothing radius increases. For instance, a power-law power spectrum filtered with a Gaussian window leads to

$$\epsilon = \left(\frac{R_s R_b}{R_h^2}\right)^{(n+3)/2} \to \left(\frac{2R_s}{R_b}\right)^{(n+3)/2}, \qquad r_1 = \left(\frac{R_s}{R_h}\right)^2 \to 2\left(\frac{R_s}{R_b}\right)^2, \tag{A.20}$$

where $R_h^2 = (R_b^2 + R_s^2)/2$. The limits hold for $R_b \gg R_s$.

Finally, the conditional probability can be written as

$$P(\nu_b|\nu_s, x)\,\mathrm{d}\nu_b = \frac{1}{\sqrt{2\pi}\,\Delta\nu_b} \exp\left[-\frac{(\nu_b - \bar{\nu}_b)^2}{2(\Delta\nu_b)^2}\right] \mathrm{d}\nu_b\,, \tag{A.21}$$

with mean $\bar{\nu}_b$ and dispersion $\Delta\nu_b$ given respectively by

$$\begin{aligned} \bar{\nu}_b &= \frac{\epsilon^2}{1-\gamma_s^2}[\nu_s(1-\gamma_s^2 r_1) - \gamma_s x(1-r_1)], \\ \Delta\nu_b^2 &= 1 - \frac{\epsilon^2}{1-\gamma_s^2}(1 - 2\gamma_s^2 r_1 + \gamma_s^2 r_1^2)\,. \end{aligned} \tag{A.22}$$

The second step consists of calculating the joint density of points with height ν_b when the field is smoothed on scale R_b, and height ν_s and scaled Laplacian x when it is filtered on scale R_s. This quantity is straightforwardly derived from the differential number density $\mathcal{N}_{pk}(\nu_s, x)$ (see equation[A.11]) and the conditional probability $P(\nu_b|\nu_s, x)$

$$\mathcal{N}_{pk}(\nu_b, \nu_s, x)\,\mathrm{d}\nu_b\mathrm{d}\nu_s\mathrm{d}x = \mathcal{N}_{pk}(\nu_s, x)\,\mathrm{d}\nu_s\mathrm{d}x\, P(\nu_b|\nu_s, x)\,\mathrm{d}\nu_b\,. \tag{A.23}$$

The integral of this expression over x, with the constraint $x > 0$, to ensure that the points with height ν_s are peaks, yields

$$\mathcal{N}_{pk}(\nu_b,\nu_s)\,\mathrm{d}\nu_b\,\mathrm{d}\nu_s = \mathrm{d}\nu_b\,\mathrm{d}\nu_s \int_0^\infty \mathrm{d}x\,\mathcal{N}_{pk}(\nu_s,x)\,P(\nu_b|\nu_s,x) =$$

$$= \frac{G(\tilde{\gamma},\tilde{x}_*)}{(2\pi)^2\,R_{*s}^3}\,\exp\left[-\frac{(\nu_s-\epsilon\nu_b)^2}{2(1-\epsilon^2)}\right]\,\frac{e^{-\nu_b^2/2}\mathrm{d}\nu_b\,\mathrm{d}\nu_s}{\sqrt{2\pi\,(1-\epsilon^2)}}. \qquad \text{(A.24)}$$

The tilde variables $\tilde{\gamma}$, $\tilde{x}_* = \tilde{\gamma}\,\tilde{\nu}$ have been introduced to express the integral in a closed form

$$\tilde{\gamma}^2 = \gamma_s^2\left[1+\epsilon^2\,\frac{(1-r_1)^2}{1-\epsilon^2}\right], \qquad \tilde{\nu} = \frac{\gamma_s}{\tilde{\gamma}}\left(\frac{1-r_1}{1-\epsilon^2}\right)\left[\nu_s\left(\frac{1-\epsilon^2 r_1}{1-r_1}\right)-\epsilon\nu_b\right]. \qquad \text{(A.25)}$$

The conditional number density $\mathcal{N}_{pk}(\nu_s|\nu_b)\,\mathrm{d}\nu_s$ of peaks with height within the interval ν_s to $\nu_s+\mathrm{d}\nu_s$ in backgrounds with height ν_b is derived by dividing the joint density $\mathcal{N}_{pk}(\nu_b,\nu_s)$ by the probability of finding a background. Taking into account that this is a Gaussian probability, the conditional number density writes

$$\mathcal{N}_{pk}(\nu_s|\nu_b)\,\mathrm{d}\nu_s \equiv \frac{\mathcal{N}_{pk}(\nu_b,\nu_s)}{P(\nu_b)}\mathrm{d}\nu_s =$$

$$= \frac{G(\tilde{\gamma},\tilde{x}_*)}{(2\pi)^2\,R_{*s}^3\sqrt{1-\epsilon^2}}\,\exp\left[-\frac{(\nu_s-\epsilon\nu_b)^2}{2(1-\epsilon^2)}\right]\,\mathrm{d}\nu_s\,. \qquad \text{(A.26)}$$

To obtain the density of peaks exceeding a given threshold at a point where the background field has height ν_b, it is necessary to integrate the above expression over ν_s with the constraint $\nu_s > \nu_c$

$$n_{pk}(\nu_c|\nu_b) = \int_{\nu_c}^\infty \mathcal{N}_{pk}(\nu\,|\nu_b)\,\mathrm{d}\nu\,. \qquad \text{(A.27)}$$

Finally, the effect produced by a background field on the peak population can be quantified by means of the *enhancement factor*, defined as the ratio

$$E(\nu_b) = \frac{n_{pk}(\nu_c|\nu_b)}{n_{pk}(\nu_c)}\,. \qquad \text{(A.28)}$$

B

Eccentricities and Semiaxes

Given a triaxial system with isodensity contours $\rho_{\rm iso}(r)$, semiaxes $a_1 \geq a_2 \geq a_3$ and labelling radii r defined as

$$r = \left[\frac{1}{3}\left(a_1^2 + a_2^2 + a_3^2\right)\right]^{1/2}, \tag{B.1}$$

the density at $\mathbf{r} = (r, \theta, \varphi)$ takes the form

$$\begin{aligned}\rho(\mathbf{r}) = \rho_{\rm iso}(r) &\left[1 - \frac{e_{\rm p}^2(r) + e_{\rm s}^2(r)}{3}\right] \\ &\times \left[\sin^2\theta\cos^2\phi + \frac{\sin^2\theta\sin^2\phi}{1 - e_{\rm sp}^2(r)} + \frac{\cos^2\theta}{1 - e_{\rm ps}^2(r)}\right],\end{aligned} \tag{B.2}$$

where the azimutal axis is taken aligned along with the major axis and $e_{\rm ps}$ and $e_{\rm sp}$ stand for the primary or secondary eccentricities, $e_{\rm p}$ and $e_{\rm s}$, respectively, defined as

$$e_{\rm p} = \left(1 - \frac{a_3^2}{a_1^2}\right)^{1/2} \qquad \text{and} \qquad e_{\rm s} = \left(1 - \frac{a_2^2}{a_1^2}\right)^{1/2}, \tag{B.3}$$

and the remaining quantity depending on the orientation of the x and y Cartesian axes relative to the minor and intermediate ellipsoid semiaxes. The spherically

averaged density at r is then

$$\rho(r) = \frac{\rho_{\rm iso}(r)}{3}\left[1 - \frac{e_{\rm p}^2(r) + e_{\rm s}^2(r)}{3}\right] G(r), \tag{B.4}$$

$$G(r) = a_1^2(r)\left[\frac{1}{a_1^2(r)} + \frac{1}{a_2^2(r)} + \frac{1}{a_3^2(r)}\right]. \tag{B.5}$$

Dividing equation (B.2) by equation (B.5), we obtain

$$1+\frac{\delta\rho(\mathbf{r})}{\rho(r)} = \frac{3}{G(r)}\left[\sin^2\theta\cos^2\phi + \frac{\sin^2\theta\sin^2\phi}{1-e_{\rm sp}^2(r)} + \frac{\cos^2\theta}{1-e_{\rm ps}^2(r)}\right]. \tag{B.6}$$

Then, using the definitions (B.3), the mean squared density contrast fluctuation over the sphere of radius r leads to

$$\left\langle\left(\frac{\delta\rho(\mathbf{r})}{\rho(r)}\right)^2\right\rangle = -\frac{2}{5}\left\{1 - \frac{3[(1-e_{\rm p}^2)^2(1-e_{\rm s}^2)^2 + (1-e_{\rm p}^2)^2 + (1-e_{\rm s}^2)^2]}{[(1-e_{\rm p}^2)(1-e_{\rm s}^2) + (1-e_{\rm p}^2) + (1-e_{\rm s}^2)]^2}\right\}(r). \tag{B.7}$$

Using the Poisson equation relating $\delta\Phi(\mathbf{r})/\Phi(r)$ to $\delta\rho(\mathbf{r})/\rho(r)$ and integrating over the solid angle, we can express the mean squared potential and mean crossed density-potential fluctuations as function of the mean squared density fluctuation (see Salvador-Solé et al. 2012b).

C

Accurate Conditional Peak Number Density

As shown in Manrique et al. (1998), the conditional number density $N^{\rm nest}(\sigma_0, \delta_{\rm c}|\sigma_0', \delta_{\rm c})$ of peaks with $\delta_{\rm c}$ per infinitesimal $\ln \sigma_0^{-1}$ subject to being located in the collapsing cloud of *non-nested* peaks with $\delta_{\rm c}$ at $\sigma_0' < \sigma_0$ is well-approximated by the integral over the distance r from the background peak out to the radius $R_{\rm p}$ of the collapsing cloud in units of $q(M,t)R$ of the conditional number density of peaks with $\delta_{\rm c}$ per infinitesimal $\ln \sigma_0^{-1}$, subject to being located at a distance r from a background peak, $N(\sigma_0, \delta_{\rm c}|\sigma_0', \delta_{\rm c}, r)$,

$$N^{\rm nest}(\sigma_0, \delta_{\rm c}|\sigma_0', \delta_{\rm c}) = C\int_0^1 {\rm d}r\, 3r^2 N(\sigma_0, \delta_{\rm c}|\sigma_0, \delta_{\rm c}, r)\,. \tag{C.1}$$

The conditional number density in the integrant on the right of equation (C.1) can be obtained, as the ordinary number density (3.16), from the conditional density of peaks per infinitesimal x and ν, subject to being located at the distance r from a background peak with ν at σ_0', calculated by BBKS. The result is (Manrique et al.

1998)

$$N(\sigma_0,\delta_{\rm c}|\sigma_0',\delta_{\rm c},r){\rm d}\ln\sigma_0^{-1} = \frac{\langle x\rangle[\tilde{\sigma}_0(r),\delta_{\rm c}]}{(2\pi)^2\,R_\star^3\,\gamma\,e(r)}{\rm e}^{-\frac{[\nu-\epsilon(r)\,\nu'(r)]^2}{2e^2(r)}}{\rm d}\ln\sigma_0^{-1}\,, \tag{C.2}$$

where $\langle x\rangle[\tilde{\sigma}_0(r),\delta_{\rm c}]$ is the average curvature of peaks with $\delta_{\rm c}$ at σ_0 located at a distance r from a background peak with identical density contrast at σ_0'. This latter function takes just the same form as the usual average curvature $\langle x\rangle(\sigma_0,\delta_{\rm c})$ for the properly normalised (by integration over x from zero to infinity) curvature distribution function

$$h(x,\sigma_0,\delta_{\rm c}) = f(x)\,{\rm e}^{-\frac{(x-x_\star)^2}{2(1-\tilde{\gamma}^2)}}, \tag{C.3}$$

$$f(x) = \frac{x^3-3x}{2}\left\{{\rm erf}\left[\left(\frac{5}{2}\right)^{1/2}x\right]+{\rm erf}\left[\left(\frac{5}{2}\right)^{1/2}\frac{x}{2}\right]\right\} + \left(\frac{2}{5\pi}\right)^{1/2}\left[\left(\frac{31x^2}{4}+\frac{8}{5}\right){\rm e}^{-\frac{5x^2}{8}}+\left(\frac{x^2}{2}-\frac{8}{5}\right){\rm e}^{-\frac{5x^2}{2}}\right], \tag{C.4}$$

but for $\tilde{x}_\star(r)\equiv\tilde{\gamma}(r)\,\tilde{\nu}(r)$ instead of $x_\star\equiv\gamma\,\nu$, being

$$\tilde{\gamma}^2(r) = \gamma^2\left[1+\epsilon(r)^2\,\frac{(1-r_1)^2}{1-\epsilon(r)^2}\right] \tag{C.5}$$

$$\tilde{\nu}(r) = \frac{\gamma}{\tilde{\gamma}(r)}\,\frac{1-r_1}{1-\epsilon(r)^2}\left[\nu\left(\frac{1-\epsilon(r)^2r_1}{1-r_1}\right)-\epsilon(r)\nu'(r)\right]. \tag{C.6}$$

In equations (C.2), (C.5) and (C.6), we have used the following notation: $e(r)=\sqrt{1-\epsilon(r)^2}$, $\epsilon(r)=(\sigma_0^2(R_{\rm h})\,/[\sigma_0\sigma_0']g(r,\sigma_0')$, and $\nu'(r)=g(r,\sigma_0')\overline{\delta(r)}/\sigma_0'$ and $r_1=[\sigma_0(R)\sigma_1(R_{\rm h})/(\sigma_1(R)\sigma_0(R_{\rm h}))]^2$, where $R_{\rm h}$ is defined as usual and $g(r,\sigma_0')$ is $\{1-[\Delta\delta'(r)]^2/\sigma_0'\}^{1/2}$, being $\overline{\delta'(r)}$ and $\Delta\delta'(r)$ the mean and rms density contrasts at r from the background peak, respectively given by

$$\overline{\delta(r)} = \frac{\gamma\delta_{\rm pk}}{1-\gamma^2}\left(\frac{\psi}{\gamma}+\frac{\nabla^2\psi}{u^2}\right)-\frac{x\sigma_0}{1-\gamma^2}\left(\gamma\psi+\frac{\nabla^2\psi}{u^2}\right) \tag{C.7}$$

$$[\Delta\delta(r)]^2 = \sigma_0^2\Bigg\{1-\frac{1}{1-\gamma^2}\left[\psi^2+\left(2\gamma\psi+\frac{\nabla^2\psi}{u^2}\right)\frac{\nabla^2\psi}{u^2}\right] -5\left(\frac{3\psi'}{u^2r}-\frac{\nabla^2\psi}{u^2}\right)^2-\frac{3(\psi')^2}{\gamma u^2}\Bigg\}, \tag{C.8}$$

where $\xi(r)$ is the mass correlation function at the separation r and scale R, ψ is the ratio $\xi(r)/\xi(0)$, ψ' is its r-derivative and u is defined as $[q(M,t)R]^2\sigma_2(R)/\sigma_0(R)$. Lastly, the factor C on the right, defined as

$$C \equiv \frac{4\pi s^3 N(\sigma_0', \delta_\mathrm{c})}{3N(\sigma_0, \delta_\mathrm{c})}\int_0^s \mathrm{d}r\, 3r^2\, N(\sigma_0, \delta_\mathrm{c}|\sigma_0', \delta_\mathrm{c}, r) \tag{C.9}$$

with s equal to the mean separation between the larger scale non-nested peaks drawn from their mean number density[1], is to correct for the overcounting of background peaks in $N(\sigma_0, \delta_\mathrm{c}|\sigma_0', \delta_\mathrm{c}, r)$ as they are not explicitly required to be non-nested.

The simpler version of the conditional peak number density given in Section 5.2.2 can be readily recovered from the present one by ignoring the radial dependence of the typical spherically averaged density profile around peaks, that is taking $\overline{\delta(r)} = \delta_\mathrm{c}$ and $\Delta\delta(r) = 0$.

[1]This must be calculated iteratively, although two iterations, starting with $C = 1$, are enough to obtain an accurate result.

References

Anderhalden D., Diemand J., 2013, JCAp, 4, 9

Appel L., Jones B. J. T., 1990, *MNRAS*, 245, 522

Ascasibar Y., Yepes G., Gottlöber S., Müller V., 2004, *MNRAS*, 352, 1109

Avila-Reese V., Colín P., Gottlöber S., Firmani C., Maulbetsch C., 2005, *ApJ*, 634, 51

Babcock H. W., 1939, Lick Observatory Bulletin, 19, 41

Bardeen J. M., Bond J. R., Kaiser N., Szalay A. S., 1986, *ApJ*, 304, 15

Bernardeau F., 1994, *ApJ*, 427, 51

Bertschinger E., Dekel A., 1989, *ApJ*, 336, L5

Bond J. R., 1989, in Astbury A., Campbell B. A., Israel W., Khana F. C., eds, , Frontiers in Physics: From Colliders to Cosmology. Singapore: World Scientific, p. 182

Bond J. R., Cole S., Efstathiou G., Kaiser N., 1991, *ApJ*, 379, 440

Bond J. R., Efstathiou G., 1984, *ApJ*, 285, L45

Bond J. R., Myers S. T., 1996, *ApJ*, 103, 41

Bond J. R., Szalay A. S., 1983, *ApJ*, 274, 443

Bower R. G., 1991, *MNRAS*, 248, 332

Bryan G. L., Norman M. L., 1998, *ApJ*, 495, 80

Bullock J. S., Kolatt T. S., Sigad Y., Somerville R. S., Kravtsov A. V., Klypin A. A., Primack J. R., Dekel A., 2001, *MNRAS*, 321, 559

Chibisov G. V., 1972, Sov. Astr., 16, 56

Cline J. M., Politzer H. D., Rey S.-J., Wise M. B., 1987, Commun. Math. Phys., 112, 217

Colafrancesco S., Lucchin F., Matarrese S., 1989, *ApJ*, 345, 3

Cole S., Lacey C., 1996, *MNRAS*, 281, 716

Coles P., 1989, *MNRAS*, 238, 319

Coles P., Melott A. L., Shandarin S. F., 1993, *MNRAS*, 260, 765

Couchman H. M. P., 1987, *MNRAS*, 225, 795

Courtin J., Rasera Y., Alimi J.-M., Corasaniti P.-S., Boucher V., Füzfa A., 2011, *MNRAS*, 410, 1911

Crocce M., Fosalba P., Castander F. J., Gaztañaga E., 2010, *MNRAS*, 403, 1353

Davis M., Efstathiou G., Frenk C. S., White S. D. M., 1985, *ApJ*, 292, 371

Dekel A., Bertschinger E., Faber S. M., 1990, *ApJ*, 364, 349

Dekel A., Bertschinger E., Yahil A., Strauss M. A., Davis M., Huchra J. P., 1993, *ApJ*, 412, 1

Dekel A., Birnboim Y., 2006, *MNRAS*, 368, 2

Del Popolo A., Gambera M., Recami E., Spedicato E., 2000, *A&A*, 353, 427

Diemand J., Kuhlen M., Madau P., Zemp M., Moore B., Potter D., Stadel J., 2008, *Nature*, 454, 735

Diemand J., Moore B., Stadel J., 2005, *Nature*, 433, 389

Doroshkevich A. G., 1970, Astrophysica, 6, 320

Doroshkevich A. G., Shandarin S. F., 1978, *MNRAS*, 182, 27

Doroshkevich A. G., Zel'dovich Y. B., Novikov I. D., 1967, Sov. Astr., 11, 233

Duffy A. R., Schaye J., Kay S. T., Dalla Vecchia C., 2008, *MNRAS*, 390, L64

Dunkley J., Komatsu E., Nolta M. R., Spergel D. N., Larson D., Hinshaw G., Page L., Bennett C. L., Gold B., Jarosik N., Weiland J. L., Halpern M., Hill R. S., Kogut A., Limon M., Meyer S. S., Tucker G. S., Wollack E., Wright E. L., 2009, *ApJS*, 180, 306

Dutton A. A., Macciò A. V., 2014, *MNRAS*, 441, 3359

Efstathiou G., Frenk C., White S. D. M., Davis M., 1988, *MNRAS*, 235, 715

Einasto J., 1965, Trudy Inst. Astrofiz. Alma-ata, 5, 87

Eisenstein D. J., Hu W., 1999, *ApJ*, 511, 5

Eke V. R., Navarro J. F., Steinmetz M., 2001, *ApJ*, 554, 114

Field G. B., 1971, *ApJ*, 165, 29

Gao L., Navarro J. F., Cole S., Frenk C. S., White S. D. M., Springel V., Jenkins A., Neto A. F., 2008, *MNRAS*, 387, 536

Gnedin O. Y., Ostriker J. P., 1999, *ApJ*, 513, 626

Gnedin O. Y., Zhao H., 2002, *MNRAS*, 333, 299

Governato F., Zolotov A., Pontzen A., Christensen C., Oh S. H., Brooks A. M., Quinn T., Shen S., Wadsley J., 2012, *MNRAS*, 422, 1231

Green A. M., Hofmann S., Schwarz D. J., 2004, *MNRAS*, 353, L23

Gross M. A. K., Somerville R. S., Primack J. R., Holtzman J., Klypin A., 1998, *MNRAS*, 301, 81

Gunn J. E., Gott J. R., 1972, *ApJ*, 176, 1

Hahn O., Paranjape A., 2014, *MNRAS*, 438, 878
Hanami H., 2001, *MNRAS*, 327, 721
Harrison E. R., 1970, *Phys. Rev. D*, 1, 2726
Heavens A., Peacock J., 1988, *MNRAS*, 232, 339
Heitmann K., Lukić Z., Habib S., Ricker P. M., 2006, *ApJ*, 642, L85
Helmi A., White S. D. M., Springel V., 2003, *MNRAS*, 339, 834
Henry J. P., 2000, *ApJ*, 534, 565
Hiotelis N., 2003, *MNRAS*, 344, 149
Hubble E., 1929, Proc. Nat. Acad. Sci., 15, 168
Huss A., Jain B., Steinmetz M., 1999, *ApJ*, 517, 64
Ishiyama T., 2014, *ApJ*, 788, 27
Jeans J., 1902, Philos. Trans. R. Soc. London A, 199, 1
Jedamzik K., 1995, *ApJ*, 448, 1
Jenkins A., Frenk C. S., White S. D. M., Colberg J. M., Cole S., Evrard A. E., Couchman H. M. P., Yoshida N., 2001, *MNRAS*, 321, 372
Juan E., Salvador-Solé E., Domènech G., Manrique A., 2014a, *MNRAS*, 439, 719
Juan E., Salvador-Solé E., Domènech G., Manrique A., 2014b, *MNRAS*, 439, 3156
Kaiser N., 1984, *ApJ*, 284, L9
Kitayama T., Suto Y., 1996, *MNRAS*, 280, 638
Klypin A. A., Trujillo-Gomez S., Primack J., 2011, *ApJ*, 740, 102
Komatsu E., Smith K. M., Dunkley J., Bennett C. L., Gold B., Hinshaw G., Jarosik N., Larson D., Nolta M. R., et al. 2011, *ApJS*, 192, 18
Kuhlen M., Strigari L. E., Zentner A. R., Bullock J. S., Primack J. R., 2005, *MNRAS*, 357, 387
Kull A., Treumann R. A., Boehringer H., 1997, *ApJ*, 484, 58
Lacey C., Cole S., 1993, *MNRAS*, 262, 627
Lacey C., Cole S., 1994, *MNRAS*, 271, 676
Lee J., Shandarin S. F., 1998, *ApJ*, 500, 14
Li Y., 2010, PhD thesis, University of Massachusetts Amherst
Li Y., Mo H. J., Gao L., 2008, *MNRAS*, 389, 1419
Lifshitz E. M., 1946, J. Phys. (USSR), 10, 116
Lin C. C., Mestel L., Shu F. H., 1965, *ApJ*, 142, 1431
Loveday J., Efstathiou G., Maddox S. J., Peterson B. A., 1996, *ApJ*, 468, 1
Lu Y., Mo H. J., Katz N., Weinberg M. D., 2006, *MNRAS*, 368, 1931
Ludlow A. D., Navarro J. F., Angulo R. E., Boylan-Kolchin M., Springel V., Frenk C., White S. D. M., 2014, *MNRAS*, 441, 378

Ludlow A. D., Navarro J. F., Boylan-Kolchin M., Bett P. E., Angulo R. E., Li M., White S. D. M., Frenk C., Springel V., 2013, *MNRAS*, 432, 1103

Ludlow A. D., Navarro J. F., Li M., Angulo R. E., Boylan-Kolchin M., Bett P. E., 2012, *MNRAS*, 427, 1322

Ludlow A. D., Porciani C., 2011, *MNRAS*, 413, 1961

Lukić Z., Heitmann K., Habib S., Bashinsky S., Ricker P. M., 2007, *ApJ*, 671, 1160

Lynden-Bell D., 1967, *MNRAS*, 136, 101

Macciò A. V., Dutton A. A., van den Bosch F. C., 2008, *MNRAS*, 391, 1940

Macció A. V., Dutton A. A., van den Bosch F. C., Moore B., Potter D., Stadel J., 2007, *MNRAS*, 378, 55

Manrique A., Raig A., Salvador-Solé E., Sanchis T., Solanes J. M., 2003, *ApJ*, 593, 26

Manrique A., Raig A., Solanes J. M., González-Casado G., Stein P., Salvador-Solé E., 1998, *ApJ*, 499, 548

Manrique A., Salvador-Solé E., 1995, *ApJ*, 453, 6

Manrique A., Salvador-Solé E., 1996, *ApJ*, 467, 504

Menanteau F., Hughes J. P., Sifón C., Hilton M., González J., Infante L., Barrientos L. F., et al., 2012, *ApJ*, 748, 7

Merritt D., Graham A. W., Moore B., Diemand J., Terzić B., 2006, *AJ*, 132, 2685

Merritt D., Navarro J. F., Ludlow A., Jenkins A., 2005, *ApJ*, 624, L85

Monaco P., 1995, *ApJ*, 447, 23

Monaco P., 1998, Fundam. Cosmic Phys., 19, 157

Muñoz-Cuartas J. C., Macciò A. V., Gottlöber S., Dutton A. A., 2011, *MNRAS*, 411, 584

Musso M., Paranjape A., 2012, *MNRAS*, 420, 369

Nakamura T. K., 2000, *ApJ*, 531, 739

Navarro J. F., Frenk C. S., White S. D. M., 1995, *MNRAS*, 275, 720

Navarro J. F., Frenk C. S., White S. D. M., 1997, *ApJ*, 490, 493

Navarro J. F., Hayashi E., Power C., Jenkins A. R., Frenk C. S., White S. D. M., Springel V., Stadel J., Quinn T. R., 2004, *MNRAS*, 349, 1039

Navarro J. F., Ludlow A., Springel V., Wang J., Vogelsberger M., White S. D. M., Jenkins A., Frenk C. S., Helmi A., 2010, *MNRAS*, 402, 21

Neto A. F., Gao L., Bett P., Cole S., Navarro J. F., Frenk C. S., White S. D. M., Springel V., Jenkins A., 2007, *MNRAS*, 381, 1450

Paranjape A., Lam T. Y., Sheth R. K., 2012, *MNRAS*, 420, 1429

Paranjape A., Sheth R. K., 2012, *MNRAS*, 426, 2789

Peacock J. A., Heavens A. F., 1985, *MNRAS*, 217, 805

Peacock J. A., Heavens A. F., 1990, *MNRAS*, 243, 133

Peebles P. J. E., 1967, *ApJ*, 147, 859

Peebles P. J. E., 1980, The large scale structure of the universe. Pinceton University Press

Peebles P. J. E., Yu J., 1970, *ApJ*, 162, 815

Penzias A. A., Wilson R. W., 1965, Astrophys. J., 142, 419

Percival W., Miller L., Peacock J. A., 2000, *MNRAS*, 318, 273

Planck Collaboration Ade P. A. R., Aghanim N., Armitage-Caplan C., Arnaud M., Ashdown M., Atrio-Barandela F., Aumont J., Baccigalupi C., Banday A. J., et al. 2014, *A&A*, 571, A16

Porciani C., Dekel A., Hoffman Y., 2002, *ApJ*, 332, 325

Prada F., Klypin A. A., Cuesta A. J., Betancort-Rijo J. E., Primack J., 2012, *MNRAS*, 423, 3018

Prada F., Klypin A. A., Simonneau E., Betancort-Rijo J., Patiri S., Gottlöber S., Sanchez-Conde M. A., 2006, *ApJ*, 645, 1001

Press W. H., Schechter P., 1974, *ApJ*, 187, 425

Raig A., González-Casado G., Salvador-Solé E., 1998, *ApJ*, 508, L129

Raig A., González-Casado G., Salvador-Solé E., 2001, *MNRAS*, 327, 939

Reed D., Gardner J., Quinn T., Stadel J., Fardal M., Lake G., Governato F., 2003, *MNRAS*, 346, 565

Reed D. S., Koushiappas S. M., Gao L., 2011, *MNRAS*, 415, 3177

Romano-Díaz E., Faltenbacher A., Jones D., Heller C., Hoffman Y., Shlosman I., 2006, *ApJ*, 637, L93

Sahni V., Coles P., 1995, *Phys. Rep.*, 262, 1

Salvador-Solé E., Manrique A., González-Casado G., Hansen S. H., 2007, *ApJ*, 666, 181

Salvador-Solé E., Manrique A., Juan E., 2016b, *in progress*

Salvador-Solé E., Manrique A., Solanes J. M., 2005, *MNRAS*, 358, 901

Salvador-Solé E., Serra S., Manrique A., González-Casado G., 2012b, *MNRAS*, 424, 3129

Salvador-Sole E., Solanes J. M., 1993, *ApJ*, 417, 427

Salvador-Solé E., Solanes J. M., Manrique A., 1998, *MNRAS*, 499, 542

Salvador-Solé E., Viñas J., Manrique A., Serra S., 2012a, *MNRAS*, 423, 2190

Sánchez-Conde M. A., Prada F., 2014, *MNRAS*, 442, 2271

Shandarin S. F., Zel'dovich Y. B., 1989, Reviews of Modern Physics, 61, 185

Sheth R. K., Mo H. J., Tormen G., 2001, *MNRAS*, 323, 1
Sheth R. K., Tormen G., 2002, *MNRAS*, 329, 61
Shu F. H., 1978, *ApJ*, 225, 83
Silk J., 1967, *Nature*, 215, 1155
Silk J., 1968, *ApJ*, 151, 459
Spergel D. N., Hernquist L., 1992, *ApJ*, 397, L75
Springel V., White S. D. M., Jenkins A., Frenk C. S., Yoshida N., Gao L., Navarro J., Thacker R., Croton D., Helly J., Peacock J. A., Cole S., Thomas P., Couchman H., Evrard A., Colberg J., Pearce F., 2005, *Nature*, 435, 629
Stadel J., Potter D., Moore B., Diemand J., Madau P., Zemp M., Kuhlen M., Quilis V., 2009, *MNRAS*, 398, L21
Stiavelli M., Bertin G., 1987, *MNRAS*, 229, 61
Sugiyama N., 1995, *ApJS*, 100, 281
Tinker J., Kravtsov A. V., Klypin A., Abazajian K., Warren M., Yepes G., Gottlöber S., Holz D. E., 2008, *ApJ*, 688, 709
Trenti M., Bertin G., 2005, *A&A*, 429, 161
Viñas J., Salvador-Solé E., Manrique A., 2012, *MNRAS*, 424, L6
Wang J., Navarro J. F., Frenk C. S., White S. D. M., Springel V., Jenkins A., Helmi A., Ludlow A., Vogelsberger M., 2011, *MNRAS*, 413, 1373
Wang J., White S. D. M., 2009, *MNRAS*, 396, 709
Warren M. S., Abazajian K., Holz D. E., Teodoro L., 2006, *ApJ*, 646, 881
Wechsler R. H., Bullock J. S., Primack J. R., Kravtsov A. V., Dekel A., 2002, *AJ*, 568, 52
Weimberg S., 1971, *ApJ*, 168, 175
White M., 2002, *ApJS*, 143, 241
White S. D. M., 1984, *ApJ*, 286, 38
White S. D. M., Efstathiou G., Frenk C. S., 1993, *MNRAS*, 262, 1023
White S. D. M., Rees M. J., 1978, *MNRAS*, 183, 341
Zel'dovich Y. B., 1970, *A&A*, 5, 84
Zel'dovich Y. B., 1972, *MNRAS*, 160, 1P
Zhao D. H., Jing Y. P., Mo H. J., Börner G., 2009, *ApJ*, 707, 354
Zhao D. H., Mo H. J., Jing Y. P., Börner G., 2003, *MNRAS*, 339, 12
Zwicky F., 1933, Helvetica Physica Acta, 6, 110

List of Figures

List of Tables

Non- Euclidean calculus and quantum physics
are enough to stretch any brain
H.P. Lovecraft

Perkele!
Finnish power-word

...of steel!
Enric Juan